International Journal of Science and Engineering Applications
Volume 5 Issue 3, 2016, ISSN-2319-7560 (Online)

Effect of Temperature on Creep behavior of Poly(vinyl chloride) Loaded with Single Walled Carbon Nanotubes

M. Abu-Abdeen
Physics Department
Faculty of Science
Cairo University
Giza, Egypt

A. I. Aboud
Physics Department
Faculty of Science
Cairo University
Giza, Egypt

G. H. Ramzy
Physics Department
Faculty of Science
Cairo University
Giza, Egypt

Abstract: Single walled carbon nanotubes (SWCNTs) were synthesized using alcohol catalyst chemical vapor deposition ACCVD method using ethanol and were characterized with TEM. The prepared SWCNTs were incorporated with different concentrations in Poly(vinyl chloride) with different concentrations. The effect of both SWCNTs concentrations and temperature on creep and creep recovery of PVC were studied. Burger's model was applied to the region of creep and material parameters like instantaneous elastic modulus, Voigt elastic modulus and viscosity, Newtonian viscosity and linear thermal expansion coefficient were calculated at different concentrations of SWCNTs and different temperatures. These parameters were found to have a maximum at 1 wt % of SWCNTs and also found to decrease with increasing temperature. The recovery relaxation time was calculated and the activation energy of chains upon heating was calculated and samples containing 5 wt% of SWCNTs was found to have a maximum of 0.36 eV.

Keywords: PVC, Carbon Nanotubes, Creep, Creep recovery

1. INTRODUCTION

Viscoelastic properties of materials are traditionally measured by uniaxial tests [1]. Creep, stress relaxation and dynamic loading tests are the commonly used techniques to measure the time-dependent analogs to elastic constants. The uniaxial creep test consists of measuring the time-dependent stretch resulting from the application of a steady axial load, and can be directly related to the viscoelastic properties. Viscoelasticity is an important characteristic of polymers. The long-term behavior of polymers is essential to estimate their life-time under load. Although creep in an anisotropic, multi-phase system, like composites, is very complex, the analysis of creep properties is important for the use of composites in long-term applications. This may be more significant in reinforced polymer nano-composites than in classic materials reinforced by glass or basalt fiber. Polymer nano-composites have some advantages in addition to the good mechanical properties: easy and fully recyclability and low density [2 –7]. Relatively poor creep resistance of thermoplastic polymers is unfavorable to their application as structural materials. Creep deformation of polymers is easy to exceed the structural limitation, and fracture of ten occurs under long-term loading. To overcome the disadvantage, works were done started their attempts at the incorporation of nano - fillers. Rigid nan fillers used to improve mechanical performance of thermoplastic polymers have received considerable attentions in recent years [8–12].Strength, stiffness and toughness of nanocomposites can be simultaneously enhanced by improving dispersion of nanoparticles in polymer matrix as well as interfacial interaction between nanoparticles and matrix [13 –15]. Previous works [16 –18] showed that the glass transition temperature of polymers was increased by the incorporation of nanoparticles owing to a good bonding at the interface that restricts motion of the polymer chains. All of the above manifests that with the aid of inorganic nano fillers, performance of thermoplastics is becoming more attractive.

The one-dimensional structure of carbon nanotubes (CNTs), their low density, their high aspect ratio, and extraordinary mechanical properties make them particularly attractive as reinforcements in composite materials. By now, hundreds of publications have reported certain aspects of the mechanical enhancement of different polymer systems by CNTs [19 – 23]. The interest in the creation of nanocomposites based on the PVC matrix may be explained by an essential role played by this polymer. Poly (vinyl chloride) presents today an object of a manifold of applications, where its considerable environmental and chemical resistance, as well excellent mechanical properties may be cited. Therefore, the physical modification of the properties of this polymer, and specially the improvement of mechanical properties, was the based idea of this work.

In the present work the effect of both single walled carbon nanotubes content and temperature on creep and creep recovery behavior will be investigated. In this respect Burger's model will be used to study the viscoelastic creep behavior and material parameters like elastic moduli, coefficients of viscosity and relaxation times, linear thermal expansion coefficient will be deduced at different SWCNTs contents. Creep recovery behavior will be also investigated and both recovery relaxation time and activation energy will be calculated.

Experimental

2.1 Materials and Preparation

2.1.a Polymer

A commercial grade of Polyvinyl chloride (PVC) was supplied from Sabic Company, Saudi Arabia. It was in the powder form (powder fraction of 90–120 μm, average size of 100 μm, density ρ_p = 1.37 g/cm^3) was used as a polymeric matrix for preparation of composites.

2.1.b Preparation of SWCNTs

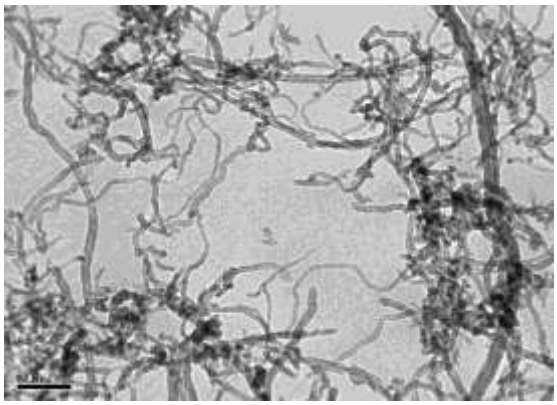

Fig. (1) Morphology of prepared CNT's as observed by TEM.

SWCNTs were grown via the alcohol catalytic chemical vapor deposition (ACCVD) technique using a 50 cm long ceramic tube furnace with diameter of 12 cm. Cobalt acetate supported catalyst was first prepared as follows. A metal acetate solution was prepared by dissolving cobalt acetate $(CH_3COOH)_2Co\text{-}4H_2O$ (99.999 %, Sigma-Aldrich) into ethanol (typically 42mg of cobalt acetate in 10 ml of ethanol) so that the concentration of each metallic species was 0.01 wt % with stirring for 10 min followed by sonication for 2 h at room temperature. For a substrate, we employed n-type Si wafer with (100) surface polished at one surface (University Wafers, USA) and a thickness of 0.5 mm. The substrate was cut into a strip of about 7×20 mm^2. The substrate was cleaned by consecutive acetone and methanol sonication for 5 min, washed with DI water and blown with dry nitrogen. The substrate piece was then submerged vertically into the prepared metallic acetate solution for 5 min. This piece was then drawn up from the solution at a constant speed of 4 cm/min. The surface of the substrate was rapidly dried at several millimeters above the liquid contact level as soon as it was removed from the solution. Right after this process, the piece was placed in a furnace and maintained at 400 ^oC for 5 min [24].

For the growth of SWCNTs, Cobalt acetate supported catalyst was placed into alumina combustion boat; whereas a 10^o inclined graphite stage was used to support the substrates and the group was then placed at the center of the tube furnace. The tube was evacuated to 150 mTorr, and samples were heated to the desired reaction temperature under 250 sccm of flowing argon. Once the growth temperature was reached (depending on the growth temperature), samples were held at that temperature for 5 min. The argon was then shut off and the tube was evacuated before the introduction of alcohol vapor. The alcohol vapor (ethanol) was then transferred into the tube furnace to achieve a pressure of 5–10 Torr. The alcohol flow rate in the growth chamber was controlled by controlling the alcohol bath temperature. After growth, the alcohol vapor was evacuated, argon was introduced again and the reaction tube was cooled to room temperature. SWCNTs growth time was kept constant at 50min unless otherwise stated [25].

Nanotubes grown in powder form were sonicated in methanol and placed onto holey/lacey carbon coated copper grids for TEM (Model 1011 JEM at 100 KV KSU, Saudi Arabia) observations to confirm both their existence and morphology and shown in Figure 1.

2.1.c Preparation of the Polymer composite

PVC was dissolved in tetrahydrofuran (THF) by slowly mixing for24 hr. SWCNTs was added to the PVC solution to get composites from SWCNTs/PVC with different weight percent (Typically, 0, 0.25, 0.35, 0.5, 0.88, 1, 1.5, 2, 2.5 and 5 wt %). The solution will be prepared in a dark laboratory bottle, by slowly mixing during 24 h at an ambient temperature. The composites of PVC with SWCNTs with different concentrations were prepared in the form of thin sheets cast from PVC solution in THF. Parts of the composites solution were spin coated on Si substrates for AFM imaging. The aim of a multi-step procedure used to prepare the PVC loaded SWCNTs nano composites was done to achieve the distribution of the carbon nanotubes in nano composites as homogeneous as possible. In the first step the SWCNTs was dispersed in the PVC solution using a combined procedure; quick mixing and ultrasonication at room temperature during 5 min., alternatively three times every procedure. The second step was the preparation of thin films with thickness of 0.1 mm cast from the nanocomposite solution in THF on a glass surface with controlled horizontal position.

.

2.2 Creep tests

The creep and creep recovery tests were carried out using TA instruments DMAQ800 machine (USA), using the tension film clamping arrangement. Specimens in the form of sheets with dimensions 9 mm length, 4 mm width and 0.1 mm thick were used. Temperature was automatically controlled and samples were left isothermally for 5 min. at 25, 30, 35, 40 or 45 ^oC before testing. The sensitivity in temperature during testing was in the range ± 0.2 ^oC. A stress of 20 MPa was suddenly applied after a constant temperature was established. The strain produced in the specimen was recorded with time for 15 min. After that, stress was removed suddenly and the recovery strain was also collected with time for 20 min.

3. Results

Among physical models for creep [26-28], the strain response $\varepsilon(t)$ of a polymer to the applied stress σ can be represented by three parts: (1) elastic or instantaneous deformation, (2) visco-elastic deformation and (3) viscous deformation. These can be represented schematically as in figure (2) and mathematically by:

$$\varepsilon(t) = \varepsilon_{elastic}(t) + \varepsilon_{visco-elastic}(t) + \varepsilon_{creep}(t) \quad (1)$$

Or

$$\varepsilon(t) = \frac{\sigma}{E_1} + \frac{\sigma}{E_2}\left[1 - \exp\left(-t\frac{E_2}{\eta_2}\right)\right] + \frac{\sigma}{\eta_1}t \quad (2)$$

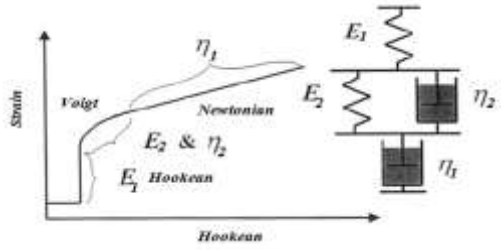

Fig (2) Quantitative Analysis of the creep curve.

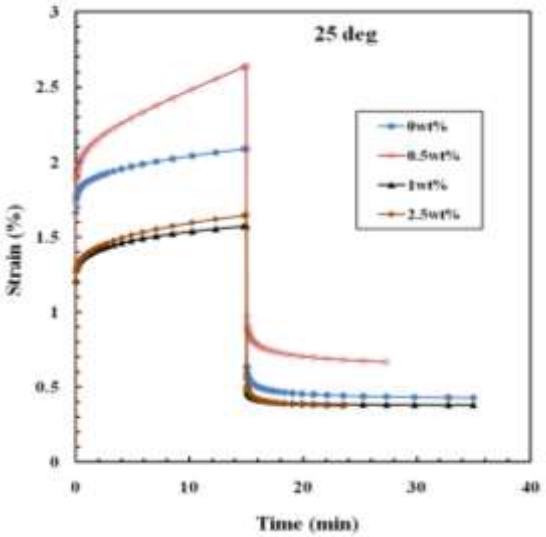

Fig. (3) Creep curves for MWCNT's loaded samples at 25 C.

where ε (*t*) is the creep strain, σ is the applied stress, *t* is time, E_1 and E_2 are the elastic moduli of the Maxwell and the Voigt springs, and η_1 and η_2 are viscosities of the Newtonian and the Voigt dashpots.

In equation (2), the first term is the instantaneous creep strain, which can result from changes in bond lengths and angles, for instance. The second term is the early stage creep strain and is due to mechanisms such as molecular chain relaxations and extensions. The last term is the long-term creep strain and is due to viscous slippage of molecular chains, for instance.

Since polymers are viscoelastic materials that have combined mechanical properties of elastic solids and viscous fluids, they respond to an external force in a manner intermediate between the behavior of an elastic solid and a viscous fluid [29,30]. Burger's model provides a mechanism to gain insight into this behavior. The DMA creep-recovery curve for PVC loaded with different concentrations of SWCNTs resembles the response predicted by Burger's model, suggesting that the macroscopic viscoelasticity of the polymer may be understood in terms of this model. The large time-independent, virtually instantaneous strain upon the impulsive increase of the stress indicates elastomeric behavior with a weak Hookean constant.

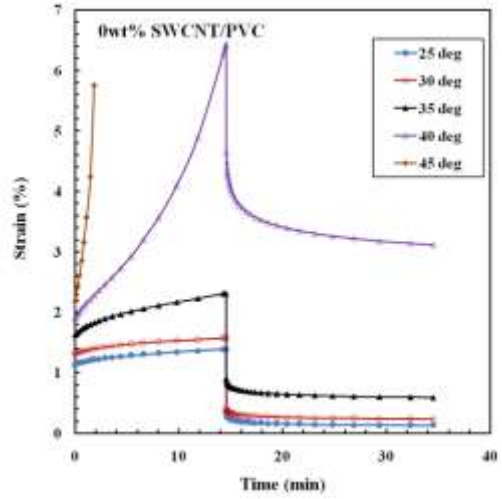

Fig. (4) Creep curves for unloaded samples at different temperatures.

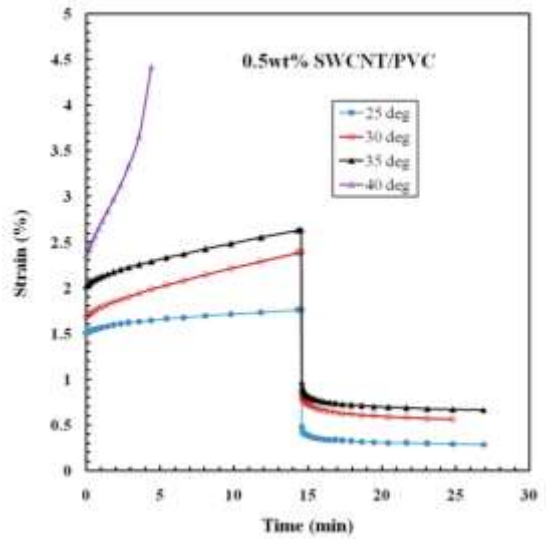

Fig. (5) Creep curves for samples loaded with 0.5 wt% SWCNT's at different temperatures.

The weaker the Hookean constant, the larger the initial fast displacement. After the weak Hookean spring reaches its maximum displacement, the polymer slowly shifts through the curvature of the Voigt region to the Newtonian region.

The creep response is time-dependent and indicates the yielding of the polymer to the stress by reorganization of its internal microscopic structure. The creep rate of SWCNT/PVC is indicative of the stability of its elastomer structure. When, after 15 min of constant stress, the stress is suddenly reduced back to 0.05 N, the polymer is able to recover from almost half of its maximum elongation. This is consistent with moderate elastomeric stability.

Figure (3) shows the creep and creep recovery for all studied samples at a temperature of 25 ^{o}C and applied stress of 20 MPa. Sample loaded with 1wt% of SWCNTs possesses minimum instantaneous strain and steady strain rate. Creep and creep recovery experiments at temperatures 25, 30, 35, 40 and 45 ^{o}C for PVC samples loaded with 0, 0.5, 1.0, 2.5 and 5.0 wt% of SWCNTs under constant stress of 20 MPa are shown in Figures (3 – 7) respectively.

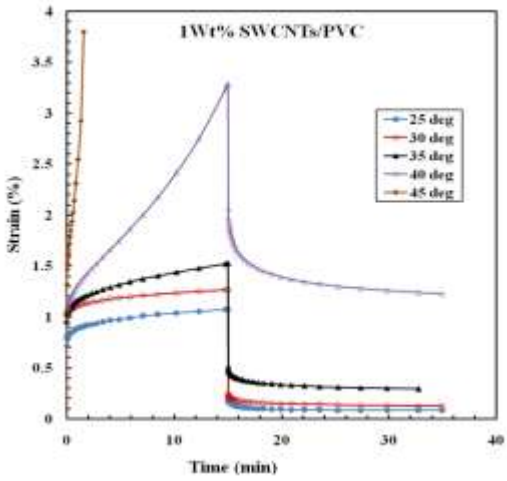

Fig. (6) Creep curves for samples loaded with 1 wt% SWCNT's at different temperatures.

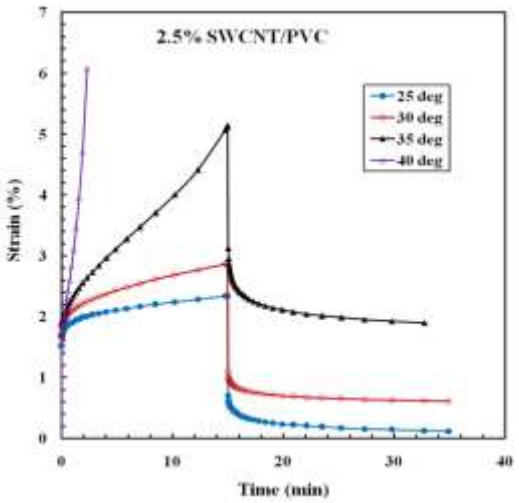

Fig. (7) Creep curves for samples loaded with 2.5 wt% SWCNT's at different temperatures.

3.1 Instantaneous deformation

The instantaneous strain as the stress was applied is found to increase linearly with temperature, as shown in Figure (8), according to the equation

$$\varepsilon_o = \varepsilon_o^{/} + \alpha T \qquad (3)$$

where $\varepsilon_o^{/}$ is a constant indicating the strain at zero Kelvin and α is the slope of the lines. From the definition of the strain ($= \Delta L / L_o$), the constant α may indicates the coefficient of linear expansion, under a constant tensile stress of 20 MPa, of the studied composites and its values are listed in table (1). The values of α, in general, decrease with increasing the weight content of SWCNTs as a result of originally high values of α of PVC over SWCNTs.

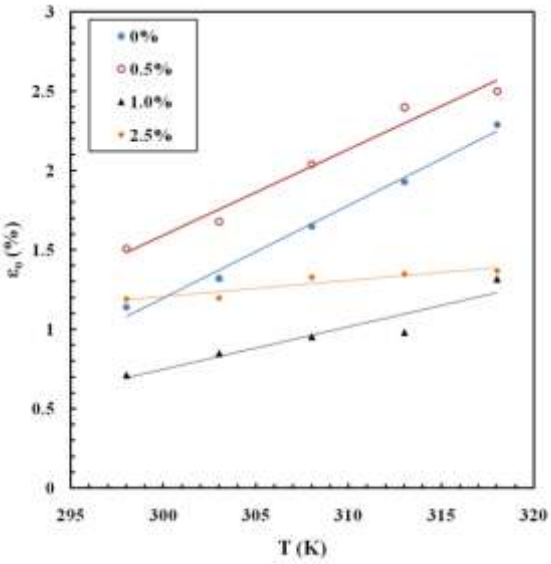

Fig. (8) The instantaneous strain versus temperature for MWCNT's loaded samples

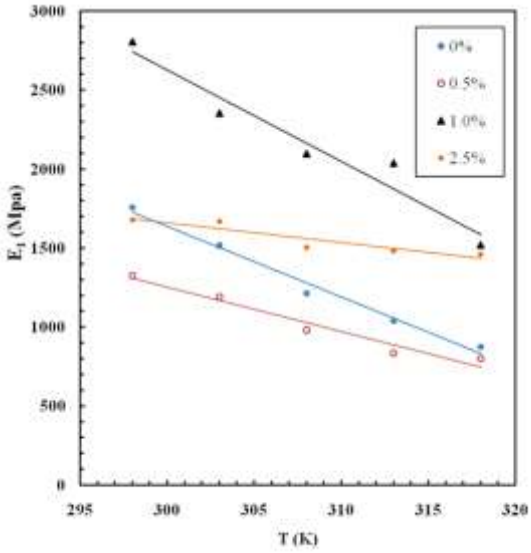

Fig. (9) The tensile elastic modulus E_1 versus temperature for all composites

The tensile elastic modulus E_1 of Maxwell springs and its dependence on temperature for all the studied composites is calculated using the first term in equation (2). The calculated data are illustrated in figure (9) and found to obey a straight line equation of the form

$$E_1 = E_{1o} - AT \qquad (4)$$

where E_{1o} is elastic modulus of Maxwell springs at zero Kelvin. The constant A represents the slopes of the lines with values listed in table (1). This constant may represent the energy density acquired by the material when the temperature increased by one degree. Samples containing 1 wt% of SWCNTs have maximum values of A which agree very well with the values of Young's modulus achieved in a previous work for these composites [29].

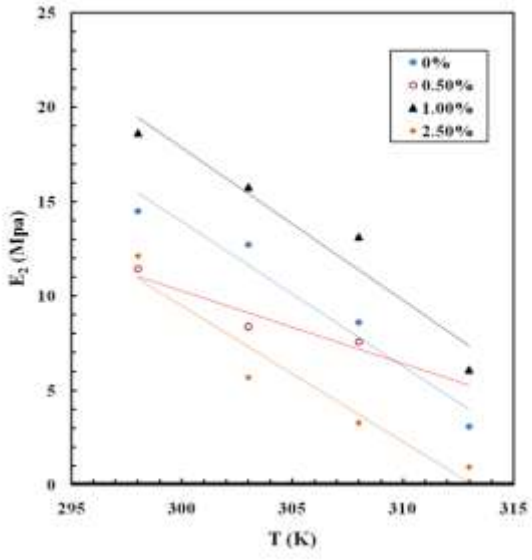

Fig. (10) The tensile elastic modulus E_2 versus temperature for all composites

Table (1)

Wt % of SWCNTs	$\alpha \times 10^{-4}$ (deg^{-1})	A $\times 10^6$ J/m^3.deg	A$'$ for E_2 J/m^3.deg	A$'$ for η_2 Pa.s/deg	E_r (eV)
0	5.80 - 59.1	44.8	0.77	0.3	0.054941
0.5	5.40 -70	28.1	0.39	1.1	0.185006
1.0	2.60 - 60	57.8	0.81	4.32	0.231495
2.5	0.90 - 50	6.74	0.46	1.06	0.50922
5	1.00 - 46	12.5	0.72	0.82	0.435218

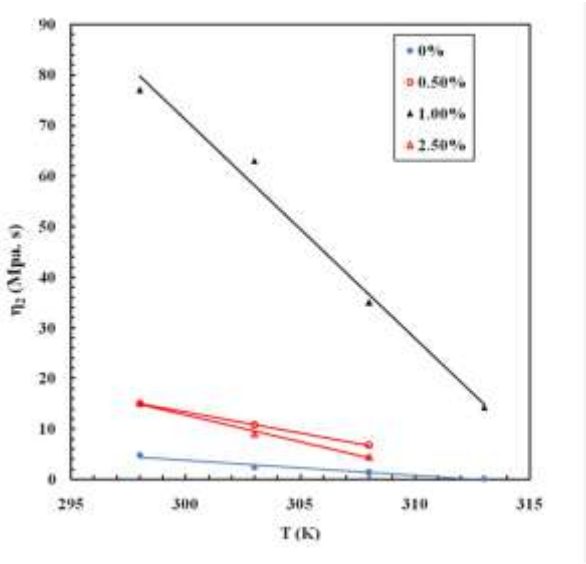

Fig. (11) The viscosity coefficient η_2 versus temperature for all composites

3.2 Visco-elastic deformation

As the stress is suddenly applied to the material, all the deformations take place instantaneously in the Hookean spring. As time goes, these deformations transfer gradually to the Voigt and dashpot describing Newtonian deformation. Both the elastic modulus E_2 and the coefficient of viscosity η_2 of the spring and dashpot of Voigt unit are calculated according to equation (2) at different concentrations of SWCNTs as well as temperature. These results are shown in Figures 10 and 11.Both E_2 and η_2 decrease linearly with increasing temperature and each of them obeys a linear function of the form:

$$\Psi_2(T) = \Psi_{o2} - A'T \tag{5}$$

where $\Psi_2(T)$ represents either E_2 or η_2 at temperature T, Ψ_{o2} is the value of either E_2 or η_2 at zero Kelvin. When $\Psi_2(T)$ describes E_2 the constant A' has the same meaning as described in equation (4) and their values are shown in table (1). As described in section 3.1, E_2 has maximum value at 1 wt% loading of SWCNTs. In the case of either A or A' when dealing with Hookean or Voigt springs, the reason behind their maxima at 1 wt% of SWCNTs may be due to the folding of Polymer chains around the length of the CNTs making additional entanglements which results in strengthen the composite. Besides, this may be due to direct bonding between chain ends and CNTs [30]. Concentrations of SWCNTs more or less than 1 wt%, may produce agglomerations which results in a less folding of polymer chains as well as less bonding between chain endings and SWCNTs. On the other hand, when $\Psi_2(T)$ describes E_2 the slope A' represents the change in viscosity of the Voigt dashpot at different concentrations of SWCNTs and its values are presented in table 1. The change in viscosity of the dashpot 2 has a maximum at 1 wt% of SWCNTs loading.

3.3 Viscous deformation

The last deformation in the creep experiments is the Newtonian viscous flow which represented by a dashpot 1. The viscosity of this dashpot is changed with temperature as well as the concentration of SWCNTs as shown in Figure 12. Maximum coefficient of viscosity is found for 1 wt% of SWCNTs and low temperature of 25 °C. Heating the material produces energy gained by polymer chains which can reorient themselves easily and this result as a decrease in the coefficients of viscosity of both dashpots. Thus we can say that both dashpots relax to their new positions under an external stress faster at higher temperatures. These relaxations are associated with characteristic times called relaxation times which related to the coefficients of viscosity according to:

$$\tau_1 = \frac{\eta_1}{\sigma}, \quad \tau_2 = \frac{\eta_2}{E_2} \tag{6}$$

Both relaxation times are calculated for all studied composites at different temperatures and shown in figures 13 and 14 and it was noted a decrease in both with temperature but with higher values of τ_1 over τ_2 at same temperature and SWCNTs loading.

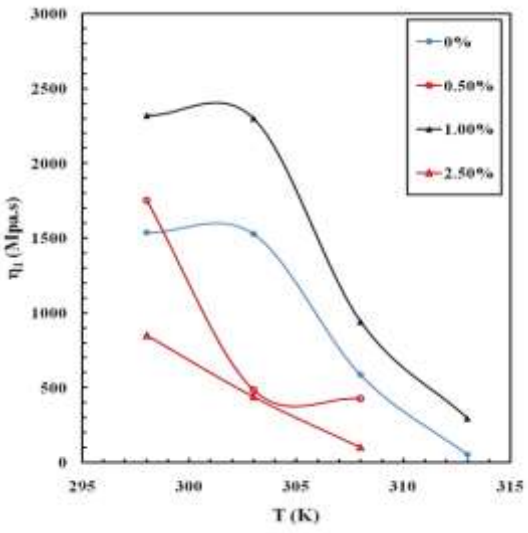

Fig. (12) The viscosity coefficient η_1 versus temperature for all composites

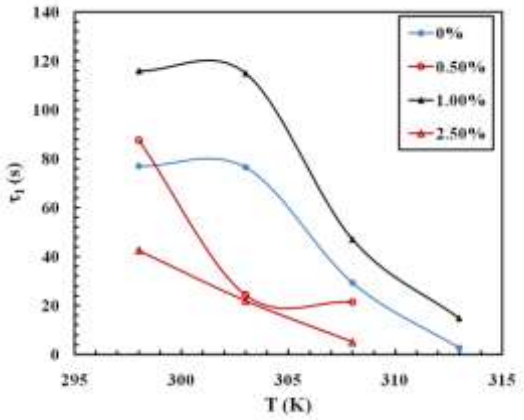

Fig. (13) The relaxation time τ_1 versus temperature for MWCNT's loaded sample

3.4 Creep recovery

In order to study the creep recovery of a test sample, after the steady creep rate was attained, the stress was suddenly removed from and the strain was continuously recorded versus time, an instantaneous strain recovery took place followed by a gradual decrease in the sample's strain which finally reached an asymptotic value. Figures (3 – 7) represent sets of tensile creep and creep recovery curves under different conditions of SWCNTs loading and temperature. In the following analysis the term tensile creep recovery, ε_r will be assigned to the recoverable strain after time t from removal of stress. It is calculated by the difference between the observed strain at time t after unloading and the asymptotic strain attained after infinite time. The recoverable strain is here assumed to decrease with time according to an exponential decay function of the type

$$\varepsilon_r = \varepsilon_{ro} \exp\left(-\frac{t}{\tau_r}\right) \tag{7}$$

where ε_{ro} and τ_r are constants. This assumption proved to be valid for the initial parts of the recovery curves on account of the straight line relations between $\log\varepsilon_r$ versus t, shown in figures 15 and 16 for samples containing 0 and 1 wt% of SWCNTs. The rest of figures describing other composites are not mentioned to avoid repetition. The constant τ_r in equation (7), which is the reciprocal of the slopes of the lines in figures 15 and 16, might be given its usual physical meaning of recovery relaxation time characterizing creep recovery. It was

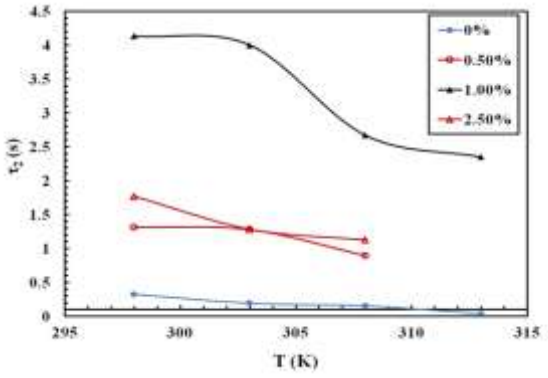

Fig. (14) Fig. (13) The relaxation time τ_2 versus temperature for MWCNT's loaded sample

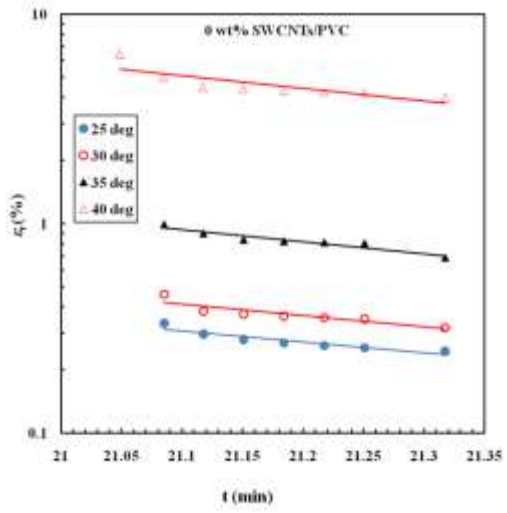

Fig. (15) The recoverable strain as a function of time at different temperatures for 0 wt% MWCNT's loaded samples.

presently calculated in every case tested and the values obtained are given in the figure 17.

The energy of creep recovery of the samples could be determined from the observed temperature dependence of the recovery relaxation time τ_r which time might be written in the form

$$\tau_r = \tau_{ro} \exp\left(\frac{E_r}{k\,T}\right) \tag{8}$$

where T is the absolute temperature, k is the Boltzmann constant and E_r is the activation energy of the relaxation process characterizing creep recovery.

A plot of the logarithm of the relaxation time τ_r versus $1/T$ yielded straight lines for all studied composites as shown in figure 17. The activation energy characterizing the relaxation process responsible for creep recovery is presented in table (1). The activation energy is increased from 0.071 to 0.37 when the weight percentage of SWCNTs increased from 0 to 5 wt%, respectively.

4. Discussion of the results

The values of E_1 and E_2 correspond to the modulus in the Hookean and Voigt regions of the creep response, respectively. The general magnitude of these parameters is an indicator of strength, with larger values corresponding to smaller strain orientations reached for a given amount of stress. In Figure 9 the Hookean E_1 values differentiate the bands from the hard and soft segments, with the hard segments generally possessing higher modulus values. This observation indicates that, during the initial stage of the impulse time-independent elastic deformation, the soft domains orient more, contributing more to the macroscopic deformation, while the hard domains orient less, contributing more to the elasticity or Young's modulus (initial strength). The trend observed for E_2 (Voigt region) is similar to that observed for E_1.

The analysis of the parameter η_1 provides insights into the slow structural rearrangement of the polymer morphology after it is already stressed and deformed. The polymer then has mobility to deform, and even after it has been strained several times its original length, the network structure is not

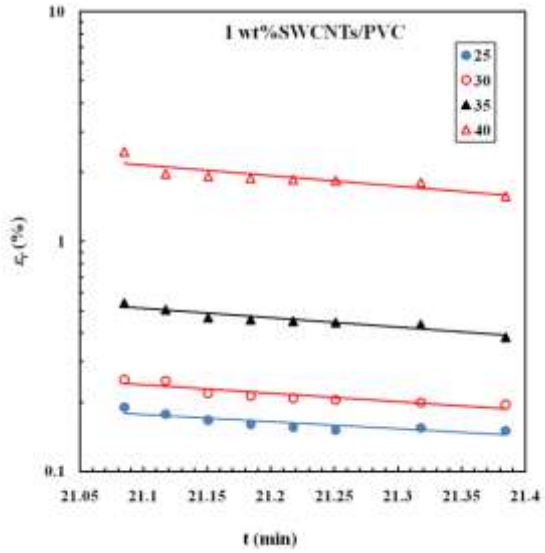

Fig. (16) The recoverable strain as a function of time at different temperatures for 1 wt% MWCNT's loaded samples.

significantly changed. As a result, upon the release of the stress, the polymer is able to recover to nearly its original length. While the Hookean (initial) region provides insights into the mobility of the morphological structure, the Newtonian region provides insights into the stability of the network structure. The slow change in this region is characteristic of the motion of a highly viscous material that undergoes slow but steady irreversible changes.

The decrease in E_1 and E_2 resulted from the increases in the instantaneous and the viscoelastic deformations as temperature increased. The decreases in η_1 and η_2 suggest an improvement in the mobility of molecular chains at higher temperature. The parameters for SWCNTs/PVC experienced the largest decreasing change, especially those containing 1 wt%. Also, η_1, which is related to the long-term creep rate, has more decreasing change over η_2 and demonstrates the large temperature-dependence of this composite. The observed creep relaxation in SWCNTs/PVC is thought to have its origin at the restoration motion of molecular segments after the removal of stress.

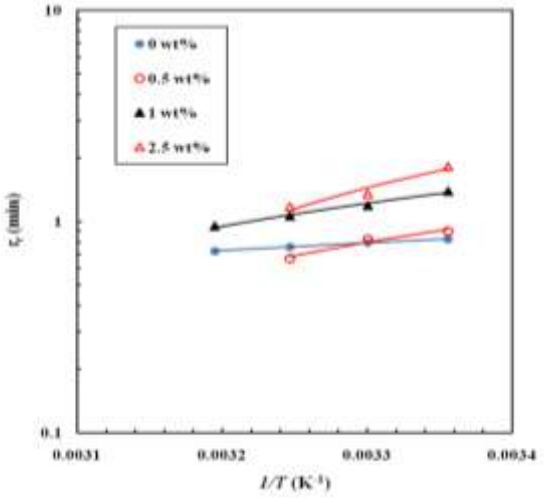

Fig. (17) The recovery relaxation time versus the reciprocal of temperature for MWCNT's loaded samples

Translational or rotational motion of macromolecular segments in a polymer is usually enhanced by thermal energy or by the action of an externally applied field of force. However, this motion is usually opposed by intermolecular forces responsible for the cohesion of the molecular aggregates. The flexibility of the molecular chain under the action of an externally applied stress depends on the ease with which the different structural elements along the chain can displace or rotate to contribute to the elastic strain. The observed energy of activating of the present relaxation mechanism is thought to describe the average height of the potential barrier created by the cohesive forces between the structural segments along and between the neighboring chains. The addition of SWCNTs increases these cohesive forces and thus increases the average height of potential barriers resulting as increase in the activation energy.

5. Conclusions

This work reports a discrete temperature-dependent creep and creep recovery spectra at different concentrations of SWCNTs, which may be used to describe the mechanical response of nonlinear viscoelastic polymers. This work supports the following specific conclusions.

1. Study of the mechanical properties of the PVC/CNTs and PVC/CNP composites depending on the content of nanofillers demonstrate an increase in Young's modulus by 3 times at concentration of 1 wt% of CNTs and 1.4 times at 2 wt% of CNP. The change in micro-hardness degree is also increased by 3.5 and 2.5 times at same concentrations. The tensile strength, strain at break decrease with increasing either nanofiller.

2. The presence of nanofillers reduces the percolation threshold from 1wt% CNP to 0.5 wt% CNTs. It is caused by high anisotropy of the CNTs and CNP and the presence of a segregated structure of them within the polymer matrix with distribution of nanofillers on the boundaries between the polymer grains.

3. Composites containing CNTs can be better employed for electronic and microwave devices working at different temperatures since their electrical conductivity is independent from temperature in the studied range.

4. Concentrations of either nanofiller in the percolation region produce a jump region in the I-V curve. The conduction mechanism is Ohmic for other composites.

6. References

[1] Mohan R, Adams D F, Nonlinear creep-recovery response of a polymer matrix and its composites, *Exp Mech*, Sept, 1985, 262.

[2] Giles JM, Black AE, Bischoff JE. Anomalous rate dependence of the preconditioned response of soft tissue during load controlled deformation. *J Biomech* 2007; 40(4):777–785.

[3] Haj-Ali RM, Muliana AH. Numerical finite element formulation of the Schapery's nonlinear viscoelastic material model. *Int J Numer Methods Eng* 2004; 59: 25–45.

[4] Zaoutsosa SP, Papanicolaou GC, On the influence of preloading in the nonlinear viscoelastic–viscoplastic response of carbon–epoxy composites Comp Sci and Tech, 70, 2010, 922-929.

[5] Varela-Rizo H, Weisenberger M, Bortz, DR, Martin-Gullon I, Fracture toughness and creep performance of PMMA composites containing micro and nanosized carbon filaments , *Compos Sci. and Tech*. Article in Press.

[6] Li, J., Ngan, A.H.W, Nanoscale fast relaxation events in polyethylene , *Scripta Materialia* 62 , 2010, (7), pp. 488-491

[7] Jia M, Xue P, Zhao Y, Wang K, Creep behavior of wood flour/poly(vinyl chloride) composites, Journal Wuhan University of Technology, Materials Science Edition 24, 2009, (3), pp. 440-447

[8] Amy, Y.-H.L., Jörg R, Physical aging and structural relaxation in polymer nanocomposites , *Journal of Polymer Science, Part B: Polymer Physics* 47,2009, (18), pp. 1789-1798

[9] Zhou, TH, Ruan WH, Yang, JL, Rong MZ, Zhang MQ, Zhang Z, A novel route for improving creep resistance of polymers using nanoparticles , *Comp Sci Tech* 67, 2007, (11-12), pp. 2297-2302

[10] Xia H, Song M, Zhang Z, Richardson M, Microphase separation, stress relaxation, and creep behavior of polyurethane nanocomposites, *J of Appl Polym Sci* 103, 2007, (5), pp. 2992-3002

[11] Devasenapathi V, Monish P, BalasivanandhaPrabu S, Experimental investigation of tensile creep behavior of polymer nanocomposites , International Journal of *Adv Man Tech* 44, 2009 (3-4), pp. 412-418

[12] Muenstedt H, Katsikis N, Kaschta J, Rheological properties of poly(methyl methacrylate)/nanoclay composites as investigated by creep recovery in shear , *Macromol 4*1, 2008, (24), pp. 9777-9783

[13] Rong MZ, Zhang MQ, Zheng YX, Zeng HM, Walter R, Friedrich K. Structure–property relationships of irradiation grafted nano-inorganic particle-filled polypropylene composites. *Polym* 2001; 42:167–83.

[14] Zhang MQ, Rong MZ, Zeng HM, Schmitt S, Wetzel B, Friedrich K. Atomic force microscopy study on structure and properties of irradiation grafted silica particles in polypropylene-based nanocomposites. *J Appl Polym Sci* 2001; 80: 2218–2227.

[15] Ruan WH, Zhang MQ, Rong MZ, Friedrich K. Polypropylene composites filled with in situ grafting polymerization modified nanosilica particles. *J Mater Sci* 2004; 39:3475–8.

[16] Ruan WH, Zhang MQ, Rong MZ, Friedrich K. Polypropylene composites filled with in situ grafting polymerization modified nanosilica particles. *J Mater Sci* 2004; 39: 3475–8.

[17] Zhang YQ, Lee JH, Rhee JM, Rhee KY. Polypropylene-clay nanocomposites prepared by in situ grafting-intercalating in melt. *Compos Sci Technol* 2004; 64:1383–9.

[18] Abu-Abdeen M. Investigation of the rheological, dynamic mechanical, and tensile properties of single-walled carbon nanotubes reinforced poly (vinyl chloride). *J Appl Polym Sci* 2012;124: 3192-9.

[19] Coleman JN, Khan U, Blau WJ, Gun'ko YK. A reviewof the mechanical properties of carbon nanotube polymer composites. *Carbon* 2006; 44:1624–52.

[20] Moniruzzaman M, Winey KI. Polymer nanocomposites containing carbon nanotubes. *Macromolecules* 2006; 39:5194–205.

[21] Miyagawa H, Misra M, Mohanty AK. Mechanical properties of carbon nanotubes and their polymer nanocomposites. *J Nanosci Nano technol* 2005; 5:1593–615.

[22] Salvetat JP, Bhattacharyya S, Byron Pipes R. Progress on mechanics of carbon nanotubes and derived materials. *J Nanosci Nano technol* 2006; 6: 1857–82.

[23] Tjong SC. Structural and mechanical properties of polymer nanocomposites. *Mater Sci Eng R* 2006;53:73–197.

[24] Murakami Y, Miyauchi Y, Chiashi S, Maruyama S, Direct synthesis of high-quality single-walled carbon nanotubes on silicon and quartz substrates, *Chem Phys Lett*, 2003, 377,49-54.

[25] Unalan HE, Chhowalla M, Investigation of single-walled carbon nanotube growth parameters using alcohol catalytic chemical vapor deposition, *Nanotech*, 2005, 16, 2153-2163.

[26] Acha BA, Reboredo MM, Marcovich NE, Creep and dynamic mechanical behavior of PP–jute composites: effect of the interfacial adhesion. *Composites, Part a – Appl Sci Man* 2007, 38, 1507–1516.

[27] Nunez AJ, Marcovich NE, Aranguren MI, 2004. Analysis of the creep behavior of polypropylene–wood flour composites. *Polym Eng Sci*, 2004, 44, 1594–1603.

[28] Marcovich NE, Villar MA, 2003. Thermal and mechanical characterization of linear low density polyethylene/wood flour composites. *J Appl Polym Sci*, 2003, 90, 2775–2784.

[29] Elias, H. Macromolecules, 2nd ed.; Plenum Press: New York,1984.

[30] Aklonis, J. J.; MacKnight, W. J. Introduction to Polymer Viscoelasticity; John Wiley & Sons: New York, 1983.

[31] Coleman J N, Khan U, Gun'ko Y K, Mechanical reinforcement of polymers using carbon nanotubes, *Adv Mater* 2006, 18, 689–706.

International Journal of Science and Engineering Applications
Volume 5 Issue 3, 2016, ISSN-2319-7560 (Online)

Empirical Study on Data Security Privacy: Data Partition for Centric Key Management Cloud

Deepika.P[1], B.V.N.Sai Kumar[1], K.Jhansi[1], K.Lavanya[1], A.V.S.Sudhakar Rao[2]

[1]Department of computer science & engineering, St. Ann's college of Engineering & Technology, Chirala, Andhra Pradesh, India.

[2]Department of Computer Science & Engineering, St.Ann's college of Engineering & Technology, Chirala, Andhra Pradesh, India.

Abstract: The Cloud Computing is a next generation platform, which provides virtualization with resource pool.There are three types of cloud service models, Infrastructure as-a-Service (IaaS), Platform-as-a-Service (PaaS) and Software-as-a-Service (SaaS).Most of the scientific research focus on IaaS model, which manage virtualization and storage. IaaS allows customer to scale based on user demand and user only pays for the resource usage. Data security plays a crucial role in cloud environment and user trust is most challenging problem of cloud services. This project proposed new methodology that secures data and provide privacy to the customer in cloud. Our technique providing security by using data partition approach and that partitioned data will be proceed further parallel for encryption mechanism. Here privacy is given by centric key management scheme.

Keywords: ***Cloud Computing, Encryption, Key Management, Service Models, Algorithm.***

1. INTRODUCTION

Cloud computing is term that describes various type of computing concepts that uses a high number of computers connected via network such as the Internet. In general Cloud computing is a type of computing that depends on sharing computing resources rather than using local servers or personal devices to perform application.

Cloud viewed as the third party, on-demand, self-service that implemented on pay-per-use mechanism and it is scalable computing resources whose services offered by the Cloud paradigm promise to reduce capital as well as operational expenditures for hardware and software.

It classified based on Location of the cloud computing and Type of services offered [1].Based on Location its types are: public cloud,private cloud, hybrid cloud, community cloud. Based ontype of services it's categorized in Infrastructure as a service(IaaS) , Platform as a Service (PaaS) , Software as a service(SaaS). Public cloud is offered by third party service provider and it involves resources that are outside the user premises. Customer has no visibility and no control over the computing infrastructure where it is hosted and this infrastructure is shared between any organizations.

If computing infrastructure is dedicated to particular organization and not shared with other than this setup is private cloud. The hybrid cloud uses hybrid approach.The above classification is well accepted in the industry. David Linthicum [2] shows further classification on the basis of service provided. These are listed below: Storage-as-aservice, Database-as-a-service, Information-as-a-service, Process-as-a-service, Application-as-a-service, Platform-as-a-service, Integration-as-a-service, Security-as-a-service,Testing-as-a-service, Infrastructure-as-a-service.

2. PROPOSED WORK

In proposed security layer, cloud-client data is not just sent to cloud directly instead data processed intelligently and sent to cloud. This mechanism ensures client data security but to provide authentication, before data processed, secure connection between client and cloud is created logically. For providing privacy to client data, we introduce a new way that deal with encryption mechanism and provide privacy to client data. User data is processed in two different passes, in first pass user data is partitioned dynamically and then partitioned encrypted using parallelism.

The limitation of cloud computing are the security issues of cloud computing. It comes to know that there are no security standards available for secure cloud computing.Users has serious concerns about confidential of sensitive information. Privacy is not provided for critical data being processed in the public accessible cloud. The main security problems involve user data privacy, data security, protection, cloud computing administration and cloud computing platform stability. Customers should have the right of the supervision and have audit of cloud computing services for fully ensure the security of customer data.

The data must be protected from virus, worms and Trojan in cloud computing platform within the network of internal and external .We introduced a new security layer between user and cloud as combined three layer (PaaS,IaaS, SaaS) that provide mechanism which deal with user data security, privacy and authentication.

To solve the problem existing we need authentication at both the side. While data sends via internet, any encryption algorithm must secure it. To address authentication we are going to use public key cryptography. Public key cryptography is most common method for authenticating a sender and receiver.

Ravi Shankar Dhakar, Prashant Sharma and Amit Kumar Gupta [3] used the Public Key cryptography. In traditional cryptography, one secret key is used for encryption and decryption at both the side. So if secret or private key is discovered by some else than message can easily be decrypted. For this reason, public key cryptography is most suitable approach on the internet. This public key system is known as asymmetric cryptography.

3.SYSTEM IMPLEMENTATION

To solve this problem we need authentication at both the side. While data sends via internet, any encryption algorithm must secure it. To address authentication we are going to use public key cryptography. Public key cryptography is most common method for authenticating a sender and receiver. In traditional cryptography, one secret key is used for encryption and decryption at both the side. So if secret or private key is discovered by some else than message can easily be decrypted. For this reason, public key cryptography is most suitable approach on the internet.

A. Selby and C. Mitchell [4] have proposed two algorithms that are used to implement RSA. The first algorithm performs modular reduction and the other performs modular multiplication. But when the bit size is large, the computation takes a lot of time. This public key system is known as asymmetric cryptography. In public key cryptography, private and public keys are generated simultaneously using the same algorithm by trusted certificate authority. In this system, private key is given to the requesting person means here any customer in cloud. Every customer has a unique private key, which is confidential. Public key is available publicly to everyone. In cloud, whenever customer wants any type of service from service providers he will make a request.

In this request, customer's digital signature is encrypted by private key after that encrypted message again encrypt using receiver's public key. Here cloud service provider is receiver. After receiving this encrypted message first receiver will decrypt by own private key and then decrypt encrypted digital signature by public key of sender. Here customer is sender.Digital signature contains customer name, serial number, expiry date. After decrypting message, cloud service provider easily come to know about their customer. Using this mechanism, we can provide perfect authentication and privacy in cloud environment.

4.SYSTEM ARCHITECTURE

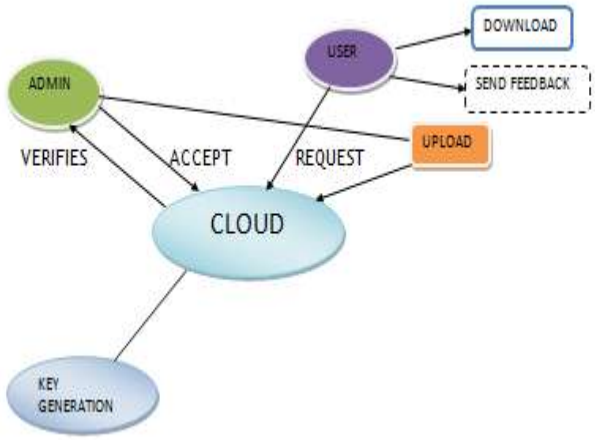

5.CODING

```
<?php
if(isset($_GET['filename']))
{
   $var_1 ="admin/upload/".$_GET['filename'];
$file = $var_1;
 session_start();
  include 'dbconn.php';
            $k1=$_POST['key'];
 echo "<br>";
            $id=$_GET['id'];


  $q=mysql_query("select `encryptfile` from `uploadfiles` where id='$id'")or die(mysql_error());


  $q1=mysql_num_rows($q);
```

```
 $a=mysql_fetch_array($q);
            $k=$a['0'];
 if($k1==$k)
 {
  $a=$_SESSION['user'];
$dt=date('d/m/y');
$q1=mysql_query("select * from download where user='$a' and date='$dt'");
$q=mysql_fetch_array($q1);
$z=$q[2];
if($z>=5)
{
echo "<script>alert('download limit exceed');window.location='downloadfiles.php';</script>";
exit;
}
if (file_exists($file)) {
   header('Content-Description: File Transfer');
   header('Content-Type: application/octet-stream');
   header('Content-Disposition: attachment; filename='.basename($file));
   header('Expires: 0');
   header('Cache-Control: must-revalidate');
   header('Pragma: public');
   header('Content-Length: ' . filesize($file));
   ob_clean();
   flush();
   readfile($file);
$z++;

mysql_query("update download set count='$z' where user='$a' and date='$dt'")or die(mysql_error());

   exit;
}
echo "<h1>Content error</h1><p>The file does not exist!</p>";
exit;
}

}
echo "<script>alert('ENTER CORRECT KEY');window.location='downloadfiles.php';</script>";
?>
```

6.RESULTS

Fig 1: Home page

Fig 2:Registrationpage

Fig 3:Login page

Fig 4:User Download File

Fig 5:Downloading Files

Fig 6:User Feedback

Fig 7:Admin Home Page

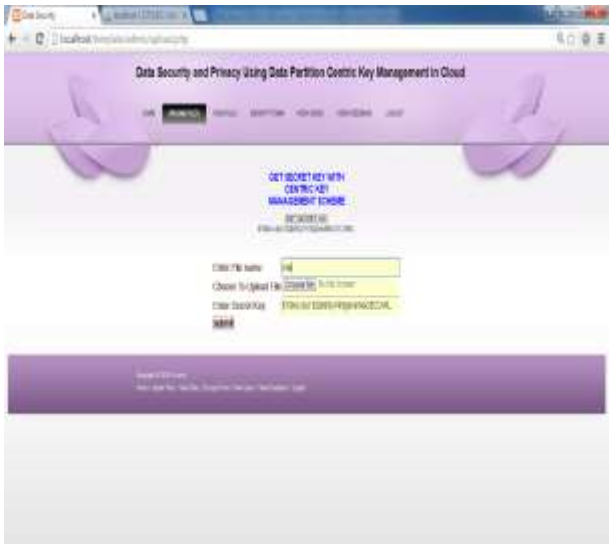

Fig 8:Upload Files

Fig 9:View Upload Files

Fig 10:Encrypt Form

Fig 11:View Users

Fig 12:View Feedback

7.CONCLUSION

This project suggests use of an "asymmetric public key cryptography" algorithm as part of the key management to ensure the authentication between client and service provider. After creating the logical authentic link between client and service provider, large client-data is partitioned and is encrypted in parallel. This project proposes a new way to provide data security, privacy & authentication on different cloud models. Especially in public-cloud model, by introducing a new layer in-between the client and the service provider (i.e. cloud) and also suggests use of an "asymmetric public key cryptography" algorithm as part of the key management to ensure the authentication between client and service provider.

8.FUTUIRE SCOPE

This mechanism provides security to client-data.The partition &encryption of user-data is done on the user side only. This approach raises the power & computational consumption at the user side which is of a great concern. In future the drawback of the project will be implemented as a advantage.

9.REFERENCES

[1]. P. Mell and T. Grance, "The NIST Definition of Cloud Computing Version 15," Nat'l Inst. of Standards and Technology, Information Technology Laboratory, vol. 53, p. 50,http://csrc.nist.gov/groups/SNS/cloud-computing/, 2010.

[2].Dripto Chatterjee, Joyshree Nath, Suvadeep Dasgupta and Asoke Nath. "A new Symmetric key Cryptography Algorithm using extended MSA method: DJSA symmetric key algorithm", 2011 IEEE.

[3] Ravi Shankar Dhakar, Prashant Sharma and Amit Kumar Gupta."Modified RSA Encryption Algorithm (MREA)", 2012 IEEE.

[4]. A. Selby and C. Mitchell. "Algorithms for software implementations of RSA", IEE PROCEEDINGS.

[5] R. Rivest, A. Shamir, and L. Adleman, A method for obtaining digital signatures and public-key cryptosystems , Commun. ACM, vol. 21, pp. 120-126, 1978.

[6] Symmetric key cryptography using random key generator, A. Nath, S. Ghosh, M.A. Mallik, Proceedings of International conference on SAM-2010 held at Las Vegas(USA) 12-15 July, 2010, Vol-2, P-239-244

[7] William Stallings, "Cryptography and Network Security", ISBN 81-7758-011-6, Pearson Education, Third Edition, pages 42-62,121-144,253-297.

[8] Atul Kahate, "Cryptography and Network Security", ISBN-10:0-07-064823-9, Tata McGraw-Hill Publishing Company Limited, India, Second Edition, pages 38-62,152-165,205-240.

[9] R. Curtmola, J. Garay, S. Kamara, and R. Ostrovsky, "Searchable Symmetric Encryption: Improved Definitions and Efficient Constructions," Proc. 13th ACM Conf. Computer and Comm. Security, pp. 79-88, 2006.

[10] M. Abdalla, M. Bellare, D. Catalano, E. Kiltz, T. Kohno, T. Lange,
J. Malone-Lee, G. Neven, P. Paillier, and H. Shi, "Searchable Encryption Revisited: Consistency Properties, Relation to Anonymous IBE, and Extensions," Proc. 25th Ann. Int'l Conf .Advances in Cryptology (CRYPTO '05), pp. 205-222, 2005.

[11] L. Wiese, "Horizontal Fragp098
7entation for Data Outsourcing with Formula-Based Confidentiality Constraints," Proc. Fifth Int'l Workshop Security (IWSEC '10), pp. 101-116, 2010.

International Journal of Science and Engineering Applications
Volume 5 Issue 3, 2016, ISSN-2319-7560 (Online)

Improving Security Levels In Automatic Teller Machines (ATM) Using Multifactor Authentication

Frimpong Twum
Department of Computer Science
Kwame Nkrumah University of Science and Technology, Kumasi, Ghana.

Kofi Nti
Department of Computer Science
Kwame Nkrumah University of Science and Technology, Kumasi, Ghana

Michael Asante
Department of Computer Science
Kwame Nkrumah University of Science and Technology, Kumasi, Ghana

Abstract: A wide variety of systems need reliable personal recognition system to either authorize or determine the identity of an individual demanding their services. The goal of such system is to warrant that the rendered services are accessed only by a genuine user and no one else. In the absence of robust personal recognition schemes, these systems are vulnerable to the deceits of an imposter. The ATM has suffered a lot over the years against PIN theft and other associated ATM frauds due to its traditional authentication mode (PIN). In this paper, we proposed a multifactor (PIN and Fingerprint) based authentication security arrangement to enhance the security and safety of the ATM and its users. The proposed system demonstrates a three tier design structure. The first tier is the verification module, which concentrates on the enrollment phase, enhancement phase, feature extraction and matching of the fingerprints. The second tier is the database end which acts as a storehouse for storing the fingerprints of all ATM users' preregistered as templates and PIN as text. The last tier presents a system platform to relate banking transactions such as balance inquiries, mini statements and withdrawal. Microsoft windows 8 was used as an operating system platform for the implementation phase, with C# programming language being the front-end development and SQL server 2010 as backend. The application evaluation was based on False Rejection Rate (FAR), False Acceptance Rate (FAR), Average Matching Time (AMT) and the Total Error Rate (TER) conducted, which show the security and reliability of the proposed system for ATM users authentication and verification.

Keywords: PIN and Fingerprint-Based; Authentication; Security; Verification; ATM; Verification; Multifactor

1. Introduction

The advancement of payment system in the modern world has gone passed cash to cheques, and then to payment cards such as credit cards and debit cards (Batiz-Lazo & Barrie, 2005) Automatic Teller Machine ATM is a terminal installed by banks or other financial institution that enables customers to perform service, like cash withdrawal or cash deposit, balance enquiry, request for bank statements, and money transfer from one account to the other. Some modern ATMs are equipped with mobile money transaction. ATMs are basically independent banking workstations which aims at providing a faster and expedient service to customers (Rasiah, 2010). Barclays bank introduced the first ever ATM in 1967, in its Hendson branch in London, which could dispense a fixed amount of cash when a user inserted a special coded card and since then, ATM has become smaller, faster and easier (Das & Jhunu, 2011). Among all departments in a financial institution, the ATM has been considered as one of the important components of electronic banking infrastructure.

The main benefit of the ATM is its ability to provide a 24hours service daily to customers and users, making the ATM an integral part of our everyday life. Nowadays, ATMs' are employed in various scenarios such as ticket vending machines, quick check-in kiosks and self-service gas stations (Luca, 2011).

ATMs are not only sited at banks, but also a lot of schools, businesses nowadays installed ATM on their premises for customer convenience and more revenue. A global ATM market forecast research lead by Retail Banking Research Limited (Mohammed, 2011) shows that there are 1.8 million ATMs deployed around the world and the figure was forecast to reach 2.5 million by 2013.

ATMs cards authentication methods have changed little since their introduction in the 1960's. The security limitations of ATM are mostly derived from the security pitfalls of the magnetic media. The data on the magnetic stripe are usually coded using two or three tracks, because, it is not difficult or expensive to have the equipment to encode magnetic stripes. The standard covering this area is International Organization for Standardization (ISO) 7811 and the technique for writing of the tracks is known as Friend-to-friend (F/2F). Thankfully, magnetic stripe feebleness has been partly addressed by the introduction of Europay, MasterCard and Visa (EMV) smartcards. Normally, the authentication design involves a trusted hardware device (ATM card or token). The Personal Identification Number (PIN) of the card holder's is usually the only means to attest the identity of the user; this approach is vulnerable to misplacement, unauthorized access, card swallowing, forgetfulness and others (Das & Jhunu, 2011), (Akinyemi, et al., 2010).

Despite the numerous cautions given to the card user, many people continue to choose easily guessed passwords and PINs such as phone numbers, birthdays and social security numbers. However, due to the limitations of this design, an intruder in possession of a user's card can discover the user's PIN with password prediction or guessing (brute force) attack. For instance, in a typical four digits PIN, one in every 10,000 users will have the same number. In spite of all security measures in place, cases of ATM crimes continue to occur globally. A current figure by European ATM Security Team (EAST) affirms that there is a rise in ATM fraud "trend", especially of skimming attacks. An upsurge of 24 % in

skimming attacks at European ATMs, matched to the first half of 2009, is reported for the first half of 2010 in the ATM Crime Report (Gunn, 2010).

In situations where a user has two or more ATM cards, all PINs needs to be memorized by the user. This can easily lead to the user initiating security problems (Adams & Sasse, 1999), thus a card holder or user may decide to write down the authentication token, or use the same authentication token (PIN) across different services or use authentication token (words) that can be found in dictionaries. A notable example of this was shown by Klein, who could crack 25% of 14,000 passwords using a dictionary attack with only 86,000 words (Jermyn, et al., 1999) and (Luca, 2011). This leads to the saying that the user is often referred to as the 'weakest link' in the security chain (Luca, 2011).

With the introduction of internet technology in recent years, the internet communication is exposed to unwanted people giving them access to pose different kinds of attacks on ATM System.

In 2013 Ghana Commercial Bank (GCB) confirms money theft from an ATM of about GH¢3 million (Obour, 2013)and a worldwide gang of criminals stole $45 million in a matter of hours by hacking their way into a database of prepaid debit cards and then draining cash machines around the globe (Modernghana, 2013). ATM's crime has become a nationwide epidemic which faces both customers and bank operators, as well (Das & Jhunu, 2011).

The security breaches in the ATM system have contributed to the less patronage and rejection of the ATM, by some customers of various banks (Ndife, et al., 2013).

The traditional (PIN) ATM cash withdrawal process flowchart is as shown in figure 1.

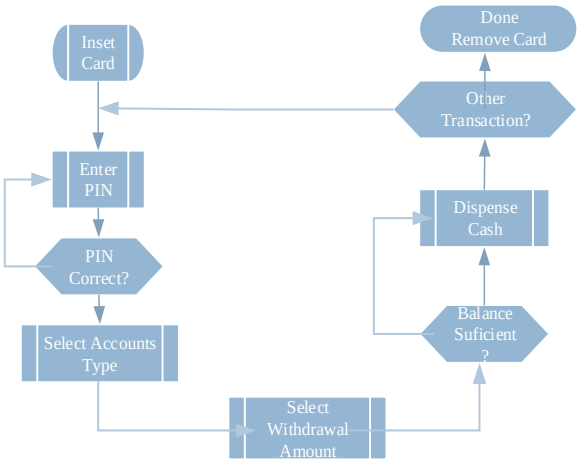

Figure 1 ATM Withdrawal PIN Based

Some method and approaches have been proposed, from text, images and biometric to increase security on ATM. This section of the research looks at some of these techniques, from their strength to weakness.

An enhanced security for ATM machine with One-Time Password (OTP) and facial recognition features was proposed by Mohsin, et al., 2015 to enhance ATM security. The OTP was used for the enrichment of security of accounts and privacy of ATM users. The face recognition technology proposed in their system was to help the ATM to identify each and every user uniquely, by using faces as a key. The researchers concluded that, there are some little flaws associated with the face recognition technique, thus the failure to detect a face when aging, beard, caps and glasses. (Mohsin, et al., 2015). ATM Transaction Security System Using Biometric Palm Print Recognition and Transaction Confirmation System was proposed by (Sanjay, et al., 2014), the researchers acknowledged that, the PIN authentication system only, as used in most ATM machines is not secured. Hence, they sort to enhance the security system by introducing palm print recognition authentication as better and further mode of ensuring security at the ATM. The proposed method was accomplished with a prototype model of an ATM simulator that mimics a typical ATM system. In their conclusion, they recorded a percentage matching of 89.43% for palm-print recognition system and a rejection rate of 10.57% (Sanjay, et al., 2014). Thus, for 53 out of every 500 customers that will visit ATM's enhanced with this authentication system are likely to have problems with their transactions. Make a Force Rejection Rate of the system to be 10.57%. Hirakawa in 2013 prospered a password enhanced mechanism called (Random Board: Password Authentication Method with Tolerance to Video-Recording Attacks) to increase or fortify up security on ATM, by preventing an observation attack for stealing user's password (thus video recording) and brute force attacks. Hirakawa acknowledges that the PIN authentication in traditional ATMs contributes to the immerse rising of ATM frauds, because this PIN, (password) are entered in open spaces which gives a chance to criminals having a mobile phone equipped with cameras and miniature cameras to spy on the user whiles entering his/her PIN. To achieve this Hirakawa proposed two modules, basic method and an improved method. In their basic method, a correct entry position of each password must be provided beforehand. Whiles, in the improved method, a user does not need to provide any information beforehand, other than the password. In his approach, the alphabet board is randomize, thus the letters changes position all times, making it difficult for an observer to see the alphabet entered by the user (Hirakawa, 2013). Lalzirtira proposed an authentication method called Graphical User Authentication to eliminate the defects in the alphanumeric authentication mode of traditional ATM's. In his research, he emphasized that graphical password which make use of images are easy for humans to remember than words or numerals. In his work he sounded that the introduction of the graphical password will eliminate the tendency of user written down their password, hence eliminating ATM frauds (Lalzirtira, 2013).

The use of images as a means of authentication in ATM system has its strength to some point and a big weakness to video recording, hence this method cannot be said to be a definite solution to ATM frauds.

A Dynamic Password (Dyna-pass) techniques was proposed to offer security to ATM transactions by Anand et.al, 2013. In their system, a user access the ATM with a debit card and his or her PIN as in the traditional system, but an SMS that contain a secret code called Dyna-pass is sent to the user mobile phone from the bank server if the PIN giving by the user is correct. The user then enters this new code received on his or her phone for confirmation, this again is checked with the bank server for confirmation, and if correct ATM transaction access is given to the user (Anand, et al., 2013).

This implies that to access a user account at the ATM, you need his or his PIN, debit card and mobile phone. Hence a person close to the user can attain all these and defraud the ATM user. In this same paper an emergency third party authentication was proposed, whereby three to four people can register in the system with own mobile numbers for a friend. So that in the event that the actual account holder can't perform a transaction, these registered people can do transaction for the actual user through the mobile phone (Anand, et al., 2013). Thus, a user is given the chance to give three or four auxiliary phone numbers in addition to his or her mobile number. Lawan proposed that, the fraudulent act associated with ATM's can be eliminated by the use of biometric authentication mechanism incorporated in the ATM security. In his report he looked at an overview of all ATM fraudulent activities and recommended approaches to element or prevents these frauds in ATM. In addition a prototype model for biometric authentication was developed to provide a solution to well-known security breaches in ATM authentication (Mohammed, 2011).

In other research work, a proposed neural network-based was adapted to match the fingerprint of users through the view of the blueprints and groove patterns of the fingerprints. This proposed module function perfectly on binary images and greyed scans; one good side of this proposed module is that, once a group is tracked, pattern can then be tracked with high accuracy. But this approach comes with a great threat where the network becomes inaccessible (Saropourian, 2009). Multi-layers of convex polygon were proposed to implement fingerprint verification to enhance security levels on ATM's. In this work, extraction of fingerprint image was found in a specified area in which the prevailing brightness value of fingerprint ranges. The major limitation is the possibility of falsifying identity and falsified authentication cannot be noticed easily. To conclude these reviewed research efforts was carried out using a single biometric check without any form of cryptography, hence, could not warrantee a dependable security solution (Myo, 2009). An authentication method called fakepointer is proposed to enhance the security levels at ATM's, which make use of a numeric key entry. With this approach, a disposable "answer selection data" is to be retrieved before each authentication. This selective information provides the background mark, like square, triangle, pentagon, hexagon of the numeric password displayed. At the authentication stage or period a user trikes the enter button, which adapts to the password according to the mark at the background. This method is open to twice video recording attack, if the "answer selection data" can be safely retrieved before each authentication. However, this research did not emphasis on how to recover it safely (Takada, 2007) cited by (Tedder, 2009). Zhao & Li proposed an interface for PIN authentication called S3PAS, this mechanism proposed numerous characters to be displayed on an interface. A user at an ATM premises assigns three places where a password character is included in a triangle. This approach guides the user from shoulder surfing attack, but again if the input is recorded; it's exposed to user password to criminal attacks (Zhao & Li, 2007). A pin-Entry password authentication technique using numeric key entry was proposed. In this approach a black or white background is randomly displayed. The ATM user does designate a password rather he/she selects a black or white as background colour for a password. A user designates the background colour by the different colour pattern with four times to enter a password entry of One (1) digit. The method is very safe against shoulder surfing, but an attacker is able to video record the input operation the password is still open to attack (Roth, et al., 2004). (Sakurai, et al., 2004; Sakurai & Munaka, 2008) cited (Hirakawa, et al., 2013) proposed a text-password entry interface known as mobile authentication. With their method every text that is selectable are arranged in a square, with each text having its own background colour. For instance, every password is numeric or alphabetic, and the texts are ordered in 6×6 square in which six colours are used, with each colour appearing only once in each row. The colour pattern of a row is the permitted colour pattern of another row. In this approach, a user provides the correct background colour and a password beforehand. At the authentication (password entry) stage, the user changes the background colour of a pass-character until it matches the correct background colour, and then presses the accept/enter button. This technique comes with a restriction that all available texts must be displayed in the square, but this approach is secure against video attack by twice recording. Their techniques is applicable to numerical passwords but still, a 12-length numerical password is required for secure use, which might be considered too long by most ATM customers. In this method, all of the texts available are presented as squares on the authentication interface. In the case of a four-character password, the columns number should be bigger than or equal to 10 for tolerance to random attacks, and the rows number should be larger than or equal to 9 for tolerance to video-recording attacks. Therefore, the numbers of available pass-texts are equal to or more than 90 for tolerance for both the attacks. And also, in a case where five-character password is used, the columns number should be equal to or greater than 7 and the rows number should be equal to or bigger than 6. Therefore, the method is not used when four or five lengthy alphanumeric password is used as a PIN for authentication (Hirakawa, 2013). A method called AWASE-E was proposed, which has 25 images, with one being a correct pass images. These images are normally displayed on the screen, similar to (Passfaces, 2005) approach, but with the ability to display on a screen in where there is no pass-image. Where the pass image is not part of the images' on the screen, then a user has to select the "no pass-image button". Although this technique offers a quieter security to ATM authentication, it's only safe when taking a shot, is not clear to the attacker (Koike & Takada, 2003) cited (Hirakawa, 2013). The techniques proposed by (Passfaces, 2005) are exposed to shoulder surfing attack, because the user designates a pass-image in the process of authentication. (Ratha, et al., 2001) proposed an embedded fingerprint system for ATM security applications, in their proposed system, bankers will have to collect customers' finger prints and mobile numbers while opening new accounts. With their system a customer wanting to perform a transaction at an ATM will get a text of a 4-digit code message on his/her GSM phone when the customer place a finger on the finger print module attached to the ATM. This message is automatically generated every the customer visit the ATM. The code received by the customer is entered into the ATM machine by pressing the keys on the touch screen. After entering it checks whether it is a valid one or not and allows the customer further access. The main disadvantage of this system is that customers with a lost phone needs a new one or has to updates his records at the bank before he/she can access his account on an ATM. An ATM enhancement technique using secured Personal Identification Image (PII) process was proposed by Santhi and Kumar. This method is secured against shoulder surfing attack, but if a recording

camera is hidden to record the authentication process, the system becomes insecure (Santhi & Kumar, 2012). A highly authenticated biometric security system is proposed by (Subh & Vanithaasri , 2012), to enhanced ATM security. The proposed method implementation however lacks the strength to exclude wrong or false feature and minutiae points from its extracted list.

In light of the above discussions, it appears clearly, that the PIN and Image's authentication approach does not guarantee sufficient ATM security.

This paper seeks to propose a multifactor authentication (PIN and Fingerprint) authentication system for dealing with modern ATM's security challenges and examine its performance.

2. Materials and method

Microsoft Visual Studio 2010 (C#) was used to develop the front end, where system user can graphically interact with the ATM. The back end (database) was developed with Microsoft Structured Query Language (MSSQL) server 2008, MSSQL is a relational database management system (RDBMS) use for creating a database for Microsoft Windows family of servers. MSSQL was chosen over other database management tool, due to its ability to provide a working environment to easily generate a database that can be easily and quickly accessed from the internet, workstation, LAN and so on. To help communicate between the fingerprint scanner a Grfinger software development kit (SDK) was employed in conjunction with the Microsoft visual studio to help in the implementation of the proposed fingerprint enrollment and authentication algorithm.

2.1 Design Concept

Figure 2 portrays the block diagram of the proposed ATM multifactor authentication system, which comprises of customer account details, PIN database, fingerprint database and an ATM machine. The following subsections explain in details how the proposed ATM multifactor Authentication will enhance the level of security on the ATM, to safeguard the users of ATM from various ATM attacks initiated by fraudsters.

The internet, is the first phase of the proposed system, serving as the working environment and platform for the proposed system to communicate between individual ATM terminals and the central bank server. Customers fingerprint and PIN databases are available on the bank servers and a relational database model is used for storing information on the fingerprint and PINs of all registered customers. These information include pattern type, and feature characteristics.

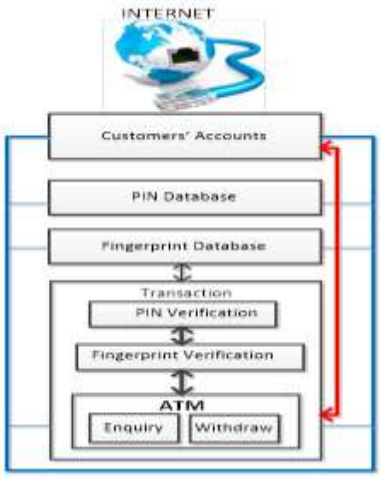

Figure 2 Conceptual Design of Proposed ATM Security Structure

Figure 3 shows the flowchart for the PIN and fingerprint verification components proposed for verifying the authenticity of a user. A user who is already enrolled onto the proposed system, will have to go through the verification process presented in figure 3.

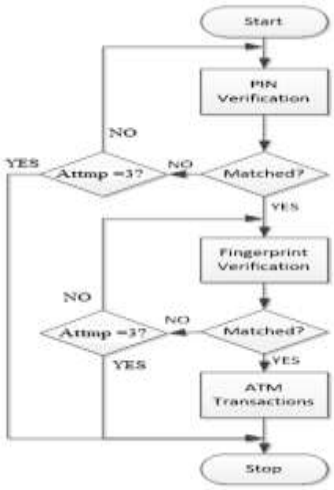

Figure 3 Flow Chart of Proposed System

For the period of image enhancement, the foreground regions of the image which are the regions containing the ridges and valleys are separated, from the background regions, which consist mostly of noise. Segmentation is performed with the view of ensuring that focus is only on the foreground regions, while the background regions are ignored. The segmented fingerprint image ridge structure will be normalized so as to standardize the level of variations in the image grey-level values. By normalizing, the grey-level values will be brought to a range that is good enough for improved image contrast and brightness. The normalized image is then filtered to remove any noise and spurious feature present. The filtering will also preserve the true ridge and valley, and this involves the ridge orientation and frequency estimations. The output obtained after filtering (filtered image) is converted to binary

format and thinned for satisfactory feature extraction. At the feature extraction stage, major features; namely ridge ending and bifurcation are located and extracted from the image. These two main features are the characteristics that establish uniqueness among different fingerprints.

The extracted features from the user template is matched with templates of the other images in the database. A user of the ATM will provide his or her PIN and if it's correct after system check, then the user is granted access to the second level of authentication (fingerprint identification), when the fingerprint of the user is scanned by the fingerprint model incorporated in this system and a match exit when compared to the one in the database during the enrollment of the user, access is granted to the user to perform his/her ATM transactions.

2.2 Software Modules Design

As a requirement of the approach used for implementing the proposed algorithm, five primary phases were required for producing consolidative software levels necessary to meet system objectives and goals. Each module design and tested separately, and then combine together to form a complete application.

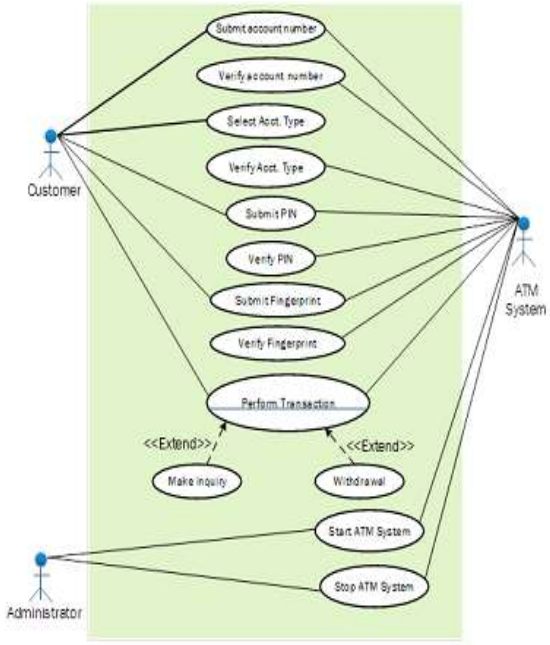

Figure 4 Use Case Diagram for Proposed ATM Multifactor Authentication Module

Figure 4 shows the Use Case Diagram for the proposed ATM multifactor authentication module. The primary actors; Administrator and customer and secondary actor; ATM system triggers the use-cases. Figure 5 shows a pictorial view of the different sub-module, and the relationships that exist between various sections of the program codes, and how each program code interact with another section.

Figure 5 Detail Code Elements and Relation

2.3 Customer Enrollment

Figure 6 shows the enrollment module. This module enables the bank to enroll customers that come to the banking hall directly into the system.

Figure 6 Module for Customer Enrollment onto the Fingerprint System

3. Implementation of Proposed ATM Multifactor Authentication System

Microsoft Windows 8 was used as an operational platform, running on a 32bit Processor with a speed 3.0 Ghz with a system memory at 3Gb.

3.1 Results and Discussions

Evaluation and testing of the proposed ATM multifactor (PIN and fingerprint) authentication system was carried out with information/data collected from randomly selected, four hundred and fifty student and staff of the Sunyani Polytechnic Sunyani, Ghana. The performance of the system was measured in terms of False Accept Rate (FAR), False Rejection Rate (FRR) and equal error rate (EER). The FAR is

the percentage of invalid inputs that are incorrectly accepted (match between input and a non-matching template). The FRR is the percentage of valid inputs that are incorrectly rejected (fails to detect a match between input and matching template) (Sainath & Tangellapally, 2010). To test the effectiveness and robustness of the proposed system, two sets of thumbprints data were used for FAR and FRR testing. Since these indicators are the commonest and simplest indicators for checking the effectiveness, accuracy and performance of fingerprint pattern matching (Iwasokun & Akinyokun, 2013). The first dataset (A) had 1,800 thumbprints, accounting for Four (4) thumbprints collected from the right thumb of each of the four hundred and fifty (450) respondents. The other dataset (B) also contained the same amount of thumbprints collected from the left thumb of respondents. Datasets (C), (D) and (E) contains 450 thumbprint each from the right thumbs of each subject with different thumb pose for intra-class variation test. All the three thousand, six hundred (3,600) thumbprints from the right and left of respondent were enrolled onto the system for a period of hundred and twenty (120) days , using a digital persona (U.are.U 4500) USB fingerprint reader with 512dpi pixel resolution and 18.1mm length by 14.6mm width capturing area.

3.2 Intra-class variations test

To ascertain how the proposed system will react to intra-class variation, each of the four hundred and fifty (450) enrolled templates in the dataset (C) was matched with templates in the dataset (C), (D) and (E) by the same client and the match score recorded. The matching score (also called weights) gives or express the measure of similarity or a distance measure between two minutiae patterns. The greater the score is, the higher is the similarity between them, and for a genuine client the score (S) must be greater than the threshold (T). Figure 7 shows a graph of the score obtain from randomly selected 20 fingerprint templates in (C) matched against fingerprint in the dataset (D) and (E) from the same respondent. The pronouncement of whether a match exists is completed by comparing the matching score (S) to a decision threshold value (T), and if $S \geq T$, then the identity claim is assumed correct.

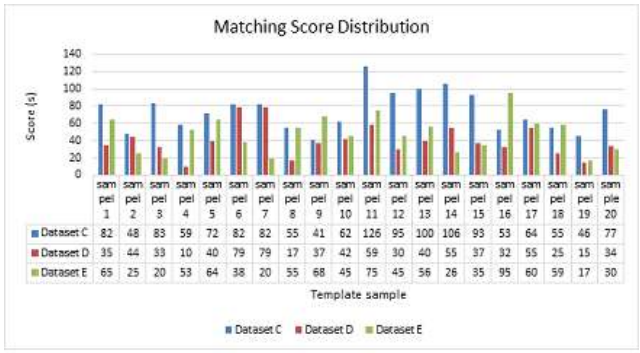

Figure 7 Intra-Class Variations Matching Score Distribution

From figure 7, it can be deduced that the scores obtained by clients differs from dataset to another dataset. These discrepancies in score rate can be attributed to the different poses clients made during the enrollment stage. If clients were to authenticated with the template stored in dataset D and E, there would have been seven (7) imposters in the dataset (D) and six (6) in the dataset (E) making a total of eleven (13) which equal 65% out of the twenty samples taken at random. From this result, it can be concluded that if client are not guided at the enrolment stage to position their thumbs well on the sensor, there will be a high rate of FAR at the authentication stage.

For FAR and FRR testing purpose, three categories of experiments I, K and L were conducted. The first category (I) experiment (FRR test), was carried out on dataset (A), by matching every single thumbprints in dataset (A) with the remaining three other thumbprints from that same thumb in dataset (A), but escaping symmetric matches, by employing the implemented fingerprint matching algorithm. This was to verify the possibility that two match-samples will be acknowledged falsely as unmatched, thus the match score will be lesser than the threshold value.

3.3 False Rejection Rate

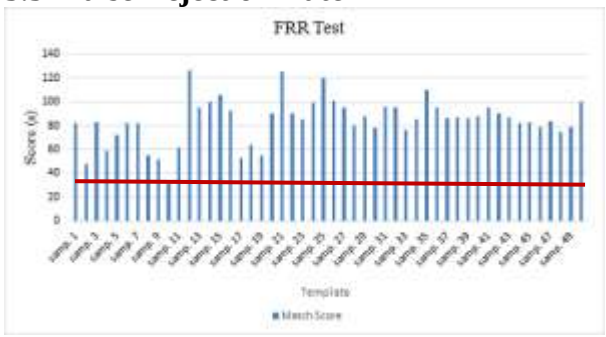

Figure 8 False Rejection Rate Score

Figure 8 shows an outcome score for randomly picked 50 (templates) samples in the FRR experiment on dataset (A).

Out of the fifty (50) samples, one (1) false reject was accounted. Thus FRR equals (2%) out of 50 as compared with 3.33% out of 30 (Manish, et al., 2011) and 10.57% (Sanjay, et al., 2014), it can be approximated that for all the four hundred and fifty samples that was put under FRR test nine (9) false rejecting will be accounted, making an overall FRR equals nine (9). The Genuine Acceptance Rate (GAR) is the fraction of genuine scores above the threshold (T). Therefore GAR =1 – FRR (1 – 0.02 = 0.98).

3.4 False Acceptance Rate

To determine FAR, the four thumbprints of each thumb, from each respondent in datasets (A) and (B) were matched with the one thousand seven hundred and ninety six (1,796) thumbprints from the 449 remaining respondents' thumbprints at different threshold values. This is to determine the probability that two non-match thumbprints will be mistakenly confirmed as a match.

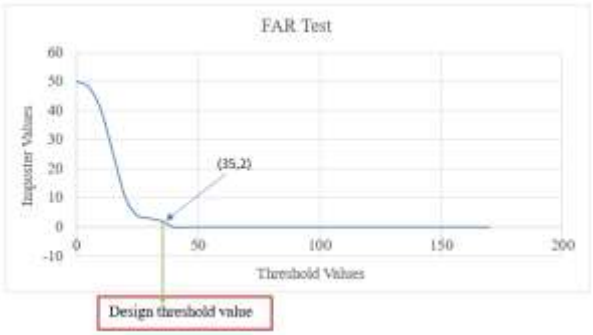

Figure 9 False Acceptance Test

Figure 9 shows the output curve for the FAR test on dataset (A). From the graph it can be realized that, for a threshold value of thirty-five (35), two imposter values were recorded as a genuine record out of fifty (50) sample taken at random. Hence FAR equals (4%) for this work as compared to (6.6%) for (Manish, et al., 2011) for 30 samples. The TER is 6% for a total access of 50 and compared to 13.3% (Manish, et al., 2011) for a total access of 30 and 8.27% (Iwasokun & Akinyokun, 2013).

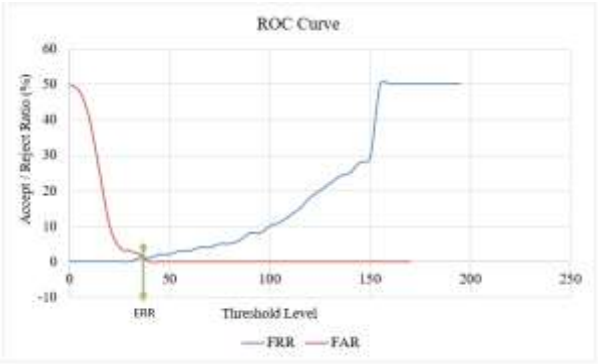

Figure 10 ROC Curve

With a TER of 6%, it shows that the developed system is 94% accurate as compared with 89.43% (Sanjay, et al., 2014). Figure 10 shows the ROC curve. An average matching time of 1.023, 1.075 and 1.155 were recorded for dataset A, B and A + B respectively.

4. Conclusions And Recommendations

The conclusions arising out of this research, based on the findings, are given below.

- ✓ The proposed fingerprint and PIN system has an overall efficiency of 94%, FAR 4%, FRR 2%, TER 6% and GAR 98%.
- ✓ Compared to other fingerprint identification and verification systems, the proposed system provides an improved performance in matching time and partial elimination of false minutiae from its fingerprint database.
- ✓ The proposed system is a good cost effective measure for implementing a well secure ATM transactions to protect ATM users from fraudsters.

The recommendations of this research could be summarized as follows:

Decision-makers need to appreciate the level of security assured through the usage of biometric systems and the transformation that can exist between the perception and the authenticity of the sense of security delivered.

The Bank of Ghana (BoG) and the Ghana Association of Bankers (GAB) which has the mandate to implement strategic actions in the banking sector of Ghana should pilot the installation of ATM enhanced with this system as a cost reduction strategy and security for their customers and clients.

The great difference obtained on Intra -class variations test in this research indicates that, if clients thumb pose at enrollment do not match with thumb pose at verification, a falsehood rejection will occur. Hence the Electoral commission (EC) of Ghana should ensure that, the thumbs of voters at enrollment and voting days are positioned well on the fingerprint scanner,

to prevent false rejection, causing confusion at voting days. Experimental validation should be conducted to confirm the results presented in this research work.

- ✓ The proposed system is a good cost effective measure for implementing a well secure ATM transactions to protect ATM users from fraudsters.

5. Acknowledgments

We give all our praises and extreme thanks to God Almighty for how far He has brought us faithfully in life.

6. References

1. Adams, A. & Sasse, M. A., 1999. Users are Not the Enemy. Commun.. *ACM 42, 12*, pp. 40-46.

2. Akinyemi, I., Omogbadegun, Z. & Oyelami, O., 2010. Towards Designing a Biometric Measure for Enhancing ATM Security in Nigeria EBanking System.. *International Journal of Electrical & Computer Sciences IJECS-IJENS 10*, pp. 68-73.

3. Anand, D. A., Dinesh, G. & Naveen, H. D., 2013. A Reliable ATM Protocol and Comparative Analysis on Various Parameters with other ATM Protocols. *International Jouranl of Communication and Computer Technologies (IJCCT), ISSN: 2278-9723*, 01(56), pp. 192-197.

4. Batiz-Lazo, B. & Barrie, . A., 2005. *The business and technology history of automated teller machine in the UK*. London, Queen Mary University, pp. 1-10.

5. Das, S. & Jhunu, D., 2011. Designing a Biometric Strategy (Fingerprint) Measure for Enhancing ATM Security in Indian E-Banking System. *International Journal of Information and Communication Technology Research*, pp. 197-203.

6. Gunn, L., 2010. *European ATM crime report. Technical Report 1.2*, s.l.: European ATM Security Team (EAST),.

7. Hirakawa, Y., 2013. Random Board: Password Authentication Method with Tolerance to Video-Recording Attacks. *International Journal of Innovation, Management and Technology, Vol. 4, No. 5*, pp. 455-460.

8. Iwasokun, G. B. & Akinyokun, O. C., 2013. A Fingerprint-based Authentication Framework for ATM Machines. *Journal of Computer Engineering & Information Technology*, pp. 1-8.

9. Jermyn, I. et al., 1999. *The design and analysis of graphical passwords.*. s.l., USENIX Association, pp. 1-1.

10. Lalzirtira, 2013. *Graphical User Authentication*, India: Department of Computer Science and Engineering National Institute of Technology Rourkela.

11. Luca, A., 2011. *Designing Usable and Secure Authentication Mechanisms For Public Spaces (Doctoral dissertation, lmu)*, s.l.: s.n.

12. Manish, . M., Ajit , S. K., Thakur, S. S. & Sinha, D., 2011. Secure Biometric Cryptosystem for Distributed System. *International Journal Communication & Network Security (IJCNS)*, Volume-I(Issue-II), pp. 28-32.

13. Modernghana, 2013. *Modernghana*. [Online] Available at: http://www.modernghana.com/news/463043/1/hackers-steal-45-million-in-atm-card-scam-federal.html [Accessed 10 June 2015].

14. Mohammed, L. A., 2011. *Use of biometrics to tackle ATM fraud*.. Malaysia,, IACSIT Press, Kuala Lumpur, pp. 331-335.

15. Mohsin, K., Saifali, K., Sharad, O. & Dr.D.R.Kalbanded, 2015. *Enhanced security for ATM machine with OTP and Facial*. s.l., Elsevier B.V., pp. 390-396.

16. Myo, N., 2009. Fingerprint Identification Based on the Model of the Outer Layers of Polygon Subtraction. *International Conference on Education Technology and Computer*, p. 201 – 204.

17. Ndife, .. A., Ifesinachi, .. E., Anthony, .. O. & Davies, .. ,., 2013. An Enhanced Technique in ATM Risk Reduction using Automated. *Volume No.4*, 06 June , pp. 1132-1138.

18. Obour, S. K., 2013. [Online] Available at: http://graphic.com.gh/news/general-news/8459-gcb-confirms-money-theft-from-atm-but-says-amount-is-lower-than-gh-3-million.html

19. Passfaces, Corporation, 2005. [Online] Available at: http://www.realuser.com/enterprise/about/about_passfaces.htm [Accessed 9 July 2015].

20. Rasiah, D., 2010. ATM Risk Management and Controls. *European Journal of Economics, Finance and Administrative Sciences , 21, ,* 2014 January.pp. 161-171.

21. Ratha, N., Connell, J. & Bolle, R., 2001. Enhancing Security and Privacy in Biometrics-based Authentication Systems. *IBM Systems Journal, vol. 40, no. 3,* pp. 614-634.

22. Roth, V., Richter, K. & Freidinger, R., 2004. A Pin-Entry Method Resilient Against Shoulder Surfing. pp. 236-245.

23. Sanjay, S. G. et al., 2014. ATM Transaction Security System Using Biometric Palm Print Recognition and Transaction Confirmation System. *International Journal Of Engineering And Computer Science,* pp. 5332-5335.

24. Santhi, B. & Kumar, R., 2012. Novel Hybrid Technology in ATM Security Using Biometrics. *Journal of Theoretical and Applied Information Technology,* pp. 217-223.

25. Saropourian, B., 2009. A new approach of finger-print recognition based on neural network," Computer Science and Information Technology, 2009. ICCSIT 2009. *ICCSIT 2009. 2nd IEEE International Conference ,* pp. 158-161.

26. Subh , M. & Vanithaasri , S., 2012. A Study on Authenticated Admittance of. *International Journal of Advances in Engineering & Technology 4,* pp. 456-463.

27. Takada, . T., 2008. FakePinter: The authentication technique which has tolerance to video recording attacks. *Information processing society of Japan (IPSJ) transaction, vol. 49, no. 9,* pp. 3051-3061.

28. Tedder, K., 2009. *A Review of Fraud Costs and Trends,* s.l.: s.n.

29. Zhao, H. & Li, X., 2007. "S3PAS: A Scalable Shoulder-Surfing Resistant Textual-graphical Password Authentication Scheme. *IEEE Advanced Information Networking and Applications Workshops,* pp. 467-472.

International Journal of Science and Engineering Applications
Volume 5 Issue 3, 2016, ISSN-2319-7560 (Online)

SACET::Result Management System

D. V. Sandeep[1], K. Mahesh[1], A.Vasudeva Rao[1], K. Mahesh[1], N LAKSHMI NARAYANA[2]

[1]UG Scholar, Department of Computer Science and Engineering, St.Ann's College Of Engineering and Technology, Chirala, Andhra Pradesh, India.

[2]Asst.Professor,Department Of Computer Science and Engineering, St.Ann's College Of Engineering and Technology, Chirala, Andhra Pradesh, India.

ABSTRACT: To solve the problems of managing the results that are obtained whenever the results are released from the University of a certain Semester Examination, the project presents a model for maintaining the records of results obtained in every semester for every year. The results are maintained in the form of records using pdf format and are maintained by the exam cell of a college. Those results are send to each and every department in the college for analysis like to know the details of the passed and failed candidates in the examination. This project contains Admin for uploading the results, Head Of the Department for viewing the results of students in their respective department as well as other department results also, Faculty for viewing the results and generating the analysis, Student for viewing the results of their own from first semester to the current semester. Experiments show that the model can effectively maintains the records of results.

Keywords: Data Mining, Jquery,PHP,Attribute Selection,DFS.

1. INTRODUCTION:

Our application is developed basing on the Data Mining concept which means process to extract information from a data set and transform it in to an understandable structure for further use. It involves database for storing the data which the user want and can retrieve the data from the database.

In our application the user interface is developed using HTML (Hyper Text Mark-up Language) in which different types of tags are used to enter the data. And to store the entered database is used and in connection to the database and HTML the server side scripting language PHP (personal-Home-Page Hypertext Pre-Processor) is used for storing and retrieving the data. The validation for the text fields is done using the java script.

[1]The Oracle Database (commonly referred to as *Oracle RDBMS* or simply as *Oracle*) is an object-relational database management system (ORDBMS) produced and marketed by Oracle Corporation.

[1]Larry Ellison and his friends, former co-workers BobMiner and Ed Oates, started the consultancy Software Development Laboratories (SDL) in 1977. SDL developed the original version of the Oracle software. The name *Oracle* comes from the code-name of a CIA-funded project Ellison had worked on while previously employed by Ampex.

Database Scheme

Most Oracle database installations traditionally came with a default schema called SCOTT. After the installation process has set up the sample tables, the user can log into the database with the username scott and the password tiger.**[2]**The name of the SCOTT schema originated with Bruce Scott, one of the first employees at Oracle (then Software Development Laboratories), who had a cat named Tiger.

[4]Oracle Corporation has de-emphasized the use of the SCOTT schema, as it uses few of the features of the more recent releases of Oracle. Most recent examples supplied by Oracle Corporation reference the default HR or OE schemas.

2. PROPOSED WORK:

Traditionally, the clients are using excel sheets to record the results of students. Those sheets have to be updated when the recounting or revaluation or supplementary examination results are released. The clients has to maintain a lot of records like there are eight semesters for a batch in their entire four years and there will be supplementary and revaluations results for every semester. They not only maintain the records of a single batch they have to maintain the records of students who are going to join in the organization every year. **[5]**So the maintenance of those records may become difficult as the client has to remember everything about each and every batch. The client will maintain the records and the analysis of the students have to done. The generation of analysis may become difficult.

To solve the problems that are obtained in the existing process, the idea is to develop an application for maintaining the records of the results and to automate the analysis process. In this the client have to upload the excel sheet which they will get from the university whenever the results are released. The uploaded file will be stored in the database and will provide a friendly environment to view the results that are uploaded and modification of the data will be automated. The application will greatly simplify and sorts the results of students department wise that are present in the organization. The generation of analysis will be automatically done by the application.

3. SYSTEM IMPLEMENTATION:

To solve the problems that are obtained in the existing process the system is implemented so that everything that the clients need is done automatically when the client will upload the file of results that will be obtained from the university whenever the results are released.

The system implementation can be explained using different modules that are present in the application

The **Admin module** consists of viewing the student results and uploading the student results and uploading the subject details of corresponding results. Admin maintains the accounts of students, faculty, head of department etc.

The **HOD module** consists of the login page for login with his unique id. By login he can view student results semester wise. Head of department can also view results according to some selected subjects.

The **Faculty module** consists of the login page for login with his unique id. By login he can view student results semester wise. And he can generate the analysis of students of particular class and branch. Faculty can also view results according to some selected subjects.

The **Student module** consists of the login page for login with his unique id. By login he can view his results semester wise. And he can logout by completing his actions that are to be performed.

4. SYSTEM ARCHITECTURE :

Dataflow diagram:

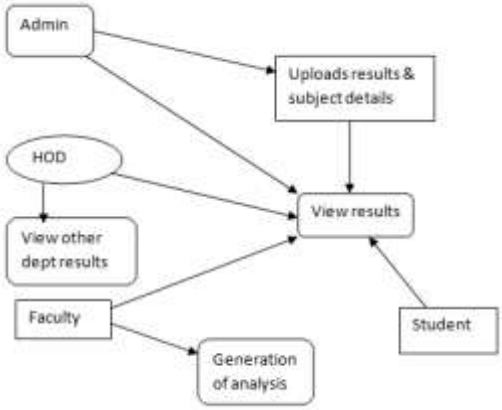

5. CODING:

Uploading A File:

```
<?php

if(isset($_POST['submit']))

{

include '../db.php';

$py=$_POST['yr'];

$s=$_POST['sem'];

$r="R".$_POST['reg'];

$date=$_POST['month']." ".$_POST['year'];
```

```
$file = $_FILES['ex']['tmp_name'];

$handle = fopen($file, "r");

while(($filesop = fgetcsv($handle, 1000, ",")) != false)

{                       $htno = $filesop[0];

if($htno=='Htno')

{           if(($filesop = fgetcsv($handle, 1000, ",")) != false)

$htno=$filesop[0];

}

$q = ociparse($c,"SELECT * FROM S$s where htno='$htno'");


$q1=oci_execute($q);

$br=substr($htno,7,1);

if($br==1)

$branch='CIVIL';

else if($br==2)

$branch='EEE';

else if($br==3)

$branch='MECH';

else if($br==4)

$branch='ECE';

else if($br==5)

$branch='CSE';

if(!$row=oci_fetch_row($q))

{           $q2         =         ociparse($c,"insert         into
S$s(htno,branch,passedyear,regulation)
values('$htno','$branch','$py','$r')");

$q3=oci_execute($q2);

}

$subcode = $filesop[1];

$subint=$filesop[3];

$subext = $filesop[4];

$subcre=$filesop[5];

if($row[4]=='')

{$u=ociparse($c,"updates$sset
sub1code='$subcode',sub1int='$subint',sub1ext='$subext',sub1
cre='$subcre',date1='$date' where htno='$htno'");

$u1=oci_execute($u);

}

else if($row[4]!='')

if($row[4]==$subcode)

{

$u=ociparse($c,"updates$sset
sub1int='$subint',sub1ext='$subext',sub1cre='$subcre',date1='$
date'where htno='$htno'");

$u1=oci_execute($u);

}

else if($row[9]=='')

{

$u=ociparse($c,"updates$sset
sub2code='$subcode',sub2int='$subint',sub2ext='$subext',sub2
cre='$subcre',date2='$date' where htno='$htno'");

$u1=oci_execute($u);

}

else if($row[9]!='')

if($row[9]==$subcode)
```

```
{$u=ociparse($c,"updates$sset
sub2int='$subint',sub2ext='$subext',sub2cre='$subcre',date2='$
date'where htno='$htno'");

$u1=oci_execute($u);

}

else if($row[14]=='')

{$u=ociparse($c,"updates$sset
sub3code='$subcode',sub3int='$subint',sub3ext='$subext',sub3
cre='$subcre',date3='$date' where htno='$htno'");

$u1=oci_execute($u);

}

else if($row[14]!='')

if($row[14]==$subcode)

{$u=ociparse($c,"updates$sset
sub3int='$subint',sub3ext='$subext',sub3cre='$subcre',date3='$
date'where htno='$htno'");

$u1=oci_execute($u);

}

else if($row[19]=='')

{$u=ociparse($c,"updates$sset
sub4code='$subcode',sub4int='$subint',sub4ext='$subext',sub4
cre='$subcre',date4='$date' where htno='$htno'");

$u1=oci_execute($u);

}

else if($row[19]!='')

if($row[19]==$subcode)

{$u=ociparse($c,"updates$sset
sub4int='$subint',sub4ext='$subext',sub4cre='$subcre',date4='$
date'where htno='$htno'");

$u1=oci_execute($u);

}

else if($row[24]=='')

{$u=ociparse($c,"updates$sset
sub5code='$subcode',sub5int='$subint',sub5ext='$subext',sub5
cre='$subcre',date5='$date' where htno='$htno'");

$u1=oci_execute($u);

}

else if($row[24]!='')

if($row[24]==$subcode)

{$u=ociparse($c,"updates$sset
sub5int='$subint',sub5ext='$subext',sub5cre='$subcre',date5='$
date'where htno='$htno'");

$u1=oci_execute($u);

}

else if($row[29]=='')

{       $u=ociparse($c,"updates$sset
sub6code='$subcode',sub6int='$subint',sub6ext='$subext',sub6
cre='$subcre',date6='$date' where htno='$htno'");

$u1=oci_execute($u);

}

else if($row[29]!='')

if($row[29]==$subcode)

{$u=ociparse($c,"updates$sset
sub6int='$subint',sub6ext='$subext',sub6cre='$subcre',date6='$
date'where htno='$htno'");

$u1=oci_execute($u);

}

else if($row[34]=='')
```

```
{ $u=ociparse($c,"updates$sset sub7code='$subcode',sub7int='$subint',sub7ext='$subext',sub7cre='$subcre',date7='$date' where htno='$htno'");

$u1=oci_execute($u);

}

else if($row[34]!='')

if($row[34]==$subcode)

{$u=ociparse($c,"updates$sset sub7int='$subint',sub7ext='$subext',sub7cre='$subcre',date7='$date'where htno='$htno'");

$u1=oci_execute($u);

}

else if($row[39]=='')

{$u=ociparse($c,"updates$sset sub8code='$subcode',sub8int='$subint',sub8ext='$subext',sub8cre='$subcre',date8='$date' where htno='$htno'");

$u1=oci_execute($u);

}

else if($row[39]!='')

if($row[39]==$subcode)

{$u=ociparse($c,"updates$sset sub8int='$subint',sub8ext='$subext',sub8cre='$subcre',date8='$date'where htno='$htno'");

$u1=oci_execute($u);

}

else if($row[44]=='')

{$u=ociparse($c,"updates$sset sub9code='$subcode',sub9int='$subint',sub9ext='$subext',sub9cre='$subcre',date9='$date' where htno='$htno'");

$u1=oci_execute($u);

}

else if($row[44]!='')

if($row[44]==$subcode)

{ $u=ociparse($c,"updates$sset sub9int='$subint',sub9ext='$subext',sub9cre='$subcre',date9='$date'where htno='$htno'");

$u1=oci_execute($u);

}

else if($row[49]=='')

{ $u=ociparse($c,"updates$sset sub10code='$subcode',sub10int='$subint',sub10ext='$subext',sub10cre='$subcre',date10='$date' where htno='$htno'");

$u1=oci_execute($u);

}

else if($row[49]!='')

if($row[49]==$subcode)

{ $u=ociparse($c,"updates$sset sub10int='$subint',sub10ext='$subext',sub10cre='$subcre',date10='$date'where htno='$htno'");

$u1=oci_execute($u);

}

else if($row[54]=='')

{ $u=ociparse($c,"updates$sset sub11code='$subcode',sub11int='$subint',sub11ext='$subext',sub11cre='$subcre',date11='$date' where htno='$htno'");

$u1=oci_execute($u);

}

else if($row[54]!='')

if($row[54]==$subcode)
```

```
{ $u=ociparse($c,"updates$sset sub11int='$subint',sub11ext='$subext',sub11cre='$subcre',date11='$date'where htno='$htno'");

$u1=oci_execute($u);

}

else if($row[59]=='')

{$u=ociparse($c,"updates$sset sub12code='$subcode',sub12int='$subint',sub12ext='$subext',sub12cre='$subcre',date12='$date' where htno='$htno'");

$u1=oci_execute($u);

}

else if($row[59]!='')

if($row[59]==$subcode)

{ $u=ociparse($c,"updates$sset sub12int='$subint',sub12ext='$subext',sub12cre='$subcre',date12='$date'where htno='$htno'");

$u1=oci_execute($u);

}

else if($row[64]=='')

{$u=ociparse($c,"updates$sset sub13code='$subcode',sub13int='$subint',sub13ext='$subext',sub13cre='$subcre',date13='$date' where htno='$htno'");

$u1=oci_execute($u);

}

else if($row[64]!='')

if($row[64]==$subcode)

{ $u=ociparse($c,"updates$sset sub13int='$subint',sub13ext='$subext',sub13cre='$subcre',date13='$date'where htno='$htno'");

$u1=oci_execute($u);

}

else if($row[69]=='')

{ $u=ociparse($c,"updates$sset sub14code='$subcode',sub14int='$subint',sub14ext='$subext',sub14cre='$subcre',date14='$date' where htno='$htno'");

$u1=oci_execute($u);

}

else if($row[69]!='')

if($row[69]==$subcode)

{ $u=ociparse($c,"updates$sset sub14int='$subint',sub14ext='$subext',sub14cre='$subcre',date14='$date'where htno='$htno'");

$u1=oci_execute($u);

}

else if($row[74]=='')

{ $u=ociparse($c,"updates$sset sub15code='$subcode',sub15int='$subint',sub15ext='$subext',sub15cre='$subcre',date15='$date' where htno='$htno'");

$u1=oci_execute($u);

}

else if($row[74]!='')

if($row[74]==$subcode)

{$u=ociparse($c,"updates$sset sub15int='$subint',sub15ext='$subext',sub15cre='$subcre',date15='$date'where htno='$htno'");

$u1=oci_execute($u);

}

}
```

```
$z=ociparse($c,"select * from subjects where reg='$r' and sem='$s'");

$z1=oci_execute($z);

oci_close($c);

if(!$row=oci_fetch_row($z))

echo "<script>alert('Upload Subjects File');window.location='upload1.php';</script>";

else

if($q1)

echo"<script>alert('ResultsSavedsuccessfully');

window.location='view.php';</script>";

else

echo "<script>alert('Upload Failed');window.location='upload.php';</script>";

}

?>
```

6. RESULTS:

Home Page:

Figure 1: Home page

Admin login page

Figure 2: Admin login page

Admin home page

Figure 3: Admin home page

Upload results Page

Figure 4: Upload results page

Upload subjects page

Figure 5: Upload subjects page

Remove faculty Page

Figure 8: Remove faculty page

View results Page

Figure 6: View results page

Add students Page

Figure 9: Add students page

Add faculty Page

Figure 7: Add faculty page

Remove students page

Figure 10: Remove students page

7. CONCLUSION:

Various organizations use various types of techniques for maintain the records of results, but by using the application which was developed will greatly simplify the process that have to be done whenever the results are released of certain semester examination and manages the information about the marks obtained by the various students in various subjects in different semesters and will greatly simplify and speed up the result analysis preparation.

8. FUTURE WORK:

This application is developed only for a certain graduation, so it can be implemented to other graduations also. The application is developed to maintain the records of a certain organization but it can be implemented to maintain the records of each every organization.

9. REFERENCES:

[1]. Sparse Social Domains Based Scalable Learning of Collective Behaviour (1) Retrieved from TRYLOGIC software solutions

[2]. Mohini .B. and Amar. J. S. (2011). Mode of processing result System. Himachal Pradesh University Journal. Pg 123

[3]. Ogbeifun,E. and Ekpeyong,(2008). Packages used n designing result processing . Volume9 , issue 2):407-412.

[4]. Wikipedia. (2014). Student information system. Retrieved from http://en.wikipedia.org/wiki/Student_information_system

[5]. Student Examination Result Processing System. (2012). Retrieved from: http://15projects.com/projects/wpcontent/uploads/2012/06/Student-Examination-Result-Processing-System.docx

International Journal of Science and Engineering Applications
Volume 5 Issue 3, 2016, ISSN-2319-7560 (Online)

Short-Term Wind Power Forecasting Using Artificial Neural Networks for Resource Scheduling in Microgrids

Abinet Tesfaye
School of Electrical and Electronic Engineering, North China Electric Power University, and Goldwind and Etechwin Electric Co., Ltd
Beijing, China

J. H. Zhang
School of Electrical and Electronic Engineering, North China Electric Power University
Beijing, China

D. H. Zheng
Goldwind and Etechwin Electric Co., Ltd
Beijing, China

Dereje Shiferaw
Department of Electrical and Computer Engineering, Adama Science and Technology University
Adama, Ethiopia

Abstract: Use of wind power as one of renewable resources of energy has been growing quickly all over the world. Wind power generation is significantly vacillating due to the wind speed alteration. Therefore, assessment of the output power of this type of generators is always associated with some uncertainties. A precise wind power prediction aims to support the operation of large power systems or microgrids in the scope of the intraday resources scheduling model, namely with a time horizon of 5-10 minutes, and this can efficiently uphold transmission and distribution system operators to improve the power network control and management. A Short-term ANN based wind power prediction model, for day-ahead energy management and scheduling in microgrids, is developed utilizing a real database of 12 months with 10 minutes time interval data from measured information of online supervisory control and data acquisition (SCADA) of Goldwind microgrid wind turbine system (Beijing, China) as well as Numerical Weather Prediction (NWP). The ANN predicted wind power has been compared with the actual power of Goldwind wind turbine system. The predicted wind power has shown acceptable agreement with the actual power output that has been recorded by the SCADA which confirms the robustness and accuracy of the ANN wind power forecasting model developed in this research paper.

Keywords: Artificial neural network, microgrid, numerical weather predictions, resource scheduling, supervisory control and data acquisition, wind power prediction.

1. INTRODUCTION

Kyoto Protocol with the aim of achieving the "stabilization of greenhouse gas concentrations in the atmosphere at a level that would prevent dangerous anthropogenic interference with the climate system" is an environmental convention [43]. By adopting this protocol, due to environmental benefits of renewable resources particularly wind power generation, utilization of these types of energy has acquired noticeable consideration in eye-catching number of countries, recently. In comparison with the environmental damages of traditional sources of energy, the ecological influences of wind power is relatively negligible [43].

In fact, wind power fuel usage is incomparable with fossil power plants as well as fuel emission. Furthermore, wind power enjoys infinitesimal progress expenses, in addition to an average cost of investigation. However, despite remarkable environmental benefits, the continuous and chaotic fluctuations of wind speed make the output power of wind farms completely stochastic and different from those of conventional units. However, instant electrical generation must be equal to the grid consumption to fulfill the network stability requirements and the spare capacity may be reduced in the power system [43].

Due to this uncertainty, it may bestow ample challenges to connect large quantities of wind power into a power system. However, this challenge is not insuperable. In order to increase the economic efficiency and acceptability of the wind power and to permit a diminishing in the punishment of an instantaneous spot market coming from extra estimation or underrating of the production, the exact prediction of wind power as well as wind velocity is required. Surely, a reliable prediction system can help distribution system operators and

power marketers to make a better decision on critical situation [43].

Nowadays, several methods have been developed to predict the wind power and speed. Existing methods can be arranged as statistical, physical and time series modeling methods based on the used prediction models [1]. The physical methods are based on local meteorological service or NWP model data of the lower atmosphere (*i.e.* in relation with atmospheric pressure degree, at 2m or 10m heights above the ground) associated with topological data like obstacles, roughness and orography. The core idea of physical approaches is to estimate generation power of the wind turbine with outsourcing these obtained data up or down to exact height of the wind turbine hub and then, utilizing the manufacturer's power curve for the logarithmic power law or the specific wind turbine. Statistical forecasting techniques are only based on one or more models. These approaches found coordination between predict and historical numerical quantity of meteorological parameters and wind power measurements associated with the power quantities coming from historical data [43].

Moreover, statistical models enjoy freedom of using NWP models; whereas, physical models must utilize NWP models [2]-[5]. Recently, it is prevalent that authors use a combination of a progressive statistical model and physical methods besides each other to reach an optimal approach that is applicable for longer horizons of forecasting system.

In these methods statistical model play supplemental role to data gathered by physical methods. In fact, models not utilizing numerical wind prediction suffer from lack of preciseness in time horizons more than 3 or 4 hours [6].

Although two main classes of techniques have been recognized for the wind prediction, (in [7] and [8], comprehensive reviews of these methods are prepared), as aforementioned, combination of statistical and physical methods are more prevalent than the others [9], [10]. Furthermore, several other spatial correlation techniques are proposed for short term wind power forecasting with the goal of achieving higher prediction accuracy [11]. However, by the passage of time, more advanced methods have been proposed. To this end, Artificial Neural Network (ANN) in [12], [13], ANN with adaptive Bayesian learning and Gaussian process approximation in [14], combination of ANN with wavelet transform in [15], fuzzy logic methods in [10], [16], Kalman filter in [17], support vector machine in [18] and some hybrid methods in [6] have been proposed for wind power prediction.

In this research paper, a new effective wind power forecasting method based on combination of measured data from SCADA and NWP model is proposed. The proposed method employs feed forward ANN with back propagation learning algorithm. In the course of the training process, the ANN utilized one year (on ten minutes interval basis) SCADA records of wind speed (as training input variable) and wind power (as training target variable).

Forecasted meteorological parameter (*i.e.* wind speed) from a NWP model is then applied as input to the developed (trained) ANN wind power prediction model in order to estimate the next day wind power output of an actual wind power system ('Goldwind microgrid wind turbine system', Beijing, China). The forecasting is for the next 24 hours with 10 minutes intervals. Simulation results show that the presented method can effectively enhance the exactness of the wind power forecasting.

The paper is organized as follows: Section 2 describes an overview of the wind power prediction. Section 3 introduces proposed model in which technique of employing SCADA system and NWP model is described. Descriptions of ANN as prediction system and the prediction results for the case-studies considered are provided in sections 4 and 5, respectively. The paper is concluded in section 6.

2. LITERATURE REVIEV OF SHORT-TERM WIND POWER FORECASTING APPROACHES

The very short-term wind power prediction techniques utilize statistical models such as ARX, ARMA and Kalman Filters; while, they are mostly based on time series approach. In this category, the input data is past values of the forecasted variable like wind generation and wind speed; whereas, explanatory variables like temperature, wind direction and humidity can be employed in order to enhance precision and applicability of the forecasting methods. This model has the capability of prediction for horizons between 3–6 hours according to this consideration that they merely use the past production data [43].

In a hierarchical classification of short-term wind power prediction approaches, two major groups are consisting: 1) those that use manufacturer's power curve or empirical curves of wind turbines to map predicted wind speed to the generation output power, and 2) techniques in which wind generation power can be calculated directly without interfering the turbines' characteristics and role of NWP model is intensively highlighted for the short-term wind power forecasting [43].

The second approach is adopted in this research which combines measured data from SCADA records and NWP model without referring manufacturer's power curve or empirical curves of wind turbines.

Table 1. An overview of methods for short-term wind power prediction

Short-Term Wind Power Prediction Models
Adaptive Neural Fuzzy System [30]
Local Polynomial Regression [31]
Bayesian Clustering by Dynamics (BCD) [32]
Support Vector Machines [33]
Mixture of Experts [33]
Locally Recurrent Neural Networks [3]
Autoregressive with Exogenous input (ARX) [34]
Autoregressive with Exogenous Input and Multi-timescale Parameter (ARXM) [35]
Random Forests [36]
Neural Networks [37]

3. WIND POWER PREDICTION MODEL

3.1 Proposed Wind Power Prediction Method

In this research paper, a short term wind power forecasting using feed forward back propagation neural network (FFNN) is presented. The basic data sources for wind power prediction are historical measurement records of wind turbine SCADA system database and numerical weather prediction (NWP). To construct the model the forecasting system used historical measurement records of SCADA system database from a real wind power system ('Goldwind microgrid wind turbine system', Beijing, China).

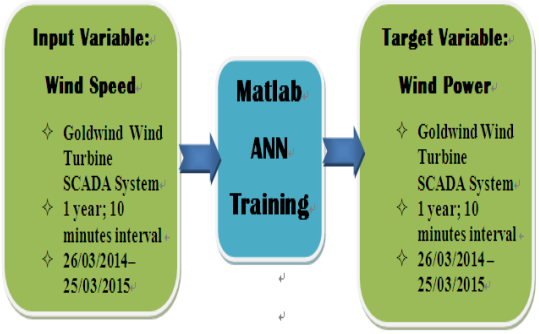

Figure 1. Block diagram illustration of ANN training

The ANN wind forecasting model has been trained utilizing 12 months data with 10 minutes interval provided from Goldwind wind turbine SCADA system. SCADA recorded wind speed and wind power data have been used as the network training input and target respectively as shown in Figure 1.

In the process of modeling, historical data provided from SCADA are used to train an ANN that effectively can estimate a transfer function between the specific patterns of input and output vectors.

Finally, the forecasted wind speed data provided from NWP model (WRF) projected around the vicinity of the wind farm has been preprocessed and applied to the developed (trained) ANN forecasting model in order to estimate wind power for the next 24 hours of the next day on 10 minutes interval basis as shown in Figure 2.

3.2 Online SCADA System

SCADA system as the nerve center and inseparable element of the wind farm plays a vital role for the prediction system. Usage of an online SCADA gives the operator freedom to oversee wind farm by supervising all of the wind turbines. This opportunity is provided for operator to set proper actions in critical situations by a 10 minutes record of the wind park turbines' information.

Moreover, this supervision system provides a comprehensive record of the wind speed and output powers as well as availability of turbines, which acts as a foundation for the short term wind power forecasting.

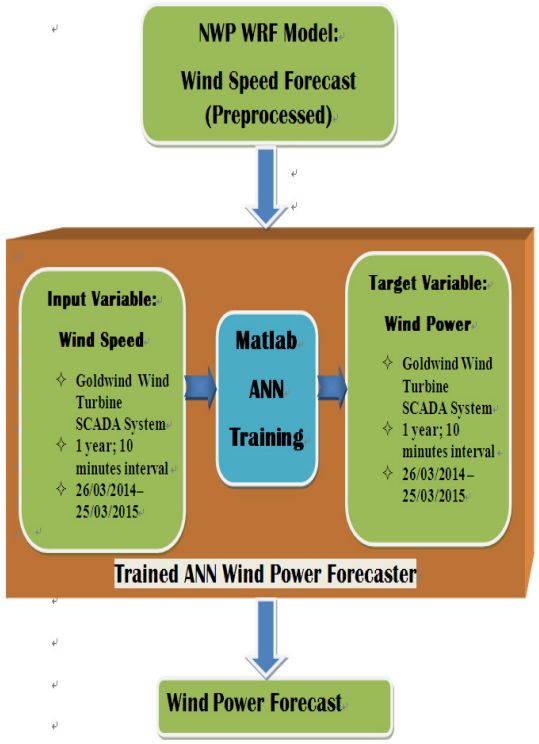

Figure 2. Block diagram illustration of ANN wind power forecaster for next day

3.3 Numerical Weather Prediction (NWP) Model

Nowadays, wind data has a non-negligible impact on wind power prediction. There are several approaches to obtain the wind data: observations, data mining and numerical weather simulations. The most straightforward and reliable way to obtain wind data is through on-site observations. However, they are not usually available.

Data mining is flexible, but its ability to downscale the weather data is limited. The NWP models use physical conservation of energy equations and this allows a more realistic downscaling of the data. In fact, high-resolution NWP of wind plays the key role for power forecasting.

In recent years, regarding availability of enhanced computational systems, many wind power estimation researches are directed utilizing NWP models wind data. This researchers use several NWP models like WRF, COSMO, MM5, and RAMS [30] - [33]. Also, various methods of extrapolation such as logarithmic law and wind shear power law have proposed by authors to provide appropriate wind information at the height of wind turbine hub (*i.e.* approximately 50 m) using meteorological data that are gathered at 10 m above of the ground (According to World Meteorological Organization (WMO) approval)[19].

4. PROPOSED FRAMEWORK OF ANN

4.1 Overview of ANN

Neural network is a powerful data modeling tool that is able to capture and represent the complex input/output relationships. An Artificial Neural Network (ANN) is an information processing paradigm that is inspired by the way

biological nervous systems, such as the brain, process information. The key element of this paradigm is the novel structure of the information processing system. It is composed of a large number of highly interconnected processing elements (neurons) working in unison to solve specific problems [45].

ANNs, like people, learn by example. An ANN is configured for a specific application, such as pattern recognition or data classification, through a learning process. Learning in biological systems involves adjustments to the synaptic connections that exist between the neurons. This is true of ANNs as well. And for the validation process ANN is followed, the human brain provides proof of the existence of massive neural networks that can succeed at those cognitive, perceptual, and control tasks in which humans are successful [45].

An illustrative representation of a multi-layer neural network is shown in Figure 3.

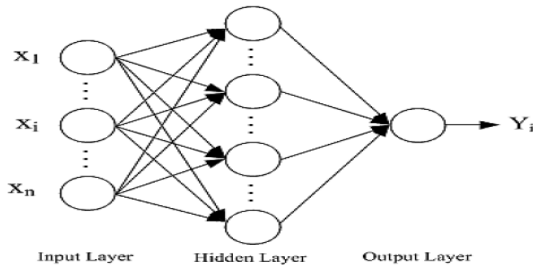

Figure 3. Multi-layer neural network

Where X_i the i^{th} input to the node (neuron) and Y_i is the output of the node.

The mathematical equation which shows the relationship between the inputs X_i to the network and the output Y_i of the network is given by equations (1) below.

$$Y_i = f_i\left(\sum_{j=1}^{n} W_{ij} X_j + b_i\right) \quad (1)$$

Where X_j is the j^{th} input to the node, Y_i is the output of the node, W_{ij} is the connection weight between the input node and output node, b_i is the bias of the node, and f_i is known as activation function that determines the property of the neural network.

The mean squared error (MSE) of the network is defined by equations (2) below.

$$MSE = \frac{1}{N}\sum_{i=1}^{N} (T_i - Y_i)^2 \quad (2)$$

Where T_i is the target at i^{th} pattern, Y_i is the prediction of the network's output at i^{th} pattern and N is the number of training set samples.

4.2 ANN Learning: Back Propagation Algorithm

There are different types of training algorithms used for ANN learning; this paper used the Levenberg-Marquardz back propagation supervised training algorithm which is described in Figure 4 below.

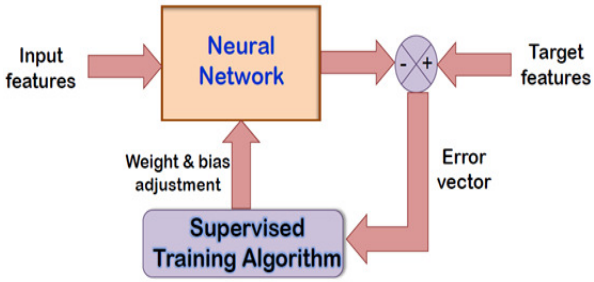

Figure 4. Back propagation supervised training algorithm

The back propagation algorithm cycles through two distinct passes, a forward pass followed by a backward pass through the layers of the network. The algorithm alternates between these passes several times as it scans the training data as described below [44]:

Forward Pass: Computation of outputs of all the neurons in the network

- The algorithm starts with the first hidden layer using as input values the independent variables of a case from the training data set.
- The neuron outputs are computed for all neurons in the first hidden layer by performing the relevant sum and activation function evaluations.
- These outputs are the inputs for neurons in the second hidden layer. Again the relevant sum and activation function calculations are performed to compute the outputs of second layer neurons.

Backward pass: Propagation of error and adjustment of weights

- This phase begins with the computation of error at each neuron in the output layer. A popular error function is the squared difference between Y_i the output of node i and T_i the target value for that node.
- This error value is calculated continuously for each data point in the training data set, and the new value of the weight W_{ij} of the connection from node i to node j is adjusted continuously until the error value reaches zero or falls below a certain threshold value.
- The backward propagation of weight adjustments along these lines continues until we reach the input layer.
- At this time we have a new set of weights on which we can make a new forward pass when presented with a training data observation.

4.3 Wind Power Forecasting Accuracy Measures

In order to evaluate the accuracy of the wind power prediction, the mean absolute error (MAE) and the mean absolute error percentage (MAPE) can be used. These criterions are defined as follows:

$$MAE = \frac{1}{N}\sum_{h=1}^{N} \left| P_h^{\,a} - P_h^{\,f} \right| \quad (3)$$

$$MAPE = \frac{100\%}{N} \sum_{h=1}^{N} \left| \frac{P_h^a - P_h^f}{P_h^a} \right| \quad (4)$$

Where P^a_h and P^f_h are the actual and forecasted wind power, respectively, at period h, and N corresponds to the number of forecasted periods. The MAE is an average of the absolute errors. In MAPE the absolute values of all the percentage errors are added and the average is computed, producing a measure of relative overall fit.

Another criterion that may be used is the standard deviation (SD) that represents a measure of how spread out the numbers is.

$$SD = \sqrt{\frac{1}{N-1} \sum_{h=1}^{N} (P^f{}_h - \overline{P})} \quad (5)$$

Where $\overline{P}$ is the wind power average.

The root mean square error (RMSE) is another frequently used measure of the differences between forecasted and the actual observed values. The RMSE is the square root of the variance. RMSE gives a relatively high weight to large errors.

$$RMSE = \sqrt{\frac{1}{N} \sum_{h=1}^{N} (P^a{}_h - P^f{}_h)^2} \quad (6)$$

The RMSE is most useful when large errors are particularly undesirable. The MAE and the RMSE can be used together to diagnose the variation in the errors in a set of forecasts [46]. The RMSE will always be larger or equal to the MAE; the greater difference between them, the greater the variance in the individual errors in the sample [46]. In this case study the MAE, RMSE and SD have been used.

5. CASE STUDY AND RESULTS

In order to evaluate performance of the proposed wind power forecasting scheme, the prediction model was built for the Goldwind microgrid wind farm, Beijing, China. This wind farm has a single wind turbine with generating capacity of 2500KW.

The wind speed and power time series of this wind farm are recorded from the 26th March 2014 to the 25th March 2015. The forecasting information is given for the next 4 days (26th March 2015 to the 29th March 2015) for every 10 minutes intervals.

The following figures present the system performance (testing of the wind power forecasting model) in the period of 26th to 29th March 2015.

Figures 5–8 show the comparison of the actual Goldwind wind turbine output power with those of the predicted output power for Goldwind microgrid wind turbine system for each of the four days ahead (26/03/2015 – 29/03/2015) of the last training date (25/03/2015) on 10 minutes time-interval basis.

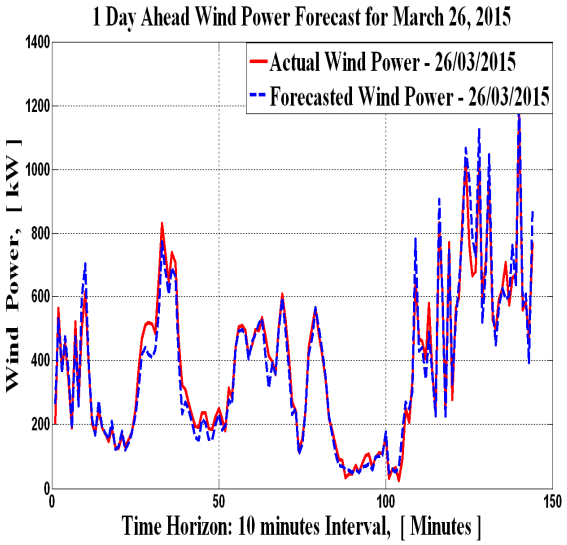

Figure 5. One Day-Ahead Wind Power Forecast for 26/3/2015

Simulation results have shown that the predicted Goldwind microgrid wind turbine output power is almost similar with the actual wind power recorded by the SCADA which indicates the effective performance of the ANN wind power forecaster model that has been developed in the paper.

Table 2 presents the forecasting errors that have been calculated for each day's forecasting simulation. In order to evaluate the accuracy of the wind power prediction model developed in this paper, it was considered the mean absolute error (MAE), the root mean square error (RMSE), and the mean absolute percentage error (MAPE) as reported in section 4.

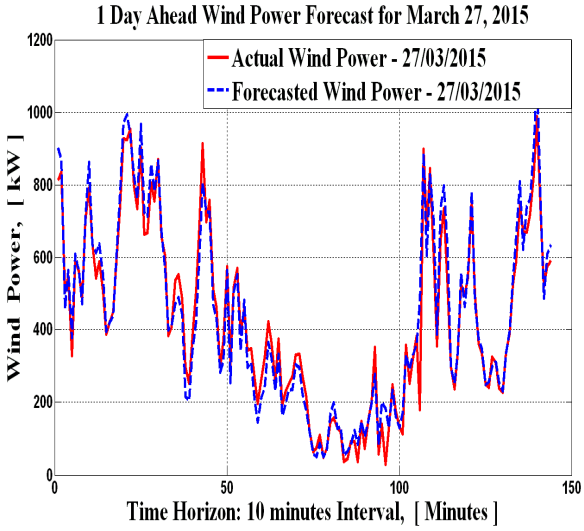

Figure 6. One Day-Ahead Wind Power Forecast for 27/3/2015

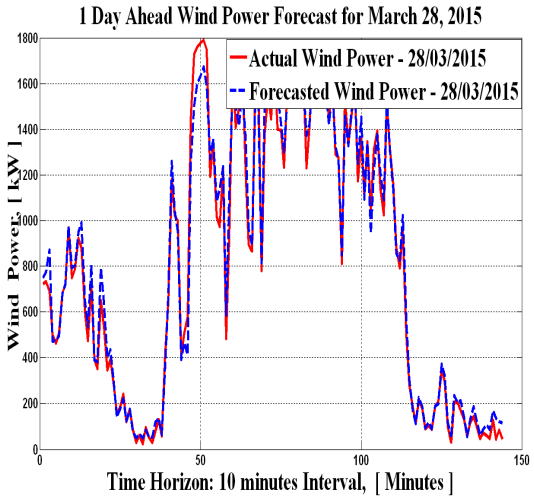

Figure 7. One Day-Ahead Wind Power Forecast for 28/3/2015

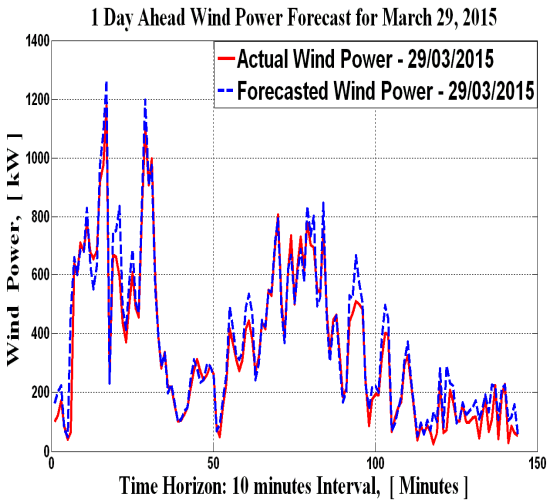

Figure 8. One Day-Ahead Wind Power Forecast for 29/3/2015

Table 2. Wind power forecasting errors of each day

Prediction Day	Prediction Accuracy Measures		
	MAE (KW)	RMSE (KW)	MAPE (%)
March 26, 2015	35.8767	50.4804	12.1620
March 27, 2015	39.2858	53.4004	15.5106
March 28, 2015	52.2056	72.5210	12.0655
March 29, 2015	41.4318	65.7079	15.6206

Prediction values of error obtained by method proposed in [6] is 17% for 24h ahead (one day ahead or 144 ten minute intervals ahead) from a specific day. While, this error values for the presented paper are 12.1620% for March 26, 2015, 15.5106% for March 27, 2015, 12.0655% for March 28, 2015 and 15.6206% for March 29, 2015 that are severely lower than [6].

Moreover, the MAE and RMSE values presented in Table 2 have shown less error values than most of the literatures reported in this paper.

Results indicate that proposed method enjoys significantly effective performance for 24h (144 ten minute intervals) ahead wind power forecasting.

6. CONCLUSIONS

In this research paper, a short term wind power prediction model, for day-ahead resource scheduling in microgrids, is proposed based on feed forward ANN for each 24 hours of the next day.

The proposed ANN prediction model is developed utilizing SCADA records of an actual wind farm ('Goldwind microgrid wind turbine system', Beijing, China) with a total installed power of 2500KW on Matlab neural network fitting tool using one year ten minutes interval data (26/03/2014 – 25/03/2015) taken from Goldwind wind turbine SCADA system.

This model was tested to predict Goldwind wind turbine output power for four days ahead of the last training date (26/03/2015 – 29/03/2015) and the results of the prediction have been compared with the actual output power of Goldwind wind turbine system. Finally, the forecasted wind speed data provided from NWP model (WRF) projected around the vicinity of the wind farm has been preprocessed and applied to the developed (trained) ANN forecasting model in order to estimate wind power for the 24 hours of the next day on 10 minutes interval.

As demonstrated by the prediction results and the prediction error measures above, the predicted wind power has insignificant error and acceptable agreement with the actual wind power taken from Goldwind wind turbine SCADA system which shows the robustness and accuracy of the ANN wind power forecasting model developed in this paper. The model has resulted in desirable prediction accuracy and therefore, the forecasted wind power can be used as one of the input quantities for day-ahead resource scheduling in microgrids with high wind energy penetration.

7. REFERENCES

[1] J. Juban, N. Siebert and G. N. Kariniotakis "Probabilistic short-term wind power forecasting for the optimal management of wind generation", in *Proc*. 2007 IEEE Lausanne Power tech, vol. 15, pp.683 - 688 , 2007.

[2] M. C. Alexiadis, P. S. Dokopoulos, and H. S. Sahsamanoglou, "Wind speed and power forecasting based on spatial correlation models," *IEEE Transactions on Energy Conversion*, vol. 14, no. 3, pp. 836–842, Sep. 1999.

[3] T. G. Barbounis, J. B. Theocharis, M. C. Alexiadis, and P. S. Dokopoulos, "Long-term wind speed and power forecasting using local recurrent neural network models," *IEEE Transactions on Energy Conversion*, vol. 21, no. 1, pp. 273–284, 2006.

[4] L. Landberg, G. Giebel, H. A. Nielsen, T. Nielsen, and H. Madsen, "Short-term prediction-an overview," *Wind Energy*, vol. 6, no. 3, pp. 273-280, 2003.

[5] G. Giebel , L. Landberg , G. Kariniotakis and R. Brownsword "State-of-the-art on methods and software tools for short-term prediction of wind energy production", in *Proc*. EWEC, 2003.

[6] G. Sideratos and N. D. Hatziargyriou, "An advanced statistical method for wind power forecasting," *IEEE Transactions on Power Systems*, vol. 22, pp. 258-265, 2007.

[7] A. Costa, A. Crespo, J. Navarro, G. Lizcano, H. Madsen, and E. Feitosa, "A review on the young history of the wind power short-term prediction," *Renewable & Sustainable Energy Reviews*, vol. 12, pp. 1725-1744, 2008.

[8] L. Ma, S. Y. Luan, C. W. Jiang, H. L. Liu, and Y. Zhang, "A review on the forecasting of wind speed and generated power," *Renewable & Sustainable Energy Reviews*, vol. 13, pp. 915-920, 2009.

[9] L. Landberg, "Short-term prediction of the power production from wind farms", *Journal of Wind Engineering and Industrial Aerodynamics*, vol. 80, pp. 207-220, 1999.

[10] I. G. Damousis, M. C. Alexiadis, J. B. Theocharis, and P. S. Dokopoulos, "A fuzzy model for wind speed prediction and power generation in wind parks using spatial correlation," *IEEE Transactions on Energy Conversion*, vol. 19, no. 2, pp. 352-361, June 2004.

[11] T.G. Barbounis, J.B. Theocharis, "A locally recurrent fuzzy neural network with application to the wind speed prediction using spatial correlation," *Neuro computing*, vol. 70, pp. 1525-1542, 2007.

[12] Palomares-Salas, J.C., de l a Rosa, J.J.G.,Ramiro, J.G., Melgar, J., et.al, "ARIMA vs. Neural networks for wind speed forecasting", in *Proc*. IEEE International Conference on Computational Intelligence for Measurement Systems and Applications, pp. 129-133, 2009.

[13] L. Shuhui, D. C. Wunsch, E. A. O'Hair, M. G. Giesselmann, "Using neural networks to estimate wind turbine power generation," *IEEE Transactions on Energy Conversion*, vol. 16, no.3, pp. 276-282, Sept. 2001.

[14] R. Blonbou, "Very short-term wind power forecasting with neural networks and adaptive Bayesian learning", *Renewable Energy*, pp. 1118–1124, 2011.

[15] J.P.S. Catalao, H.M.I. Pousinho, V.M.F. Mendes, "Short-term wind power forecasting in Portugal by neural networks and wavelet transform", *Renewable Energy*, pp. 1245-1251, 2011

[16] G. Sideratos and N. Hatziargyriou, "Using radial basis neural networks to estimate wind power production," in *Proc*. IEEE Power and Energy Soc. General Meeting, pp. 1-7, 2007.

[17] P. Louka, G. Galanis, N. Siebert, G. Kariniotakis, P. Katsafados, I. Pytharoulis and G. Kallos, "Improvements in wind speed forecasts for wind power prediction purposes using Kalman filtering," *Journal of Wind Engineering and Industrial Aerodynamics*, vol.96, pp. 2348-2362, 2008.

[18] D. Ying, J. Lu, Q. Li, "Short-term wind speed forecasting of wind farm based on least square-support vector machine," *Power Systems Technology*, vol.32, no. 15, pp. 62-66, 2008.

[19] Y. Charabi "Arabian summer monsoon variability: teleconexion to ENSO and IOD", *Atmospheric Research*, pp. 105–117, 2009.

[20] P. Pinson, L.E.A. Christensen, H. Madsen, P. Sørensen, M.H. Donovan, and L.E. Jensen,"Regime-switching modelling of the fluctuations of offshore wind generation," *Journal of Wind Engineering & Industrial Aerodynamics*, vol. 96, no. 12, pp. 2327–2347, 2008.

[21] G. Kariniotakis, E. Nogaret, and G. Stavrakakis, "Advanced Short-Term Forecasting of Wind Power Production," in *Proc*. European Wind Energy Conference EWEC'97, Ireland, pp. 751–754, October 1997.

[22] I.G. Damousis and P. Dokopoulos, "A fuzzy model expert system for the forecasting of wind speed and power generation in wind farms," in *Proc*. IEEE International Conference on Power Industry Computer Applications PICA 01, pp. 63–69, 2001.

[23] I.J. Ramírez-Rosado and L.A. Fernández-Jiménez, "Next-day wind farm electric energy generation forecasting using fuzzy time-series," in *Proc*. International Conference on Modeling, Identification, and Control, Innsbruck, Austria, pp. 237–240, 2003.

[24] G. Kariniotakis, E. Nogaret, A.G. Dutton, J.A. Halliday, and A. Androutsos, "Evaluation of Advanced Wind Power and Load Forecasting Methods for the Optimal Management of Isolated Power Systems," in *Proc*. European Wind Energy Conference EWEC'99, pp. 1082–1085, Nice, France, March 1–5, 1999.

[25] E.A. Bossanyi, "Short-Term Wind Prediction Using Kalman Filters," *Wind Engineering*, vol. 9, no. 1, pp. 1–8, 1985.

[26] S. Alpay, L. Bilir, S. Ozdemirny, and B. Ozerdem, "Wind speed time series characterization by Hilbert transform," *International Journal of Energy Research*, vol. 30, pp. 359–364, 2006.

[27] R.E. Abdel-Aal, M.A. Elhadidy, and S.M. Shaahid, "Modeling and forecasting the mean hourly wind speed

time series using GMDH-based abductive networks," *Renewable Energy*, vol. 34, no. 7, pp. 1686–1699, July 2009.

[28] C.W. Potter and M. Negnevistky, "Very short-term wind forecasting for Tasmanian power generation," *IEEE Transactions on Power Systems*, vol. 21, no. 2, pp. 965–972, 2006.

[29] T.H.M. El-Fouly, E.F. El-Saadany, and M.M.A. Salama, "Grey Predictor for Wind Energy Conversion Systems Output Power Prediction," *IEEE Transactions on Power Systems*, vol. 21, no. 3, pp. 1450–1452, 2006.

[30] M. Negnevitsky, P. Johnson, and S. Santoso, "Short term Wind Power Forecasting using hybrid intelligent systems," in *Proc*. IEEE Power Engineering Society General Meeting, pp. 1–4, June 24–28, 2007.

[31] Ismael Sanchez, "Short-term prediction of wind energy production," *International Journal of Forecasting*, vol. 22, no. 1, pp. 43–56, 2006.

[32] Shu Fan, James R. Liao, Ryuichi Yokoyama, and Luonan Chen, "Forecasting the Wind Generation Using A Two-stage Hybrid Network Based on Meteorological Information," Information and Communications Engineering, Osaka Sangyo University, 2006.

[33] R. Jursa, "Wind power prediction with different artificial intelligence models," in *Proc*. European Wind Energy Conference EWEC'07, Milan, Italy, May 2007.

[34] Mario J. Duran, Daniel Cros, and Jesus Riquelme, "Short-Term Wind Power Forecast Based on ARX Models," *Journal of Energy Engineering*, vol. 133, no. 3, pp. 172–180, Sept. 2007.

[35] A. Yamaguchi, T. Ishihara, K. Sakai, T. Ogawa, and Y. Fujino, "A Physical-Statistical Approach for the Regional Wind Power Forecasting," in *Proc*. European Wind Energy Conference EWEC'07, Milan, Italy, 2007.

[36] Lionel Fugon, Jérémie Juban, and G. Kariniotakis, "Data mining for Wind Power Forecasting," in *Proc*. European Wind Energy Conference EWEC'08, Brussels, Belgium, April 2008.

[37] A. Kusiak, H.-Y. Zheng, and Z. Song, "Wind Farm Power Prediction: A Data-Mining Approach," *Wind Energy*, vol. 12, no. 3, pp. 275–293, 2009.

[38] Kariniotakis, G.N., Pinson, P., "Uncertainty of short-term wind power forecasts a methodology for on-line assessment", in *Proc*. 2004 International Conference on Probabilistic Methods Applied to Power Systems, pp. 729-736, 2004.

[39] J. Connors, D. Martin, and L. Atlas, "Recurrent neural networks and robust time series prediction", *IEEE Transactions on Neural Networks*, vol. 5, pp. 240 - 254, 1994.

[40] E. Atashpaz-Gargari and C. Lucas, "Imperialist Competitive Algorithm: An Algorithm for Optimization Inspired by Imperialistic Competition", in *Proc*. IEEE Congress on Evolutionary Computation (CEC 2007), pp. 4661-4667, 2007.

[41] Sh. Mollaiy Berneti, M. Shahbazian, "An Imperialist Competitive Algorithm Artificial Neural Network Method to Predict Oil Flow Rate of the Wells", *International Journal of Computer Applications*, 2011.

[42] National Climate Data and Information Archive, [On-line]. Available: http://www.climate.weatheroffice.gc.ca

[43] Ghadi, M. Jabbari, S. Hakimi Gilani, H. Afrakhte, and A. Baghramian, "A novel heuristic method for wind farm power prediction: A case study", *International Journal of Electrical Power & Energy Systems*, 2014.

[44] ocw.mit.edu

[45] ijecs.in

[46] www.eumetcal.org.uk

[47] stonito.com

[48] M. Jabbari, Ghadi, S. Hakimi Gilani, H. Afrakhte and A. Baghramian, "Short-Term and Very Short-Term Wind Power Forecasting Using a Hybrid ICA-NN Method," *International Journal of Computing and Digital Systems*, vol. 3, No. 1, 63-70 (2014).

International Journal of Science and Engineering Applications
Volume 5 Issue 3, 2016, ISSN-2319-7560 (Online)

Power System Stabilizer Design for Multi-machine Power System Using Genetic Algorithm

Abinet Tesfaye
School of Electrical and Electronic Engineering, North China Electric Power University, and Goldwind and Etechwin Electric Co., Ltd
Beijing, China

Dereje Shiferaw
Department of Electrical and Computer Engineering, Adama Science and Technology University
Adama, Ethiopia

J. H. Zhang
School of Electrical and Electronic Engineering, North China Electric Power University
Beijing, China

D. H. Zheng
Goldwind and Etechwin Electric Co., Ltd
Beijing, China

Abstract: This paper uses genetic algorithm (GA) framework integrated with the classical Lyapunov's parameter optimization method employing an Integral of Squared Error (ISE) criterion to optimally tune the parameters of the power system stabilizers (PSSs) for a multi-machine system, consisting of three machines and ten interconnected buses, which is taken from the national electric power grid of Ethiopia. The issue of optimally tuning the parameters of the PSS is converted into an optimization problem that is solved via the GA algorithm. Within the GA process, a potential solution – the PSS parameter setting – is coded as an individual, which is part of a population of such potential solutions randomly generated, and by applying the survival of the fitness principle based on each individual's fitness with respect to the objective, a sound basis for finding the best individual, i.e. global optimum solution, is created. Simulation results are presented to show the effectiveness of the proposed approach, for various system loading conditions and other disturbances such as perturbation in mechanical torque inputs to the machines, and have been performed with satisfactory results with the design and integration of PSS to the power system investigated in this paper.

Keywords: Dynamic stability, electromechanical oscillations, genetic algorithm (GA), Integral of Squared Error (ISE), Lyapunov equation, power systems, power system stabilizers (PSSs).

1. INTRODUCTION

PSSs are auxiliary control devices on synchronous generators, used in conjunction with their excitation systems to provide control signals toward enhancing the system damping of electromechanical oscillations and extending power transfer limits, thus maintaining reliable operation of interconnected power systems.

Up to now conventional PSSs (CPSSs) are used in the industry because of their simplicity and their relatively good performance around the nominal operating point (Rogers, 2000).

However, conventional PSS based on a single operating condition cannot maintain adequate system stability over a wide range of operating conditions. In many instances, inadequate tuning procedures of PSS based on the sequential design have led to the destabilization of the entire system (Rogers, 2000). There is a need to find a systematic tuning procedure of PSS so as to achieve optimum parameter settings over a wide range of operating conditions [16].

Genetic algorithm based applications to tune the parameters of PSS have been reported in [5]-[8]. A GA based optimization method has been used in [6] to tune the parameters of a rule-based PSS; this way, the advantages of the rule-based PSS such as its robustness, less computational burden and ease of realization are maintained. Introduction of GAs helps obtain an optimal tuning for all PSS parameters simultaneously, which thereby takes care of interactions between different PSS [21].

In [7], simultaneous tuning for all the PSS in the system using a GA based approach has been developed. The GA seeks to shift all eigenvalues of the system within a region in the stable domain. In [8], a multiobjective design of PSSs in a multi-machine power system operating at various loading conditions and system configurations is achieved using a GA search process. A multiobjective problem is formulated to optimize a

composite set of objective functions comprising the damping factor, and the damping ratio of the lightly damped electromechanical modes, and the effectiveness of the suggested technique is confirmed through eigenvalue analysis and nonlinear simulation results.

Zhang and Coonick [5] proposed a GA based computational procedure to select PSS parameters simultaneously in multi-machine power systems, by solving a set of inequalities that represent the objectives of optimization problem.

In [8], a GA based tuning technique of fixed structure damping controllers over a prespecified set of operating conditions is proposed and demonstrated for large-scale realistic systems. It is emphasized here the importance of an accurate fitness function and the fact that a power system expert's input in the designing stage of the optimization process is very important, and sometimes required to select the best solution out of a pool of solutions resulted from the algorithm [24].

The proposed method, in this research paper, integrates the classical parameter optimization approach, involving the solution of Lyapunov equation, within a genetic search process. The method ensures that for any operating condition within a pre-defined domain, the system remains stable when subjected to small perturbations. The optimization criterion employs a quadratic performance index that measures the quality of system dynamic response within the tuning process. The solution thus obtained is globally optimal and robust. The proposed method has been tested on the lead-lag type PSS structure. System dynamic performances with PSS tuned using the proposed technique are satisfactory for different load conditions and system configurations both for the nominal and off-nominal operating conditions.

The paper is organized as follows: Section 2 introduces the dynamic stability model of the power system. Section 3 describes an overview of genetic algorithm. Designing the PSSs and optimal tuning of the parameters is described in section 4. Eigenvalue analysis and time domain simulations are provided in section 5, and the paper is concluded in section 6.

2. SYSTEM MODEL

The system considered in this paper is a three machine ten-bus power system taken from the national electric power grid of Ethiopia. It comprises of three synchronous generators (MEWA, AWASH2, and KOKA) which are interconnected together through a distribution and transmission network of ten buses in a ring network topology as shown in Figure 1.

Each machine is represented by the two-axis model (d-q axis). The machines are equipped with a simple AVR (Yu, 1983). The dynamics of the system are described by a set of nonlinear differential equations. However, for the purpose of controller design, these equations are linearized around the nominal operating conditions [16].

The transfer function block diagram in Figure 2 describes the dynamics of the i^{th} machine in a multi-machine power system [10], where $\Delta\omega_i$ is the angular speed deviation, $\Delta\delta_i$ is rotor angle deviation, $\Delta E'_{qi}$ is q-axis transient air-gap voltage deviation, ΔE_{fdi} is excitation voltage deviation, ΔT_{mi} is mechanical torque deviation, ΔT_{ei} is electrical torque deviation, T'_{doi} is d-axis transient time constant, K_{Ai} is excitation system gain, T_{Ai} is excitation system time constant, M_i is inertia constant of the i^{th} machine.

This is a generalization of the extensively used single machine connected to its terminal bus or infinite bus transfer function block diagram [2] and takes into account the interaction between machines via **K** matrices, which are square matrices with order equal to the number of generators (n_g).

These **K** matrices are derived from the electric torque expression (K1, K2), field winding circuit equation (K3, K4), and from the terminal voltage magnitude (K5, K6), and the diagonal elements of the **K1, K2**, … , **K6** matrices determine the machine's dynamics, while the off-diagonal elements model the dynamic interactions between machines. Observe that in this block diagram the PSS is not represented, for convenience [19].

The number of state variables is n_v x n_g, where n_v is the number of state variables used to model one machine and its excitation system.

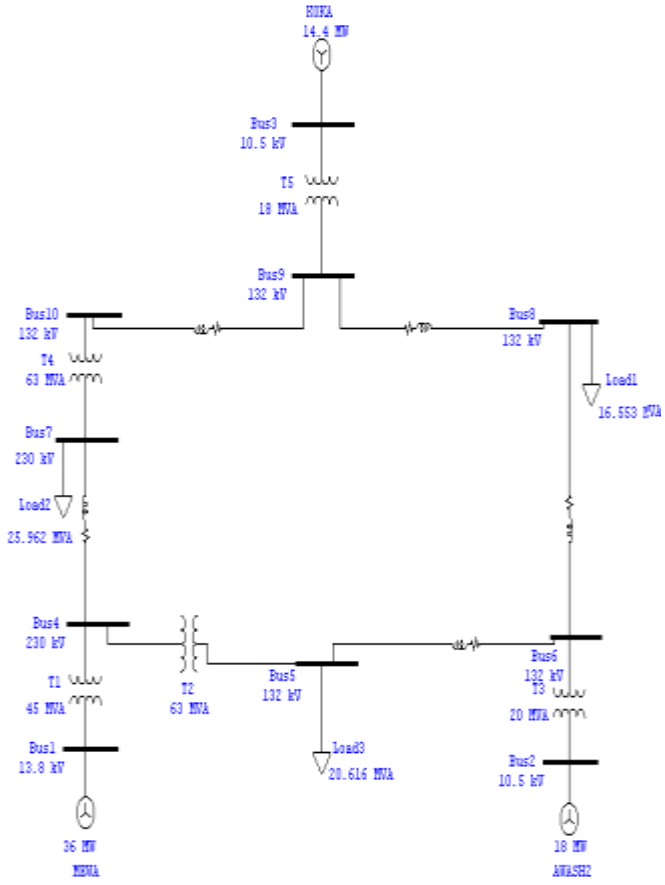

Figure 1. Three-machine ten-bus power system (Source: Ethiopian National Electric Power Grid)

Based on the transfer function block diagram (Figure 2), the system dynamics can be expressed by a set of linear differential equations in the small-perturbation variables $\Delta\omega_i$, $\Delta\delta_i$, $\Delta E'_{qi}$, ΔE_{fdi} as follows:

$$\begin{aligned}
\frac{d}{dt}(\Delta\omega_i) &= \frac{D_i}{M_i}\Delta\omega_i - \frac{K_{1i}}{M_i}\Delta\delta_i - \frac{K_{2i}}{M_i}\Delta E'_{qi} + \frac{1}{M_i}\Delta T_{mi} \\
\frac{d}{dt}(\Delta\delta_i) &= 2\pi f\Delta\omega_i \\
\frac{d}{dt}(\Delta E'_{qi}) &= -\frac{K_{4i}}{T'_{doi}}\Delta\delta_i - \frac{1}{T'_{doi}K_{3i}}\Delta E'_{qi} + \frac{1}{T'_{doi}}\Delta E_{fdi} \\
\frac{d}{dt}(\Delta E_{fdi}) &= -\frac{K_{Ai}K_{5i}}{T_{Ai}}\Delta\delta_i - \frac{K_{Ai}K_{5i}}{T_{Ai}}\Delta E'_{qi} - \frac{1}{T_{Ai}}\Delta E_{fdi} + \frac{K_{Ai}}{T_{Ai}}\Delta u_{Ei}
\end{aligned} \tag{1}$$

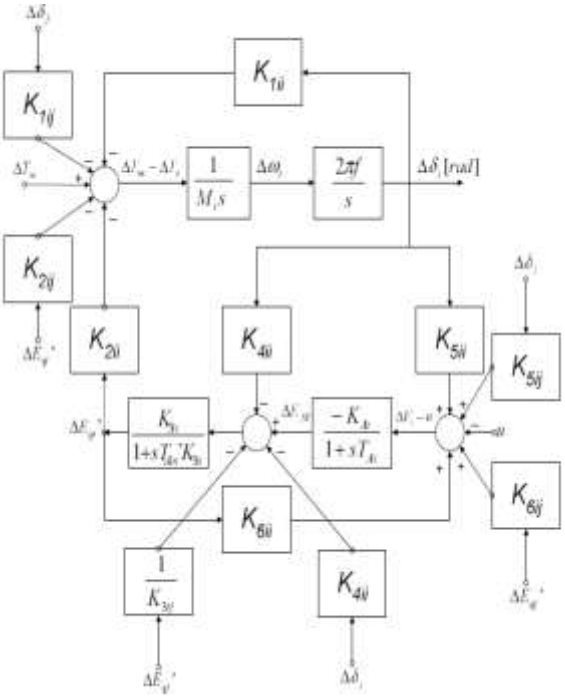

Figure 2. Transfer function block diagram representation of a multi-machine system for small-signal stability analysis

Using vector-matrix notation and the above set of equations (1), the state-space model for the three-machine system is expressed as follows:

$$\frac{d}{dt}\underline{X}(t) = \mathbf{A}.\underline{X}(t) + \mathbf{B}.\underline{U}(t) + \mathbf{\Gamma}.\underline{p}(t) \qquad (2)$$

Where $\underline{X}(t)$, $\underline{U}(t)$ and $\underline{p}(t)$ are state, control and perturbation vectors, respectively and they are expressed as follows:

$$\underline{X}(t) = [\Delta\omega_1(t)\ \ \Delta\delta_1(t)\ \ \Delta E'q_1(t)\ \ \Delta Efd_1(t)\ldots$$
$$\Delta\omega_2(t)\ \ \Delta\delta_2(t)\ \ \Delta E'q_2(t)\ \ \Delta Efd_2(t)\ldots$$
$$\Delta\omega_3(t)\ \ \Delta\delta_3(t)\ \ \Delta E'q_3(t)\ \ \Delta Efd_3(t)]^T$$

$$\underline{U}(t) = [\Delta u_1(t)\ \ \Delta u_2(t)\ \ \Delta u_3(t)]^T$$

$$\underline{p}(t) = [\Delta T_{m1}\ \ \Delta T_{m2}\ \ \Delta T_{m3}]^T$$

A, **B** and **Γ** are the state, control and perturbation matrices, respectively.

3. OVERVIEW OF GENETIC ALGORITHM

Genetic Algorithms are global search techniques providing a powerful tool for optimization problems by miming the mechanisms of natural selection and genetics. These operate on a population of potential solutions applying the principle of survival of the fittest to produce better and better approximations to a solution. In each generation, a new set of approximations is created by selecting the individuals according to their level of fitness in the problem domain and breeding them together using operators borrowed from natural genetics [11]. Thus, the population of solutions is successively improved with respect to the search objective by replacing least fit individuals with new ones (offspring of individuals from the previous generation), better suited to the environment, just as in natural evolution [20].

According to Goldberg [11] and [25], GAs are different from other optimization and search procedures in four ways:

a. GA work with a coding of the parameter set, not the parameters themselves.

b. GA search from a population of points, not a single point.

c. GA use payoff information, not derivatives or other auxiliary knowledge.

d. GA use probabilistic transition rules, not deterministic rules.

Figure 3 shows a flowchart diagram of genetic algorithm.

The process commences with random generation of a pool of possible solutions, i.e. the population and the individuals that form it. Each individual in the population, also called chromosome is represented by a string, which is formed by a number of sub-strings equal to the number of the problem's variables. Each variable is coded in a suitable coding system (binary, integer, real-valued, etc). The population size and the chromosome size are kept constant during the whole search process.

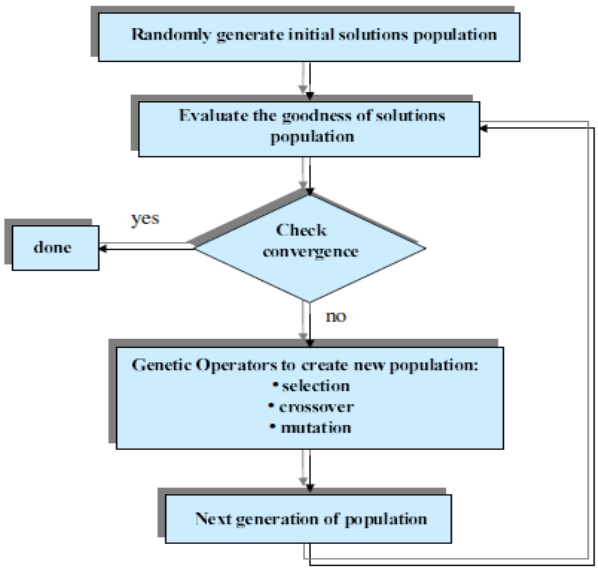

Figure 3. Genetic algorithm flowchart diagram

4. DESIGN OF THE PSS

The main goal of this study is to optimize the parameters of the PSSs such that controllers simultaneously stabilize a family of system models. It was found that a double stage lead-lag network with time constants T_1-T_4 and gain K_c is sufficient to provide adequate damping to the multi-machine power system shown in Figure1.

Optimization techniques based on Lyapunov method and GAs are applied to tune the parameters of a fixed structure lead-lag PSS whose transfer function has the following form (i.e., speed input):

$$G_{PSS}(s) = \frac{\Delta u_i(s)}{\Delta \omega_i(s)} = K_{Ci}.\left[\frac{sT_{Wi}}{1+sT_{Wi}}\right].\left[\frac{1+sT_{1i}}{1+sT_{2i}}\right].\left[\frac{1+sT_{3i}}{1+sT_{4i}}\right] \qquad (3)$$

Where, K_{Ci} is the stabilizing gain, T1-T_4 represent suitable time constants of the lead-lag circuit. T_W is the washout time constant needed to prevent steady-state offset of the voltage.

The block diagram of the lead-lag PSS on the i^{th} machine for dynamic stability studies is shown in Figure 4.

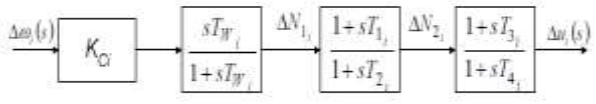

Figure 4. Transfer function block diagram for lead-lag PSS

The PSS parameters to be optimized are the time constants, T_{1i}, T_{2i}, T_{3i}, T_{4i} and gain K_{Ci}. A washout time constant T_{Wi} = 10 seconds is chosen at all machines in order to ensure that the phase-lead and gain contributed by the washout block for the range of oscillation frequencies normally encountered is negligible [4]. The number of PSS parameters to be optimized is reduced by considering the PSS to comprise two identical cascaded lead-lag networks. Therefore, $T_{1i} = T_{3i}$ and $T_{2i} = T_{4i}$. Also, $T_{2i} = T_{4i} = 0.05$ seconds is assumed fixed from physical realization considerations [2]. Thus, the optimization problem reduces to determining T_{1i} and K_{Ci} (i = 1, ... , n) only.

4.1 Conventional Design of Lead-Lag PSS (CPSS)

For the sake of clarity, the state-space model of the multi-machine system without PSS is re-stated below:

$$\frac{d}{dt}\underline{X}(t) = \mathbf{A}.\underline{X}(t) + \mathbf{B}.\underline{U}(t) + \mathbf{\Gamma}.\underline{p}(t) \quad (4)$$

A, **B** and **Γ** are the state, control and perturbation matrices. The associated state, control and perturbation vectors are given below:

$$\underline{X}(t) = [\Delta\omega_1(t)\ \ \Delta\delta_1(t)\ \ \Delta E'q_1(t)\ \ \Delta Efd_1(t)\ldots$$
$$\Delta\omega_2(t)\ \ \Delta\delta_2(t)\ \ \Delta E'q_2(t)\ \ \Delta Efd_2(t)\ldots$$
$$\Delta\omega_3(t)\ \ \Delta\delta_3(t)\ \ \Delta E'q_3(t)\ \ \Delta Efd_3(t)]^T$$

$$\underline{U}(t) = [\Delta u_1(t)\ \ \Delta u_2(t)\ \ \Delta u_3(t)]^T$$

$$\underline{p}(t) = [\Delta T_{m1}\ \ \Delta T_{m2}\ \ \Delta T_{m3}]^T$$

The control vector $\underline{U}(t)$ is a vector of stabilizing signals that represents the PSS output at different machines.

The dynamic equations of the PSS in state-space form, as obtained from the transfer function block-diagram (Figure 4), are given below:

$$\frac{d}{dt}(\Delta N_{1i}(t)) = K_{Ci}\frac{d}{dt}(\Delta\omega_i) - \frac{1}{T_{Wi}}\Delta N_{1i}(t)$$
$$\frac{d}{dt}(\Delta N_{2i}(t)) = \left[\Delta N_{1i}(t) - \Delta N_{2i}(t) + T_{1i}\frac{d}{dt}(\Delta N_{1i}(t))\right].\frac{1}{T_{2i}} \quad (5)$$
$$\frac{d}{dt}(\Delta u_i(t)) = \left[\Delta N_{2i}(t) + T_{3i}\frac{d}{dt}(\Delta N_{1i}(t)) - \Delta u_i(t)\right].\frac{1}{T_{4i}}$$
$$\forall i = 1,2,3$$

where ΔN_{1i} and ΔN_{2i} are the state-variables associated with each PSS. T_{Wi} is the washout time constant, T_{1i}, …, T4i are the phase-lead time constants and K_{Ci} is the stabilizer gain of the PSSs corresponding to each synchronous generator in the power system.

Equations (5) above may be arranged in standard vector-matrix form as shown in (6), which represents the state-space model of the system with PSSs at all machines:

$$\frac{d}{dt}\underline{X}_{PSS}(t) = \mathbf{C}.\underline{X}(t) + \mathbf{D}.\underline{X}_{PSS}(t) + \mathbf{\Gamma}_1.\mathrm{p} \quad (6)$$

where,

$$\underline{X}_{PSS}(t) = [\Delta N_{11}(t)\ \ \Delta N_{21}(t)\ \ \Delta u_1(t)\ldots$$
$$\Delta N_{12}(t)\ \ \Delta N_{22}(t)\ \ \Delta u_2(t)\ldots$$
$$\Delta N_{13}(t)\ \ \Delta N_{23}(t)\ \ \Delta u_3(t)]^T$$

C, **D** and $\mathbf{\Gamma_1}$ are the matrices associated with the PSS model with appropriate dimensions.

By defining the following augmented state-vector

$$\underline{X}_C(t) = [\underline{X}(t)\ \ \ \underline{X}_{PSS}(t)]^T$$

The state-space model of the closed-loop system (composite system) becomes:

$$\frac{d}{dt}\underline{X}_C(t) = \mathbf{A}_C.\underline{X}_C(t) + \mathbf{\Gamma}_C.\underline{p} \quad (7)$$

where $\mathbf{A}_C = \begin{bmatrix} A & B_1 \\ C & D \end{bmatrix}$, and $\mathbf{\Gamma}_C = [\Gamma\ \ \ \Gamma_1]^T$

$\mathbf{B_1}$ in $\mathbf{A_C}$ is a re-defined control matrix, with $\underline{b}_1$, $\underline{b}_2$, $\underline{b}_3$ the column vectors of **B**.

$$\mathbf{B}_1 = [\underline{0}\ \ \underline{0}\ \ \underline{b}_1\ \ \underline{0}\ \ \underline{0}\ \ \underline{b}_2\ \ \underline{0}\ \ \underline{0}\ \ \underline{b}_3]$$

By applying the coordinate transformation in the state-space given in (8), the perturbation term in (7) can be eliminated.

$$\underline{X}'(t) = \underline{X}_C(t) - \underline{X}_C(\infty) \quad (8)$$

Hence, (7) reduces to the standard state-variable form:

$$\frac{d}{dt}\underline{X}'(t) = \mathbf{A}_C.\underline{X}'(t) \quad (9)$$

where $\underline{X}'(0) = -\underline{X}(\infty) = -\mathbf{A_C}.\mathbf{\Gamma}_C.\underline{\mathbf{P}}$ is the initial state of $\underline{X}'(t)$, which is also the steady-state value of $\underline{X}(t)$.

Conventionally, the PSS tuning methods used for multi-machine systems have either used a sequential approach or a simultaneous approach. The choice of a suitable performance index is extremely important for the design of PSS.

In this work, a performance index as given in (10), where $\underline{X}$ is the state vector, and **Q** – the weighing matrix – is positive semi-definite and comprises the importance attached to different state-variables in the optimization process, has been used.

$$J = \int_0^\infty (X^T.Q.X)dt \quad (10)$$

The performance index J can be evaluated using the relation:

$$J = \underline{X}^T(0).\mathbf{P}.\underline{X}(0) \quad (11)$$

Where $\underline{X}(0)$ is the initial state of the state-vector, and **P** is a positive definite symmetric matrix obtained by solving the following Lyapunov equation:

$$\mathbf{A}^T.\mathbf{P} + \mathbf{P}.\mathbf{A} = -\mathbf{Q} \quad (12)$$

where **A** is the state matrix of the system.

By appropriate choice of **Q** matrix elements, various penalization weights can be assigned to state variables (which in this case are deviations from steady-state conditions) and a desirable dynamic performance for the system can be achieved.

As described in previously, by an appropriate choice of **Q** the performance criterion, and hence the optimal PSS parameters, can be manipulated according to design engineer's requirements. In this work, an Integral of Squared Error (ISE) criterion that seeks to minimize the square of the power angle deviation from its steady-state value (**Δδ**) is chosen. Subsequently, the state variable **Δδ** is penalized for deviations by being assigned a high weight in the **Q** matrix, and the PSS parameters are obtained accordingly.

In the following analysis, the Lyapunov method was applied to multi- machine PSS tuning using the sequential approach.

The weighing matrix **Q** is now the sum of the squares of each machine's power angle deviation from their respective steady-state value. Mathematically, this can be written as:

Thus,

$$\mathbf{Q} = \text{diag}[0\ \ 1\ \ 0\ \ 0 \quad 0\ \ 1\ \ 0\ \ 0 \quad 0\ \ 1\ \ 0\ \ 0], \text{ and}$$

$$J = \int_0^{\infty} \sum_{i=1}^{3} (\Delta\delta_i - \Delta\delta_{iSS})^2 dt \qquad (13)$$

In order to obtain the optimal values of K_C and T_1, the following procedure has been used:

1. Choose a set of PSS parameters for which the state matrix of the composite system (including the PSS) is nonsingular.

2. Fix the value of T_1 and vary K_C over a wide range of values and determine the performance index, using (13). It is observed that for a fixed T_1, when K_C increases, the performance index J decreases continuously attaining a minimum J_{min} and then start increasing again as K_C increases further.

3. Carry out Step-2 for various values of T_1 and determine the minimum $J_{min.}$

Using the approach described in the above steps, the parameters of each PSS can be obtained through a sequential optimization approach. Various combinations of tuning sequences were tried out and the best system performance was obtained with MEWA (Gen-1)–AWASH2 (Gen-2)–KOKA (Gen-3) sequence.

4.2 GA Based Design of Lead-Lag PSS (GA-PSS)

The proposed Lyapunov method based genetic algorithm is initiated by generating randomly an initial population of binary coded individuals, where each individual represents a possible solution for the PSS parameters.

A basic requirement for obtaining a feasible solution to the Lyapunov equation is that the state-matrix **A** should be stable. Fulfillment of this condition is ensured by stability screening. The entire population of individuals in each generation is screened in order to ensure that only those individuals (each of them representing a PSS parameter set) that provide a stable system over the whole operating domain D, are allowed to proceed further in the optimization process.

This also brings about significant reduction in the computational burden. Individuals resulting in unstable systems for an operating point within the domain D ("bad individuals") are assigned a very high value of J_{AVG}, where J_{AVG} is the mean value of performance indices over the N_{op} points of the operating domain D, and given by (14). The bad individuals are gradually phased out from the population within a few generations.

$$J_{AVG} = \frac{1}{N_{op}} \sum_{P,Q} \left(\int_0^{\infty} (X^T.Q.X) dt \right) \qquad (14)$$

$$\forall P, Q \in D$$

Every individual (chromosome) of the current population is evaluated for J_{AVG} and a basis for the biased selection process is then established. To avoid premature convergence and speeding up of the search when the convergence is approached, the objective values obtained for each individual are mapped into fitness values through a ranking process.

The rank-based fitness assignment overcomes the scaling problems of the proportional fitness assignment. The individuals will be ranked in the population in descending order of their fitness with respect to the problem domain. The higher the individual's fitness is, the higher is its chance to pass-on genetic information to successive generations.

The next generation will be populated with offspring, obtained from selected parents. The selection is a process used to determine the number of trials for one particular individual used in reproduction. The selection process uses the stochastic universal sampling method, a single-phase sampling algorithm with minimum spread, zero bias and time complexity in the order of the number of individuals (N_{IND}).

Recombination of the selected individuals is carried out with pairs of individuals from the current population using a multi-point crossover process having a certain probability [19]. The individuals in the pairs will exchange genetic information with each other, thereby creating two new individuals, the offspring. After that, each individual in the population will be mutated with a given probability, through a random process of replacing one allele of a gene with another to produce a new genetic structure.

The GA employed in this study uses an elitist strategy in which the offspring is created with a prespecified generation gap and reinserted in the old population by replacing the least fit predecessors. Most fit individuals are allowed to propagate through successive generations and only a better individual may replace them [17].

The GA stops when a pre-defined maximum number of generations is achieved or when the value returned by the objective function, being below a threshold, remains constant for a number of iterations.

4.3 PSS Parameters

The parameters of the CPSS, the GA-PSSs are listed in Tables 1-2, respectively. It can be seen that for both CPSS and GA-PSSs, T_1=T_3, T_2 = T_4 = 0.05 and T_W = 10 seconds. This is in accordance with the general practice, and thus the optimal PSS parameter obtained from the optimization solutions are T_1 and K_C for each PSS at each generator of the power system considered in this paper.

Table 1. Parameters of the CPSS

Parameters	MEWA (Gen-1)	AWASH2 (Gen-2)	KOKA (Gen-3)
K_C	2.97	1.09	0.73
T_W (sec)	10	10	10
T_1 (sec)	0.10	0.14	0.26
T_2 (sec)	0.05	0.05	0.05
T_3 (sec)	0.10	0.14	0.26
T_4 (sec)	0.05	0.05	0.05

Table 2. Parameters of the GA-PSS

Parameters	MEWA (Gen-1)	AWASH2 (Gen-2)	KOKA (Gen-3)
K_C	3.0	1.2	0.8
T_W (sec)	10	10	10
T_1 (sec)	0.12	0.18	0.23
T_2 (sec)	0.05	0.05	0.05
T_3 (sec)	0.12	0.18	0.23
T_4 (sec)	0.05	0.05	0.05

5. CASE STUDY AND SIMULATION RESULTS

In order to test the robustness of the PSSs, three different operating conditions were considered. The different operating conditions (represented by light, nominal and heavy loading) are given in Table 3. It might be noted that these load conditions at buses 5, 7 and 8, are same as those load variations expected in the system, except that the corresponding generation levels are obtained here using an OPF simulation with "minimizing losses" as objective.

The simulation results are presented in two ways, first the system eigenvalues with and without PSSs are presented, and in the second the system dynamic responses are plotted for both the GA based PSS and the ISE technique based PSS. The dynamic responses are plotted for rotor angle deviations of all the system generators following a 1% step change in mechanical torque input on MEWA (Gen-1) generator.

Table 3. Three different loading conditions for examining the performance of the PSSs

Cases	MEWA (Gen-1)		AWASH2 (Gen-2)		KOKA (Gen-3)	
	P_e	Q_e	P_e	Q_e	P_e	Q_e
Light	0.17	0.03	0.11	-0.11	0.90	-0.12
Nominal	0. 35	0.1027	0.13	0.07	0.10	-0.1081
Heavy	0.468	0.87	0.18	0.60	0.144	0.546

All the values are given in per-unit

5.1 Eigenvalue Analysis

The eigenvalues of the open-loop system without PSS and the closed-loop system equipped with the CPSSs, and the GA-PSSs are listed in Table 4. It can be seen from the open-loop eigenvalues listed in Table 4, that there are two eigenvalues which lie in the right half of the S-plane (has positive real part). This shows that there are electromechanical oscillations persistent in the system and the system remains dynamically unstable without PSS.

Columns 2 and 3 in Table 4 show the eigenvalues obtained with the CPSSs, and the GA-PSSs, respectively. It can be seen that for all the loading cases, the CPSSs provide acceptable damping ratio. The GA-PSSs provide "consistent" damping ratio across the range of operating conditions considered. Furthermore, all the eigenvalues obtained with the CPSSs, and the GA-PSSs lie to the left of the complex S-plane (have negative real parts). This shows that the electromechanical oscillations in the system are damped out and the system has gained its dynamic stability.

Table 4. Eigenvalues of the open-loop system (without PSS), closed-loop system with CPSS, and GA-PSS

System Eigenvalues Without PSS	System Eigenvalues With CPSS	System Eigenvalues With GA-PSS
-5.32 + j22.9	-2.2526 ± j21.1140	-2.8935 ± j22.4227
-5.32 – j22.9	-2.5951 ± j17.7718	-1.6304 ± j16.8463
-5.35 + j19.4	-4.4733 ± j16.1442	-4.8087 ± j16.7140
-5.35 – j19.4	-0.6712 ± j9.2975	-0.3606 ± j9.0937
-0.00801 + j16.0	-0.2654 ± j5.9188	-0.8613 ± j6.0866
-0.00801 - j16.0	-4.7354 ± j9.7216	-3.9211 ± j9.4440
-5.10 + j10.8	-18.1360 ± j0.0806	-20.3341 ± j1.5866
-5.10 – j10.8	-23.3570	-25.2256
0.0128 + j5.39	-22.6372	-24.7753
0.0128 - j5.39	-22.0002	-15.9589
-0.0163 + j8.44	-17.6208	-16.2935
-0.0163 - j8.44	-0.1001	-0.1004
	-0.1000	-0.1000
	-0.1001	-0.1000

From an eigenvalue point of view, the performance of GA-PSSs is better than that of the CPSSs over the range of operating conditions considered. For nominal and heavy loading cases, the damping ratio provided by the GA-PSS is greater than damping ratio provided by the CPSS.

5.2 Time Domain Simulations

Non-linear time domain simulations have been performed to evaluate the performances of the system under various loading conditions discussed in the above sections.

For all the following simulations, the dynamic responses are plotted for rotor angle and speed deviations of the system generators following a 1% step change in mechanical torque input on MEWA (Gen-1) generator. The responses are plotted for both the GA based PSS (GA-PSS) and the ISE technique based PSS (CPSS).

Figure 5 and Figure 6, respectively, show the time response of rotor angle and angular speed deviations of all the machines of the system without PSS, when a 1% step perturbation in mechanical torque input occurs at the shaft of MEWA (Gen-1) generator.

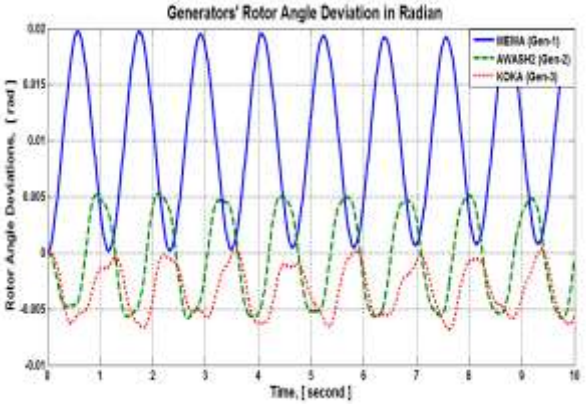

Figure 5. Rotor angle deviations without PSS

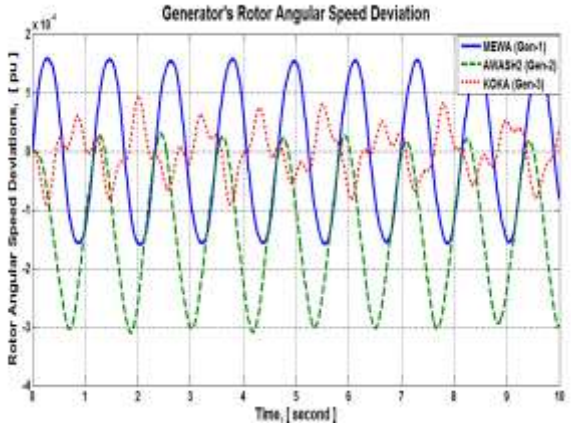

Figure 6. Rotor angular speed deviations without PSS

As has been demonstrated by Figures 5 and 6, the system is unstable under small perturbations and requires additional stabilizing control signals from PSSs.

Figures 7 and 8 show the plots for the nominal operating load condition. The GA based PSS has a lower peak off-shoot and smaller oscillations and an overall better damped response.

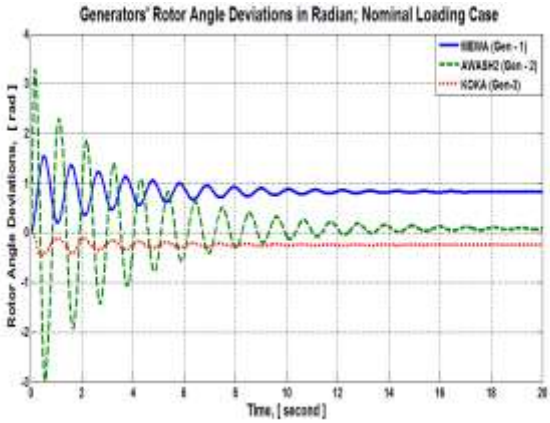

Figure 7. Rotor angle deviations with CPSS:

nominal load condition

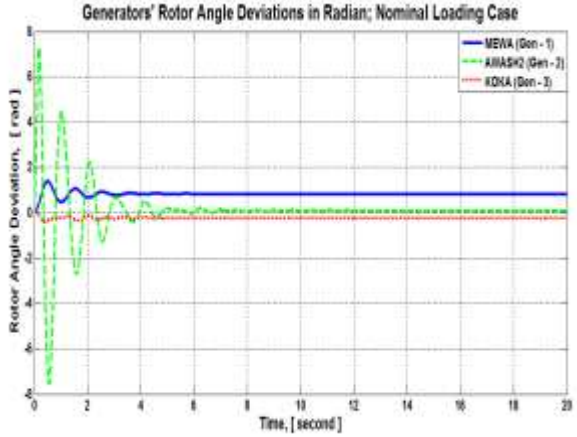

Figure 8. Rotor angle deviations with GA-PSS:

nominal load condition

Figures 9 and 10 show the plots for the heavy operating load condition. It is evident that the GA based PSS performs distinctly better as compared to the ISE technique based PSS (CPSS).

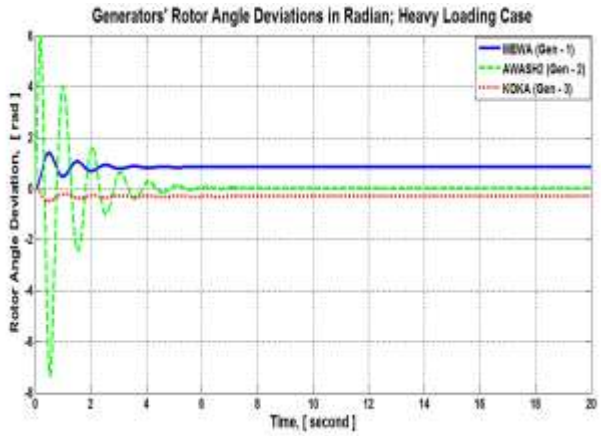

Figure 9. Rotor angle deviations with CPSS:

heavy load condition

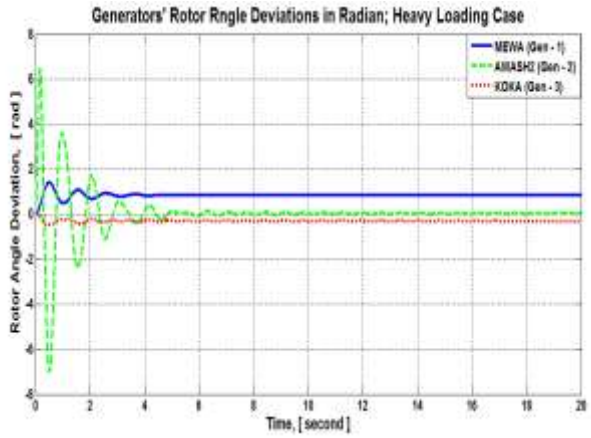

Figure 10. Rotor angle deviations with GA-PSS:

heavy load condition

Figures 11 and 12 show the plots for the light operating load condition. In this case, the GA based PSS and the ISE technique based PSS both do provide satisfactory responses.

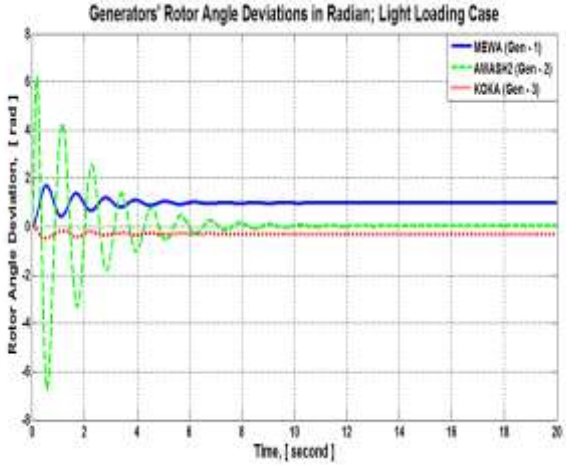

Figure 11. Rotor angle deviations with CPSS:

light load condition

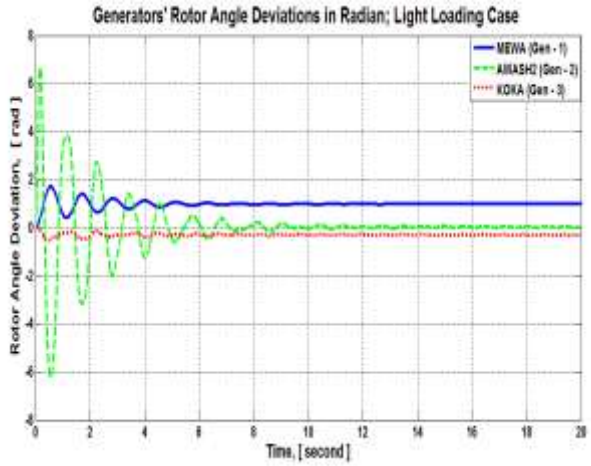

Figure 12. Rotor angle deviations with GA-PSS:

light load condition

6. CONCLUSIONS

Power system stabilizer design for multimachine power system using GA has been presented in this paper. The issue of tuning the parameters of the PSSs has been converted into an optimization problem which is solved via GA. Without PSSs, it has been demonstrated that the operation of the multimachine power system considered in this paper is dynamically unstable (has poorly damped electromechanical oscillations). The low frequency electromechanical oscillations have been completely damped out and the power system examined, in this research paper, has become dynamically stable with the design and integration of PSSs.

Moreover, eigenvalue analysis show that the GA-PSSs perform better than the CPSSs and give adequate and consistent damping for all the three-cases considered. Matlab nonlinear time domain simulations are presented to confirm the eigenvalue analysis results. The main advantage of GA is that it is simple, easy to use and has few genetic operators, and robust to solve the fitness function used to tune the optimal PSS parameters.

7. REFERENCES

[1] B.E. Eliasson and D.J. Hill, "Damping Structure and Sensitivity in the Nordel Power System", *IEEE Transactions on Power Systems*, Vol. 7, No. 1, February 1992, pp. 97-105.

[2] F.P. DeMello and C. Concordia, "Concepts of synchronous machines stability as affected by excitation control," *IEEE Trans. on Power Apparatus and Systems*, Vol. PAS-88, April 1969, pp. 316-329.

[3] W.G. Heffron, R.A. Phillips, "Effect of modern amplidyne voltage regulator on under-excited operation of large turbine generators," *IEEE Transactions on Power Apparatus and Systems*, Vol. PAS-71, August 1952, pp. 692-697.

[4] P. Kundur, M. Klein, G.J. Rogers and M.S. Zywno, "Application of power system stabilizers for enhancement of overall system stability," *IEEE Transactions on Power Systems*, Vol. 4, May 1989, pp. 614-626.

[5] Y.L. Abdel-Magid, M.A. Abido, S. Al-Baiyat and A.H. Mantawy, "Simultaneous stabilization of multi-machine power systems via genetic algorithms," I*EEE Transactions on Power Systems*, Vol. 14, November 1999, pp. 1428-1439.

[6] Y.L Abdel-Magid, M.A. Abido, "Optimal multiobjective design of robust power system stabilizers using genetic algorithms," *IEEE Transactions on Power Systems*, Vol. 18, No. 3 , August 2003, pp.1125-1132

[7] P. Zhang and A.H. Coonick, "Coordinated Synthesis of PSS Parameters in Multi-Machine Power Systems Using the Method of Inequalities Applied to Genetic Algorithms," *IEEE Transactions on Power Systems*, Vol. 15, No. 2, May 2000, pp. 811-816.

[8] A.L.B. Do Bomfim, G.N. Taranto, D.M. Falcao, "Simultaneous tuning of power system damping controllers using genetic algorithms," *IEEE Transactions on Power Systems*, Vol. 15, No. 1, February 2000, pp. 163-169.

[9] P. Kundur,"A Course on Power Stability and Control," ABB T&D University, Ludvika, Sweden, April 2000.

[10] Yao-Nan Yu, *Electric Power System Dynamics*, Academic Press 1983.

[11] D.E. Goldberg, *Genetic Algorithms in Search, Optimization and Machine Learning*, Addison-Wesley Publishing Company Inc., January 1989.

[12] "Western Electricity Coordinating Council Policy Statement on Power System Stabilizers" [Online]. Available: http://www.wecc.biz

[13] "General Transmission System Design Requirements for the Interconnection of New Generators (Resources) to the NEPOOL System" [Online]. Available: ttp://www.iso-ne.com

[14] B.E. Eliasson, "Damping of Power Oscillations in Large Power Systems", PhD thesis TFRT-1032, Department of Automatic Control, Lund University of Technology, Lund, Sweden, May 1990.

[15] Ethiopian national electric power grid, 2012.

[16] K FOLLY, "Power System Stabilizer Design for Multimachine Power System Using Population-Based Incremental Learning", *Power Plants and Power Systems Control*, 2006, 2007.

[17] K. Bhattacharya, "Lyapunov's method based genetic algorithm for multi-machine PSS tuning", 2002 IEEE Power Engineering Society Winter Meeting Conference Proceedings (Cat No 02CH37309 PESW-02), 2002.

[18] Bhattacharya, K., "Tuning of power system stabilizers in multi-machine systems using ISE technique", *Electric Power Systems Research*, 199806.

[19] Andreoiu, A., and K. Bhattacharya, "Robust tuning of power system stabilisers using a Lyapunov method based genetic algorithm", *IEEE Proceedings – Generation, Transmission and Distribution*, 2002.

[20] www.elkraft.chalmers.se

[21] www.ijmer.com

[22] www.elteknik.chalmers.se

[23] waste.org

[24] Shayeghi, H., and A. Ghasemi, "A multi objective vector evaluated improved honey bee mating optimization for optimal and robust design of power system stabilizers", *International Journal of Electrical Power & Energy Systems*, 2014.

[25] He Ren-mu, "Genetic algorithm based design of power system stabilizers", 2004 IEEE International Conference on Electric Utility Deregulation Restructuring and Power Technologies Proceedings, 2004.

[26] Shayeghi, H., "Multi-machine power system stabilizers design using chaotic optimization algorithm", *Energy Conversion and Management*, 201007.

[27] www.edi-info.ir

[28] Aalok Dubey, "Simultaneous Stabilization of Multimachine Power System Using Genetic Algorithm", *Proceedings of the 41st International Universities Power Engineering Conference*, September 2006.

[29] Liu, N., J. Chen, L. Zhu, J. Zhang, and Y. He, "A Key Management Scheme for Secure Communications of Advanced Metering Infrastructure in Smart Grid", *IEEE Transactions on Industrial Electronics*, 2012.

[30] www.docstoc.com

[31] Adrian Andreoiu, "On Power System Stabilizers: Genetic Algorithm Based Tuning and Economic Worth as Ancillary Services", PhD thesis, Department of Electric Power Engineering, Chalmers University of Technology, Goteborg, Sweden, 2004.

International Journal of Science and Engineering Applications
Volume 5 Issue 3, 2016, ISSN-2319-7560 (Online)

Field Drying of Cassava in a Solar Tent Dryer equipped with a Solar Chimney

J. K. Afriyie
Department of Mechanical Engineering
Kumasi Polytechnic
P. O. Box KS 854, Kumasi, Ghana

O-W. Achaw
Department of Chemical Engineering
Kumasi Polytechnic
P. O. Box KS 854, Kumasi, Ghana

K. A. Aikins
Department of Agricultural Engineering, College of Engineering
Kwame Nkrumah University of Science and Technology
Kumasi, Ghana

C. K. K. Sekyere
Department of Mechanical and Manufacturing Engineering
University of Energy and Natural Resources
P. O. Box 214, Sunyani, Ghana

A. Bart-Plange
Department of Agricultural Engineering, College of Engineering
Kwame Nkrumah University of Science and Technology
Kumasi, Ghana

Abstract: The performance of a solar tent dryer equipped with a solar chimney, as against that of open sun drying, was examined in the drying of cassava. An initial no-load trial was done, followed by trials with the dryer loaded with cassava. One drying trial was performed with the crops on the lower shelf, another with the crops on the upper shelf and a third trial with the dryer loaded on both the lower and upper shelves. In each drying trial, some cassava were also dried in the open sun which results were compared to that of the dryer. In the no-load process, the temperature inside the dryer increased with height due to thermo-syphon effects. But this trend was distorted by the evaporation of moisture from the crops during the drying processes, especially at the initial stages. About 75% to 80% of the drying process occurred within the first two days and nights of the drying periods. The open-sun drying was faster at the initial stages of drying, especially when the crops were on the lower shelf or the dryer was fully loaded. But the performance of the dryer overtook that of the open sun drying at later stages of drying. Thus, the dryer started more slowly but finished earlier than the open-sun drying. The best drying performance was observed when the crops were high up the dryer, though only a small amount of crops could be allowed at this height due to the design of the dryer.

Keywords: cassava; crop drying; solar chimney; natural ventilation

1. INTRODUCTION

About 65% of Ghana's workforce is made up of rural-based farmers (Owusu-Baah, 2004). Yet the food in the Ghanaian markets is generally not enough. This is partly caused by post-harvest losses, which is being compounded by increase in Ghana's population. The farmers need to dry their crops to enable them preserve and sell the crops at appropriate time in their prime marketable condition at remunerative prices. Crop drying helps in reducing the moisture content to a level below which deterioration does not occur and the product can be stored for a definite period (Sharma et al., 2009). As noted by Sharma et al. (2009) there has been very little penetration of solar drying technology. The farmers normally dry their crops by spreading them on mats in the open sun, sometimes even on bare ground by the road side (figure 1). This way of crop drying is not that efficient, and the crops are exposed to rain, pest, rodents and various forms of unhygienic conditions.

Crop drying is the removal of moisture from crop into the surrounding air. The drying process is enhanced whenever the vapour pressure of moisture in the crop is higher than the partial pressure of vapour in the air. The vapour pressure in the crop increases with increase of crop temperature. On the other hand, the vapour pressure in the air reduces as the relative humidity (*RH*) of the air reduces, and this can be achieved by increasing the air temperature (Rogers and Mayhew, 1993; Jain and Tiwari, 2004). Thus crop drying becomes very effective when both the crop and the surrounding air are constantly warm. As the moisture escapes from the crop into the air, the air becomes more humid and needs to be replaced with less humid air for the drying process to proceed effectively. So a current of warm air is mostly required for effective drying process.

A crop dryer normally requires a heating device to preheat and reduce the relative humidity of the air en route to the crops in a drying chamber. There are two main types of crop dryers; the forced-convection (or forced-ventilation) and the natural-convection (or natural-ventilation) types. The forced-ventilation dryer uses an electrically or a mechanically powered blower to blow the drying air through the crop. The natural-convection dryer depends on the natural buoyancy flow of air created by the thermo-syphon effect through the

system. The use of electricity is too expensive for the farmers who live far away from the national electricity grid. The use of heating sources like wood may also be expensive or unfriendly to the environment. The afore-mentioned challenges can be avoided through the use of simple and cheap natural convection solar crop dryers to help generate income for the farmers, and meet the present and future demand for food in the community. These dryers are normally not too expensive to construct, and all the parts are locally available. Developing these dryers in the rural areas would also provide jobs for the artisans and youth in the rural areas and help to curb the rural-urban drift among the youth.

Figure 1 Open-sun drying of cassava on bare ground

Picture taken at Abofour in the Ofinso District in the Ashanti Region of Ghana

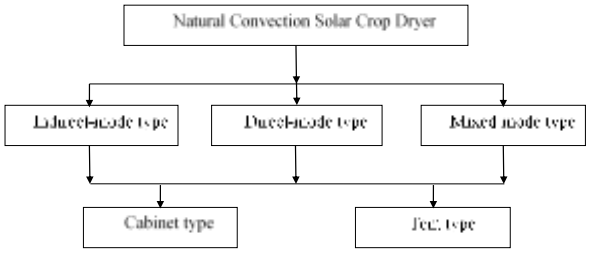

Figure 2 Types of natural convection solar crop dryers

As depicted in figure 2, a natural convection solar dryer is normally one of three kinds. The indirect-mode type is equipped with a preheating device to preheat the air before it encounters the crops in the drying chamber. The walls of the drying chamber are opaque so that the crops have no contact with sunlight. The direct-mode dryer has no air preheater, and the radiant energy passes through the transparent walls of the drying chamber whose content, including the crops, serve as the main absorber for heating the drying air. The mixed-mode dryer has an air preheating device and also transparent drying-chamber walls to allow maximum radiant energy utilisation. Earlier reports indicate that the direct-mode type is highly inefficient due to poor ventilation, leading to excessively high temperatures with high humidity in the drying chamber (Ekechukwu and Norton, 1997; Ekechukwu, 1999b). Unless the dryers are well designed, the crops at times end up partially cooked rather than properly dried. Singh et al. (2004) however report that the direct-mode dryer can be more efficient than the indirect-mode dryer, the only problem at times being the poor quality of the produce, especially those that are sensitive to sunlight. On the other hand, the direct-mode dryer is the least expensive and has the highest chance of patronage among farmers in the developing countries most of whom have low economic base and can only afford the direct-mode dryer.

Some reports on chimneys show that, properly designed solar chimneys can boost the flow of air through an enclosure (Chantawong et al., 2006; Chen et al., 2003; Ekechukwu, 1999a; Ferreira et al., 2008; Ong, 2003; Ong and Chow, 2003;). The use of a solar chimney was combined with the effect of an appropriately inclined roof of the drying chamber for the so-called tent-dryer effect and a suitable inlet-exit area ratio to improve the ventilation in the direct-mode dryer (Afriyie et al., 2009; Afriyie et al., 2011; Afriyie and Bart-Plange, 2012; Afriyie et al., 2013). The works were performed on a laboratory model of the dryer constructed to constitute on one half symmetry of a tent dryer, with a slanted roof only on one side. The current work has been performed in the field on a fully symmetrical tent dryer with slanted roof on both sides to ensure stability against the local winds.

Figure 3 shows a functional architecture of the tent dryer. In operation, radiant energy of short wavelength from the sun is transmitted through the transparent drying-chamber and chimney glazings to fall on the absorbers in the dryer. The absorbers, after absorbing this radiant energy, in turn emit heat energy of long wavelength which cannot pass through the glazing back into the atmosphere. This trapped energy heats up the air in the drying chamber and chimney. As explained in the earlier reports, cold air enters the dryer through the bottom inlet, gets heated up and dries the crops inside the chamber. The drying air, which becomes more humid after moisture absorption from the crops, enters the solar chimney where it is heated again to become less dense and is then driven upwards to exit through the top vent into the surroundings. This brings about a continuous flow where the cold, dense air is drawn in to displace the warm air through the dryer (Afriyie et al., 2009; Afriyie et al., 2011; Afriyie and Bart-Plange, 2012; Afriyie et al., 2013).

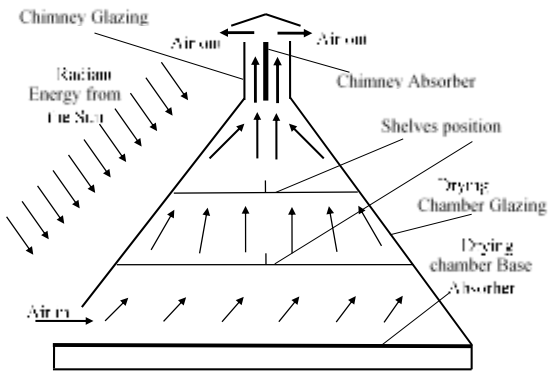

Figure 3 Functional architecture of the tent dryer equipped with a solar chimney

The test crop is cassava, a crop which is widely cultivated and harvested in the tropical and subtropical regions. It is a drought-tolerant, staple food crop which is increasingly becoming an important input in animal feed and human diet, processed in various ways in both the food and non-food industry (Olufayo and Ogunkunle, 1996; Pongsawatmanit et al., 2006; Cansee et al., 2008; Onyenwoke and Simonyan, 2014). It offers flexibility to resource-poor farmers because it serves as either subsistence or a cash crop (Stone, 2002).

Fresh cassava is, however, highly moisture laden, with high water quality. It therefore undergoes rapid postharvest deterioration, with a shelf life of the order of 24 to 48 hours after harvest (Andrew, 2002). Delayed processing of the cassava tubers will reduce the purity and functional properties of the starch produced from it (Lola et al., 2012). The high initial moisture content also makes it uneconomical to transport the fresh ones before drying. This brings about the need to dry the crop as close to the harvest point as possible, and the direct-mode dryer is most suitable for this. The objective of the current work is to investigate the performance of the fully triangular cross-sectioned solar tent dryer in the drying of cassava on the field, in relation to open-sun drying.

2. MATERIALS AND METHODS

2.1 Experimental Set Up

Using the results of works on the laboratory model, the solar tent dryer with its solar chimney was built to the dimensions shown in Appendix (Table A1). The dryer had a wooden framework. The wooden base of the drying chamber was covered with a steel sheet, painted black to act as radiant energy absorber. Along the base perimeter were beams of wood that extended downwards to limit the airflow and therefore the heat loss by convection underneath the base. The chimney absorber consisted of a sheet of steel, also covered with black paint, which run across the width of the dryer. The glazing of both the drying chamber and chimney was made of transparent glass sheet. The pictorial view of the dryer can be found in figure 4.

Three clocks (SAKURA QUARTZ CLOCK), each with a hygrometer and a thermometer as integral unit, were positioned in the drying chamber to measure the relative humidity and temperature at various time intervals during the day. The measuring positions were 0.25 m above the base of the dryer, 0.40 m above the lower shelf (i.e. 0.75 m above the base) and 0.30 m above the upper shelf (or 1.35 m above the base). A fourth SAKURA unit was used outside to measure the relative humidity and temperature of the environment and the dryer inlet. The inlet data were taken in the middle of the dryer inlet (i.e. at 0.15 m above the base at inlet). A hand-held liquid-in-glass thermometer was used to measure the chimney air temperature (at 1.85 m above the base). The liquid-in-glass thermometer was also used to check the thermometer readings on the SAKURA clocks for accuracy and consistency. There were two shelves for the drying crops, the lower and upper shelves, each with four trays of rectangular cross section. Each tray had mosquito net at the bottom to support the cassava, whilst allowing the air to flow through the system. The trays on the upper shelf were designated H1, H2, H3 and H4, whilst the lower shelf had L1, L2, L3 and L4 (figure 5). The length and width of each tray on the upper shelf were 0.69 m and 0.22 m respectively, whilst those of each tray on the lower shelf were 0.69 m and 0.45 m respectively.

Figure 4 Pictorial view of a solar tent dryer equipped with a solar chimney

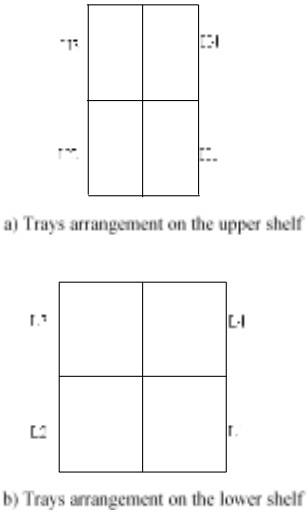

Figure 5 Arrangements of drying trays on the shelves in the dryer

2.2 Determining the Moisture Contents

A sample of the crop was sent to a nearby Chemical Engineering Laboratory of Kumasi Polytechnic, Kumasi, Ghana, to determine the initial moisture content on wet basis ($MC_{w.b.}$). An oven (wagtech; model GP-100-SLAD-250-HYD) and a precision weighing scale (METTLER TOLEDO

AL 204 wagtech; Max 210, e = 0.001, Min 0.01, d = 0.0001g) were used for determining the $MC_{w.b.}$ by the formula

$$Initial\,MC_{w.b.} = \frac{Initial\,mass\,of\,sample - Final\,mass\,of\,sample}{Initial\,mass\,of\,sample} x100\,\% \quad (1)$$

The dry solid mass of crop m_s on each tray in the dryer was then determined from the initial $MC_{w.b.}$ as

$$m_s = \frac{100 - Initial\,MC_{w.b.}}{100} x\,Initial\,m_t \quad (2)$$

where m_t is the total mass of crop (together with the moisture) on the tray. With the help of the solid mass m_s, the moisture content on dry basis $MC_{d.b.}$ on each tray at any instance of the drying process was determined from the total mass m_t on the tray at that instance from the equation

$$MC_{d.b.} = \frac{m_t - m_s}{m_s} x100\,\% \quad (3)$$

The $MC_{d.b.}$ was used for the calculations, as the denominator m_s remained constant throughout the drying process. The conversion back to $MC_{w.b.}$ was done through the equation

$$MC_{w.b.} = \frac{100\,MC_{d.b.}}{100 + MC_{d.b.}} \quad (4)$$

A mechanical kitchen weighing scale with a capacity of 5 kg, whose accuracy was verified to two decimal places with the laboratory precision weighing scale (METTLER TOLEDO) indicated earlier, was used for determining the mass of crop in the field trials.

2.3 The Trials

A no-load trial was first performed on the dryer for a whole day without any crop in the dryer, in order to examine the temperature and relative humidity profile within and around the dryer. This was repeated for the next three days. The no-load trial was followed by an under-load trial, with only the lower shelf loaded with trays of cassava (Trial UL1) for six days to allow the crop to dry appreciably. The dryer was then loaded only on the higher shelf for another under-load trial (Trial UL2) for six days. A third six-day under-load trial was later performed, with the dryer fully loaded on both the lower and upper shelves (Trial UL3). Each under-load trial also included the drying of some crops outside the dryer on three trays which were placed at the same level as the lower shelf but at different locations in the open sun. The open-sun drying served as control drying for its performance to be compared with the performance of the dryer under the same environmental conditions. The crops were cut into quadrants of average radius 0.03 m with average length 0.05 m. The average loading density on each tray, both inside and outside the dryer, was 12.3 kg/m^2. The inlet of the dryer, as well as the top of the control trays, was covered in the night and when it rained, to prevent the sucking in of moisture at those periods.

Readings of relative humidity and temperature were taken at two-hourly intervals. The no-load trial on each day began at 08 hours in the morning and ended at 18 hours in the evening at local times. The first day of the under-load trial began at noon, after the crops had been prepared and cut to the required sizes. The crops were weighed at the beginning and end of each drying day.

2.4 Data Analysis

Analysis of variance (ANOVA) was performed on the data recorded, and the average mean was analysed by Duncan's test at 95% confidence level a ($p < 0.05$). The statistical software used was SAS (SAS Institute Inc., Cary, NC, USA).

3. RESULTS

The temperature and also relative humidity of the environment and dryer inlet varied from morning till evening on each day of the experiments. To eliminate the effects of variations in the external conditions at various times of the trials, the temperature rise above ambient at various heights and the corresponding relative humidity difference in relation to the ambient conditions were used to analyse and compare the heating at various heights of the dryer. Figure 6 shows the mean temperature rise above ambient at various heights in the dryer and their corresponding mean relative humidity differences with the ambient conditions at various local times for the no-load trial. The highest temperatures above ambient, with the highest gradients, are generally observed for the local times 12 and 14 hours. This is followed by the local times 10 and 16 hours. Those temperature variations were found to be significant from the mean-comparison analyses with the SAS software. The extent of temperature variations and gradients, however, reduced for the local time 18 hours. At local time 08 hours, there was no significant increase of temperature with height, and the temperatures at the heights of 0.75 and 1.35 m (in the drying chamber) and at height 1.85 m (inside the chimney) were even slightly lower than the ambient temperature. The relative humidity variations at various positions, which were recorded only up to the top of drying chamber, showed an opposite trend to that of the temperature variations, decreasing as the air rose up the dryer, with the exception of the variation at local time 08 hours.

In figure 7a, the temperature variations in the second drying day (the first full drying day from 08 hours to 18 hours) is used to represent the variations within the initial stages of drying whilst figure 7b shows the variation at a later stage (the fourth drying day) of Trial UL1. On day 2 of Trial UL1 the temperature dropped in the local times 10, 12 and 14 hours from the height 0.25 m to 0.75 m, where the drying air passed through the crops on the lower shelf, before rising again in the top of drying chamber and in the chimney. In the local times 08 and 18 hours the temperatures generally fell as the air rose up the drying chamber (at height 1.35 m) and chimney (height 1.85 m). On day 4, the temperature variations became more like those of the no-load trials in figure 6. In figure 8a, the rise in temperature with height on day 2 was interrupted from height 0.75 m to 1.35 m, as the air encountered the crops on the upper shelf, before the temperature rose again into the chimney. As indicated in figure 8b, the interruption in the temperature variation was less pronounced so that the trend on day 4 again tended to follow that of the no-load trial more closely.

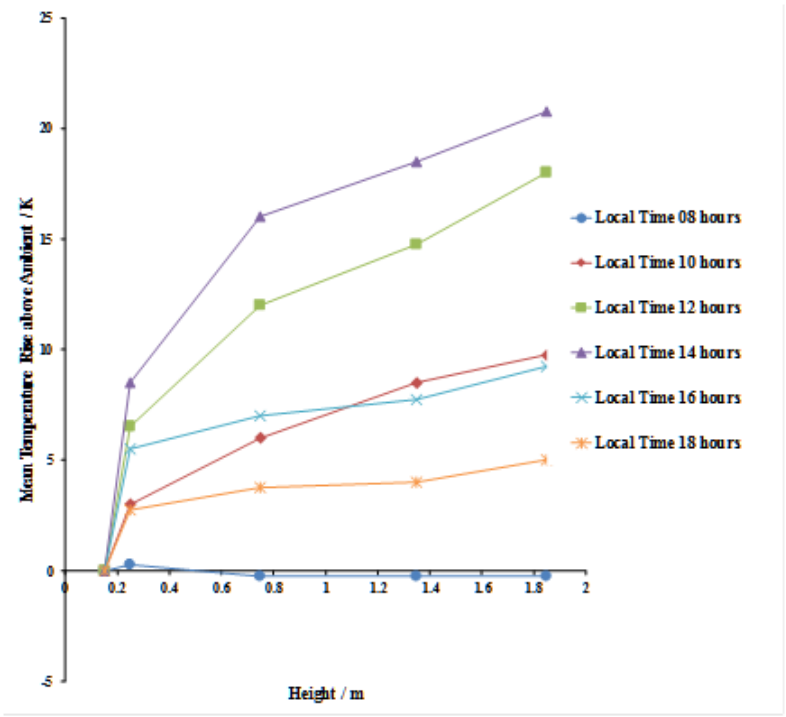

a) Mean Temperature Rise above Ambient vs Height

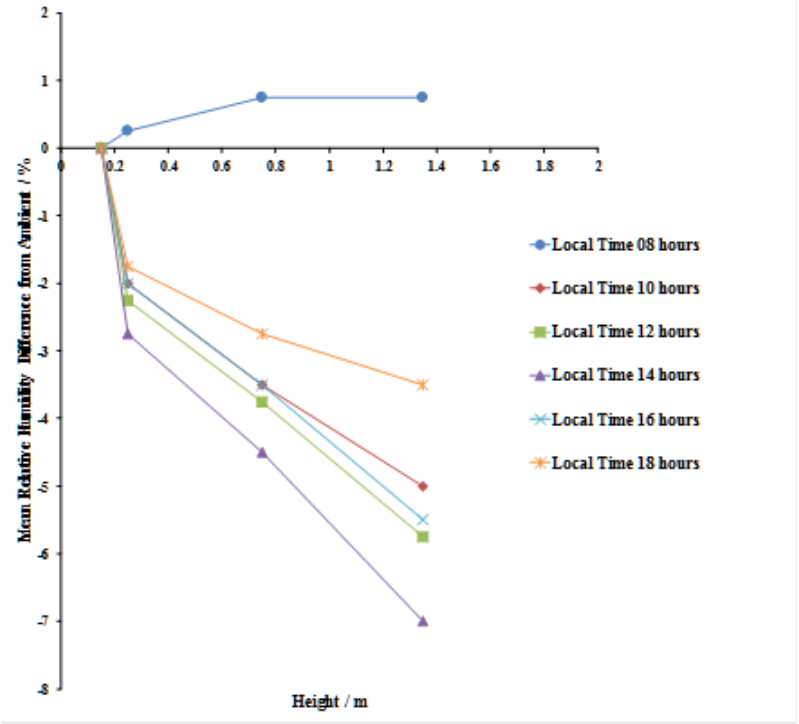

b) Mean Relative Humidity difference from Ambient vs Height

Figure 6 Variation of the mean temperature above ambient and the mean relative humidity difference from ambient with height inside the dryer for the no-load trial

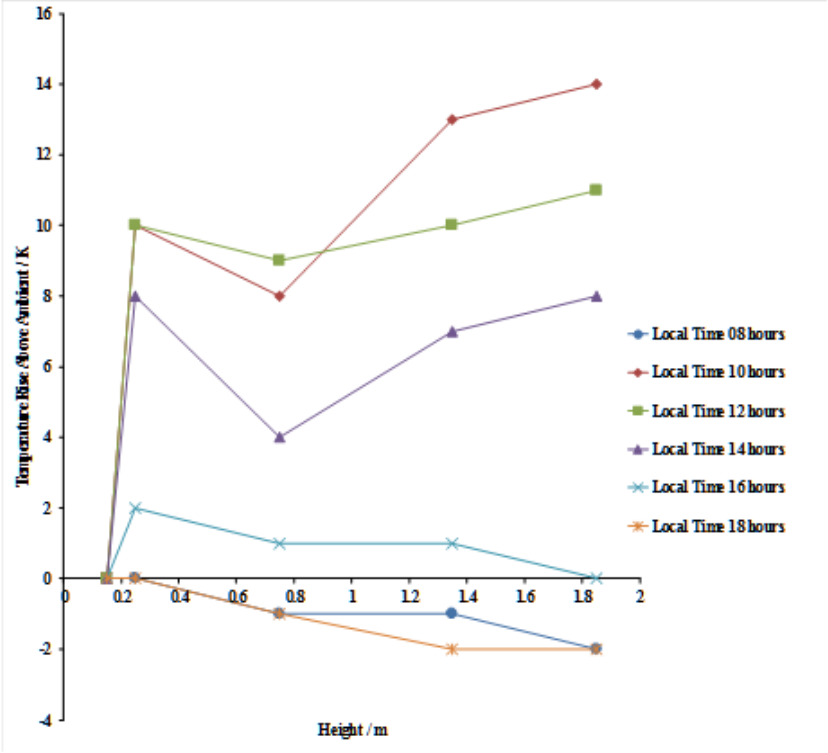

a) Temperature above Ambient vs height, Day 2

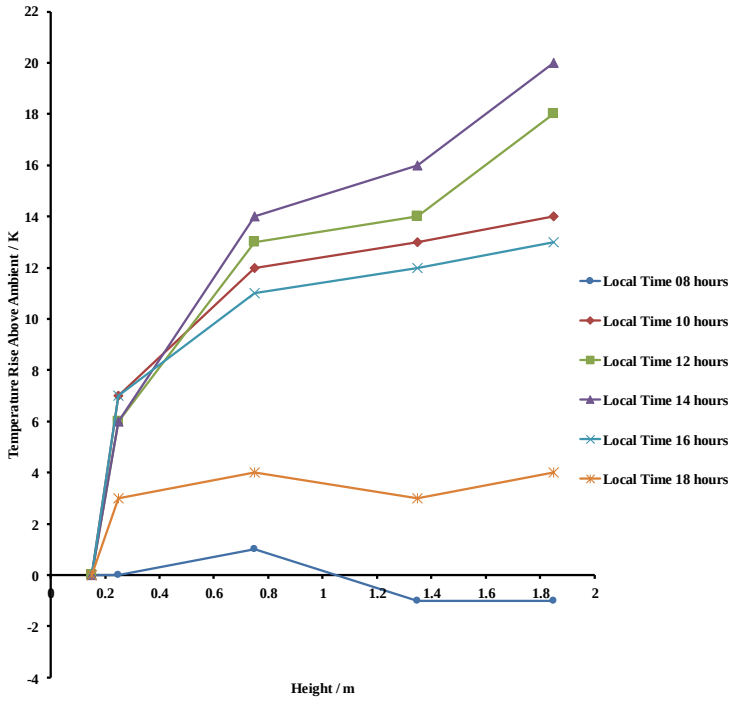

b) Temperature above Ambient vs height, Day 4

Figure 7 Variation of temperature above ambient with height inside the dryer for the Trial UL1: crops on the lower shelf

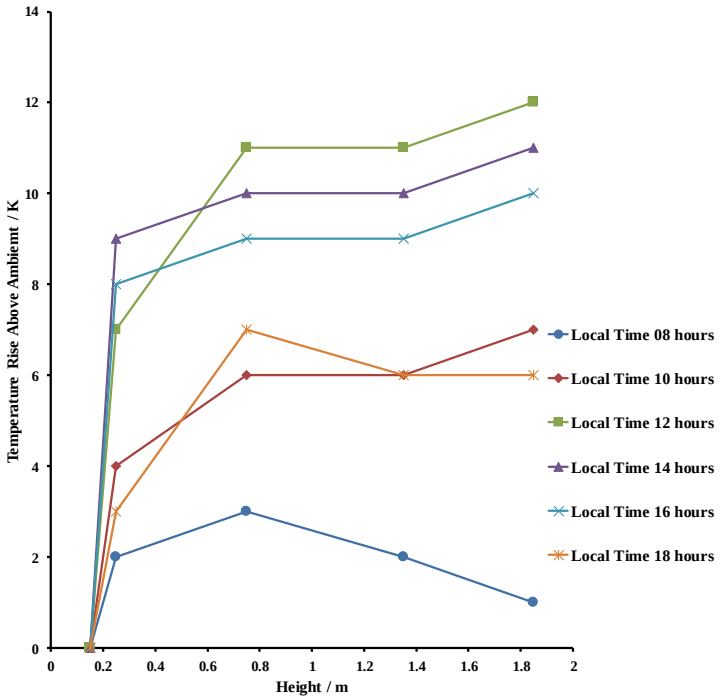

a) Temperature above Ambient vs height, Day 2

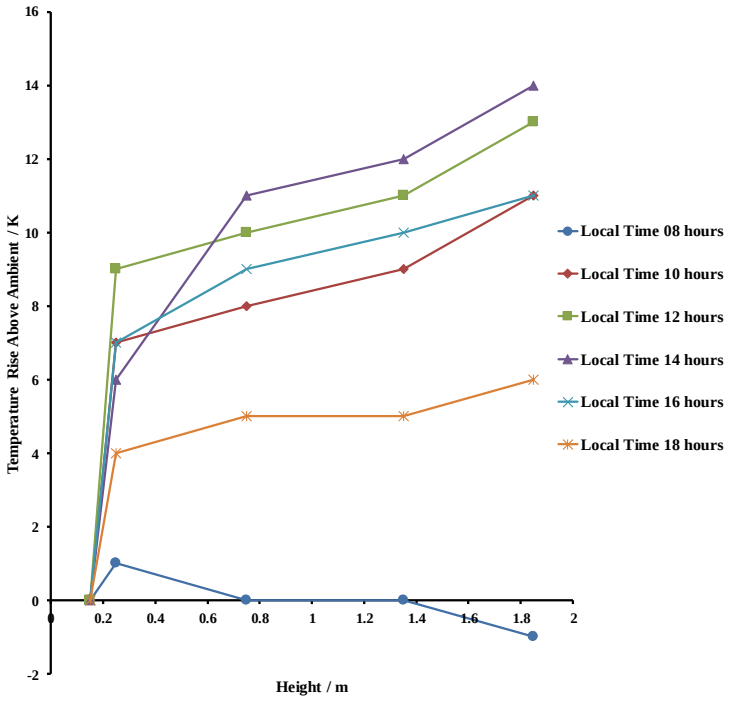

b) Temperature above Ambient vs height, Day 4

Figure 8 Variation of the temperature above ambient with height inside the dryer for the Trial UL2: crops on the upper shelf

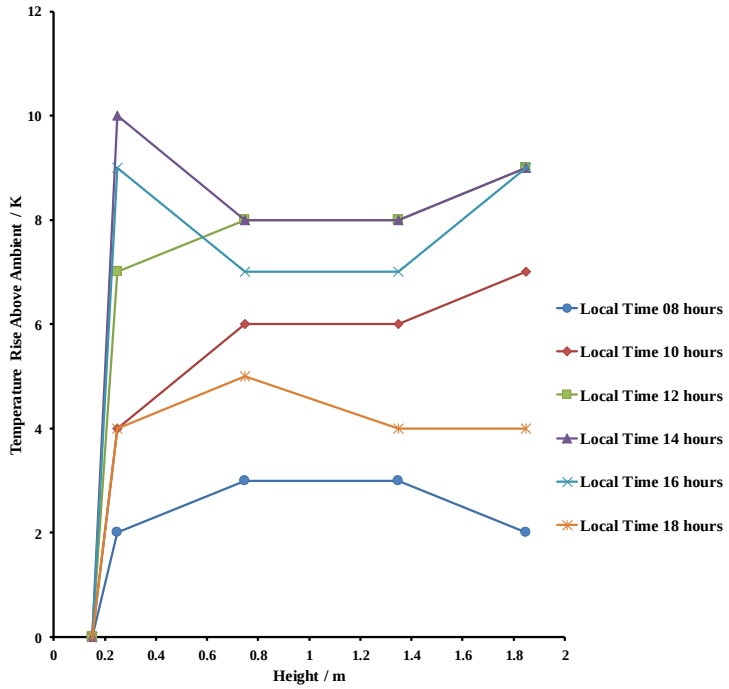

a) Temperature above Ambient vs height, Day 2

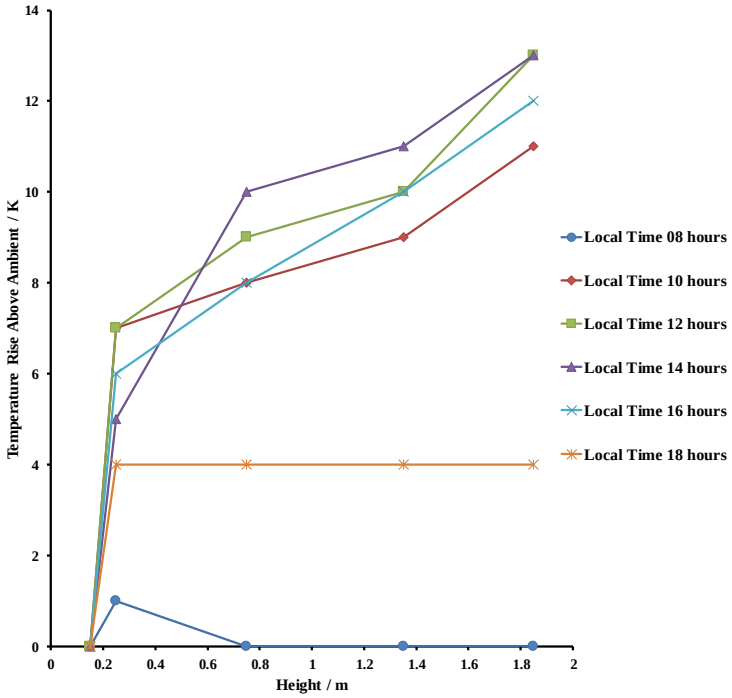

b) Temperature above Ambient vs height, Day 4

Figure 9 Variation of the temperature above ambient with height inside the dryer for the Trial UL3: dryer fully loaded

With the dryer loaded on both the lower and upper shelves, the second-day temperature variation pattern in figure 9a was far more deviated from that of the no-load trial. The variation pattern on day 4, however, again followed similar trends to that of the no-load trial (figure 9b). In all the trials the temperatures inside the dryer were generally higher than the environment or inlet temperature (represented by height 0.15 m on the graphs) apart from few instances of local times 08 and 18 hours.

Figures 10 to 12 show the variation of moisture content on dry basis ($MC_{d.b}$) of the crops on various days of the under-load trials. The drying time from 12 to 18 hours on the abscissa axis indicates the variations in the six-hour period of the first day; from 18 to 28 hours is for the ten-hour drying period (local times 08 to 18 hours) of the second day; 28 to 38 hours is for the third day; 38 to 48 hours, 48 to 58 hours and 58 to 68 hours are for the fourth, fifth and sixth days respectively. The vertical lines at times 18, 28, 38, 48, 58 and 68 hours show the *MC* drop from the self-drying at various nights when the sun was not shining.

Starting from an initial moisture content on dry basis (db) of 178% in Trial UL1 (figure 10), the crops on the control tray dried faster on the first day, with the mean MC_{db} dropping to 109%, whilst the mean MC_{db} in the dryer got to 129%. The ANOVA analyses with the SAS software showed a high significant difference between the two means. The cassava in the dryer became brownish by the end of the first day. By the end of day two, the mean MC_{db} in the dryer had fallen to 45%, just below that of the control at 47%. After overtaking that of the control, the drying process inside the dryer continued to be faster to end the third day with a mean MC_{db} of 19% whilst that of the control was at 32%. By the end of the third day, the cassava in the open sun looked more brownish than that in the dryer. The mean MC_{db} values fell to around 6% and 20% in the dryer and on the control tray respectively by the end of day five, and stayed around these values with no significant variation up to the end of day six. Most of the drying occurred within the first two days with the MC_{db} dropping from around 178% to 37%, and from 178% to 42%, for the dryer and control respectively, by the morning of day three (figure 10). As indicated by the vertical lines, most of the night drying also occurred within this period. The night drying from the fourth day on wards was not significant. In the graphs, the point for the previous night and the next morning are almost merging, so that the vertical lines are not that visible from the fourth day.

Starting with an initial MC_{db} of 186%, d.b. in Trial UL2, the MC_{db} dropped to 126% in the dryer whilst that of the control dropped to 123% on day one (figure 11). The crops in the dryer again looked brownish whilst those in the open sun still looked whitish after the first day. By the morning of the second day both moisture content values had dropped to around 116% with no significant difference. On the second day, drying was faster in the dryer, ending the day with MC_{db} 45%, whilst that of the control was 59%. The gap in MC_{db} between the crop in the dryer and that of the control tray continued to be wider (as compared to that in Trial UL1) up to the end of the fifth day when the value in the dryer got to around 6% and remained around this figure up to the end of the sixth day with no significant variation. The MC_{db} of the control crop was around 25% at the end of day five, and this fell further to around 20% by the end of day six. The crop in the open sun again appeared more brownish than that in the dryer by the end of day three. Like the results in Trial UL1, most of the drying occurred within the first two days and nights, with the MC_{db} dropping from 186% to 42% and from 186% to 55% for the dryer and control tray respectively by the morning of the third day.

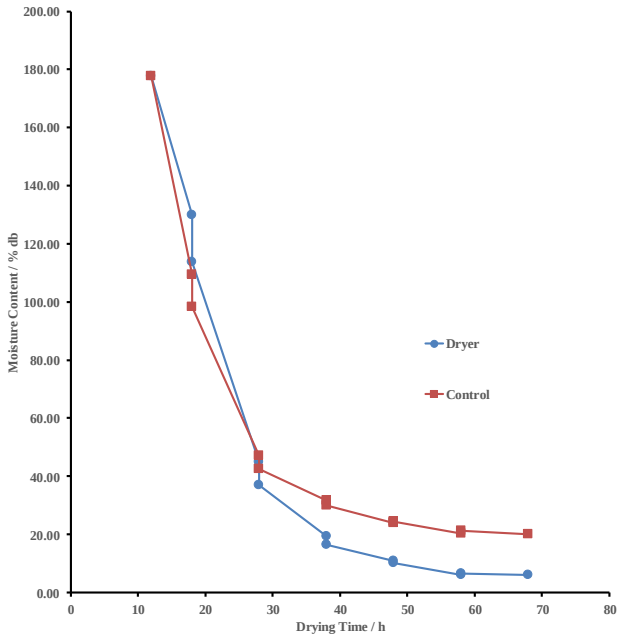

Figure 10 **Variation of Moisture Content on dry basis with Time for Trial UL1; crops on the lower shelf only**

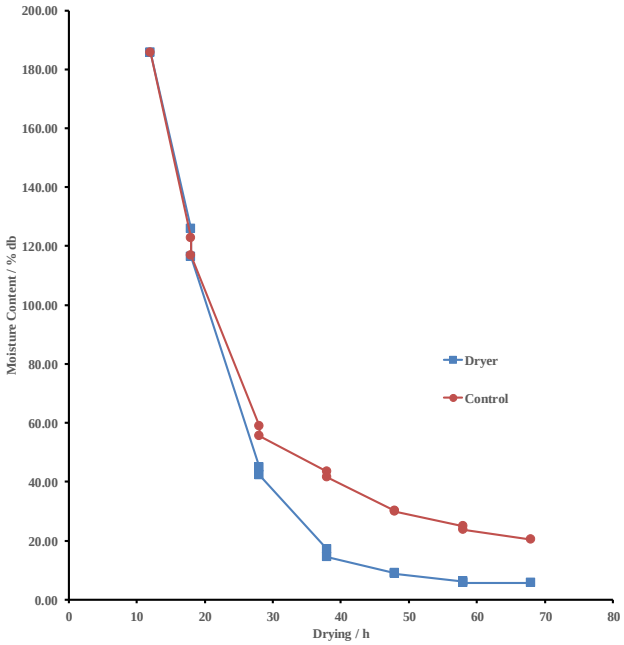

Figure 11 **Variation of Moisture Content on dry basis with Time for Trial UL2; crops on the upper shelf only**

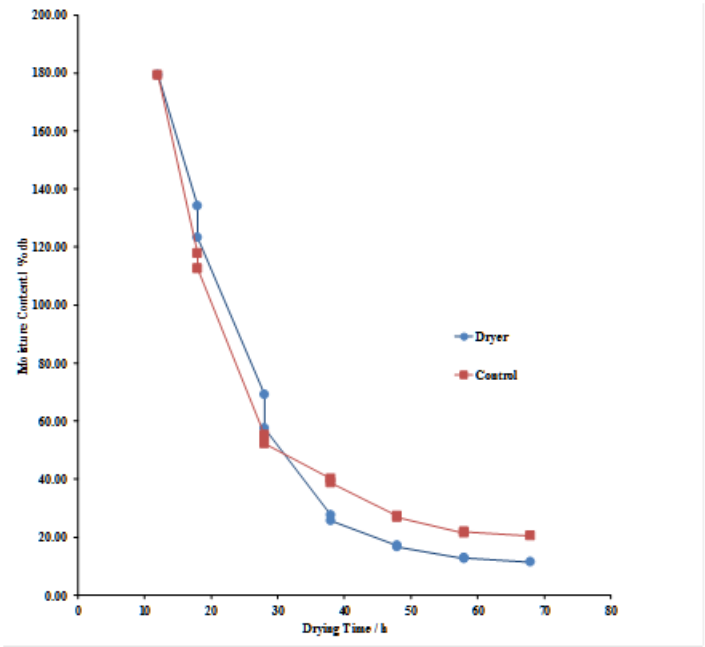

Figure 12 **Variation of Moisture Content on dry basis with Time for Trial UL3; dryer at full load**

In Trial UL3, the control crops dried faster than the crops in the dryer during the first two days (figure 12). The drops in MC_{db} were from 179% to 55% and 179% to 52% for the dryer and control tray respectively. The drying performance of the dryer overtook that of the control tray during the third day and continued to dry faster than the control till the end of the sixth day. The dryer ended the sixth day with MC_{db} of 11%, whilst that of the control tray was at 21%. As in the case of the first two trials, the cassava in the dryer appeared brownish whilst that on the control trays still looked whitish after the first day, but the control cassava became more brownish from day three onwards. The gap in MC_{db} between the dryer and control tray from the third day onwards was closer than those of trials UL1 and UL2. Again as shown in figure 12, a high proportion of the drying process took place within the first two days and nights, like the first two trials.

4. DISCUSSIONS

The increase in temperature with height observed in the no-load trial in figure 8a during the local times 10, 12 and 14 hours is attributable to air heating inside the dryer from the intense radiant energy from the sun at those local times. The

whole system then functioned as a heated chimney. In a heated chimney the air heating process induces a buoyancy flow of air up the dryer with a thermo-syphon effect in which the warm, less dense air is displaced upwards by cold, denser air from outside so that the lower part of the chimney remains colder than the upper part (Incropera et al., 2007).

The margin of temperature increase reduced around the local time 16 to 18 hours. This is attributable to the low energy intensity as the sun set at that time. In the morning around 08 hours the intensity was very low and the whole system functioned like a normal chimney in which the temperature fell as the air rose up the unheated chimney, as noted by Ekechukwu and Norton (1997) and also observed by Afriyie et al. (2009). The fall in relative humidity (*RH*) at various heights where the temperature rose could be attributed to the fact the absolute humidity of air inside the dryer remained constant during the no-load trial. This constant absolute humidity meant that the *RH* should fall as the temperature rose. The *RH* for the local time 08 hours then showed an upward trend in response to the temperature which showed a downward trend (figure 6).

The interruption to the thermo-syphon induced upwards temperature gradient, as the air passed through the lower shelf (positioned between the heights 0.25 m and 0.75 m) in the Trial *UL1* may be attributed to the fact that part of the available energy was used for moisture removal from the crop. So the air temperature fell or did not increase any significantly during the air passage through the crops on the lower shelf at the initial stages, as indicated on the second day of drying in figure 7a, during which most of the drying occurred (figure 10). Similarly, the interruptions to the thermos-syphon effects that occurred as the drying air moved across the higher shelf from the heights 0.75 m to 1.35 m in Trial *UL2* (figure 8a) and across the lower and upper shelves from 0.25 m to 0.75 m and from 0.75 m to 1.35 m respectively in Trial *UL3* (figure 9a) are attributable to the use of part of the energy for moisture evaporation in addition to air heating.

During the later stages of drying the temperature gradient in all the under-load trials, as shown in figures 7b, 8b and 9b, tended to approach that of the no-load trials (figure 6a). This could be attributed to the slowdown of the drying processes at this stage of relatively low *MC*, as shown in figures 10, 11, and 12.

During the initial stages of drying, the control tray (in the open sun) dried faster than the dryer, especially when the crops were loaded on the lower shelf or when the dryer was at full load. Similar results were observed by Jain and Tiwari (2004). The total energy for moisture removal from the crop, at any given temperature and pressure, is the sum of the latent heat of vaporisation and the binding energy of the moisture in the crop. As noted by Mujumdar (1997) the binding energy can be negative for starches at low temperatures. Eighty percent of carbohydrate produced in cassava is made up of starch (Onyenwoke and Simonyan, 2014). This means that the energy of moisture removal from a starchy crop like cassava, under atmospheric conditions, can be lower than the heat of vaporisation of water in the initial stages of drying especially when the *MC* is high. This is further supported by Aviara and Ajibola (2002) that the heat of vaporization is low at high moisture contents. Normal local winds can therefore do a good job in removing large amounts of the unbound and free moisture from the crop in the initial stages of drying when the initial moisture content is high (Ekechukwu, 1999a; Okos et al., 1992).

At later stages of drying, the moisture becomes more strongly bound to the crop so that more air heating, rather than airflow, is required to remove this bound moisture from the crop. With more heating inside the dryer than outside, the dryer then performed better and overtook the performance in the open sun at later stages of drying. The night self-drying processes were caused by heat inertial effects where some energy stored in the system at periods of sunshine was used in the night for drying. The substantial proportions (about 75% to 80%) of the drying processes that occurred within the first two days and nights for both inside the dryer and in the open sun are also attributable to the ease of moisture removal at high *MC*.

The best overall drying performance of the dryer in relation to that of open sun was observed in trial *UL2* in which the crops were high up the dryer. At this height, the shading effect of the crop shelf was much reduced so that there was a high view factor between the drying-chamber base absorber and the atmospheric dome around the dryer. This enhanced the radiant energy absorption at the base and a subsequent effective air heating of the drying air en-route to the crops. Further, the slant side of the dryer allowed a smaller quantity of crops at this higher level than that at the lower level for about the same quantity drying air which is more effectively heated. This tends to provide a solution to the challenge of ineffective air heating in the direct-mode dryer observed by Afriyie et al. (2009). The relatively poorest drying performance observed in UL3 is attributable to the increased quantity of crops to be dried by practically the same amount of heated air, although the dryer still performed better in the end than the open-sun drying.

The browning of the crop inside the dryer at the initial stages may be attributed to non-enzymatic activity caused by the level of water activity at that time. The water activity of crop increases with high *MC* and also with high temperature (Mujumdar, 1997; Okos et al., 1992; Belessiotis and Delyannis, 2011). Higher temperature inside the dryer than outside, together with high moisture, caused fast browning of the crop in the dryer at the initial stages. At later stages, there was still a considerable amount of moisture in the crop being dried in the open sun, and this continued to cause discoloration so that those crops became more brownish than those inside the dryer.

5. CONCLUSION

A full solar tent equipped with a solar chimney was used to dry cassava and the drying performance was compared with that of open-sun drying. During daytime the whole system functioned as solar heated chimney, so that there was an upward temperature gradient with height which resulted in a downward gradient of the relative humidity, in the no-load process. Early in the morning, a period of low radiant energy intensity, the system functioned like a normal chimney with negative temperature gradient up the chimney. In the initial stages of the drying process, the daytime no-load temperature gradient was distorted as the available energy had to be shared between the drying process and the air heating process.

Drying still continued after sunset as a result of the heat inertial of the system. About 75% to 80% of the drying process occurred within the first two days and nights of the whole period for both the dryer and open-sun drying. The open-sun drying generally did better than the dryer at the initial stages, when cassava drying required more airflow than air heating. Further, high temperatures and lack of effective airflow in the dryer caused browning of the cassava at the

initial stages. The dryer performance, however, overtook that of the open-sun drying at later stages, even at full load. The best performance of the dryer was when the crops were high up the dryer, but only a small amount of crops could be allowed at this height due to the slant sides of the dryer. To enhance the drying process and prevent browning of the crops within the first two days of the drying process, the side doors of the dryer could be opened and covered with only mosquito nets to allow the dryer to make effective use of the airflow from the local winds, while, at the same time, keeping insects and rodents at bay. The side doors could then be closed from the third day onwards to make use of the high temperature for further drying improvement. It can therefore be concluded that in addition to the fact that it is more hygienic, the structurally stable full tent dryer equipped with a solar chimney can end up with a much smaller moisture content of cassava than the moisture content from drying in the open-sun.

6. APPENDIX

Table A1 Dimensions of the solar tent dryer equipped with a solar chimney

Part of dryer	Dimension
Width of drying chamber base (perpendicular to inlet airflow)	1.50 m
Length of drying chamber base (in the direction of inlet airflow)	1.70 m
Height of drying chamber	1.50 m
Thickness of drying chamber base	0.03 m
Roof angle of drying chamber to the horizontal plane	60^0
Dryer inlet width	120 cm
Dryer inlet gap	0.30 m
Height of chimney walls (glazed)	0.48 m
Height of chimney roof (glazed)	0.20 m
Height of chimney absorber	0.48 m
Chimney gap	0.40 m
Chimney roof angle to the horizontal	38^0
Exit gap	0.06 m
Height of lower shelf from the base of drying chamber	0.35 m
Height of upper shelf from the base of drying chamber	1.05 m

7. ACKNOWLEDGEMENT

The authors would like to express their sincere thanks to the Departments of Chemical Engineering and Mechanical Engineering of Kumasi Polytechnic, Kumasi, Ghana, for the use of their equipment and facilities. Further appreciations are expressed to the Kumasi Polytechnic as a whole for the use of its premises for the physical experimentations.

8. REFERENCES

Afriyie, J. K., Nazha, M. A. A., Rajakaruna, H. and Forson, F. K. (2009). Experimental investigations of a chimney-dependent Solar Crop Dryer. Renewable Energy 34 (1), 217–222.

Afriyie, J. K., Nazha, M. A. A., Rajakaruna, H. and Forson, F.K., (2011). Simulation and optimisation of the ventilation in a chimney-dependent Solar Crop Dryer. Solar Energy 85, 1560-1573.

Afriyie, J. K. and Bart-Plange, A. (2012). Performance Investigation of a chimney-dependent Solar Crop Dryer for different inlet areas with a fixed outlet area. *International Scholarly Research Network ISRN Renewable Energy, Article ID 194359, 9 pages doi:10.5402/2012/194359*

Afriyie, J. K., Nazha, M. A. A., Rajakaruna, H. and Forson, F. K. (2013). Mathematical modelling and validation of the drying process in a chimney-dependent Solar Crop Dryer. *Energy Conversion and Management 67, 103-116*.

Andrew W. (2002). Cassava utilization, storage, and small scale processing. *Natural resource institute, Chatham maritime. UK, 14, 270-290.*

Belessiotis V. and Delyannis E. (2011). Solar drying. *Solar Energy 85, 1665-1691*

Cansee, S., Watyotha, C., Thivavarnvongs, T., Uriyapongson, J. and Varith, J. (2008). Effects of temperature and concentration on thermal properties of cassava starch solutions. *Songklanakarin J. Sci. Technol. 30 (3), 405-411*

Chantawong, P., Hirunlabh, J., Zeghmati, B., Khedari, J., Teekasap, S. and Win, M. M. (2006). Investigation on thermal performance of glazed solar chimney walls. *Solar Energy 80, 288–297*.

Chen, Z. D., Bandopadhayay, P., Halldorsson, J., Byrjalsen, C., Heiselberg, P. and Li, Y. (2003). An experimental investigation of a solar chimney model with uniform wall heat flux. *Building and Environment, 38, 893-906.*

Ekechukwu O. V. (1999a). Review of solar-energy drying systems I: an overview of drying principles and theory. *Energy Conversion and Management, 40, 593-613.*

Ekechukwu, O. V. (1999b). Review of solar-energy drying systems II: an overview of solar drying technology. *Energy Conversion and Management, 40, 616–655.*

Ekechukwu, O. V. and Norton, B. (1997). Design and measured performance of a solar chimney for natural circulation solar energy dryers. *Renewable Energy, 10 (4), 81–90.*

Ferreira, A. G., Maia, C. B., Cortez, M. F. B., and Valle, R. M. (2008). Technical feasibility assessment of a solar chimney for food drying. *Solar Energy 82, 198–205.*

Incropera F. P., De Witt D. P., Bergman T. L. and Lavine, A. S. (2007). Introduction to heat transfer, 5th edition, John Wiley & Sons Inc., Hoboken, New Jersey.

Jain, D. and Tiwari, G. N. (2004). Effect of greenhouse on crop drying under natural and forced convection I: Evaluation of convective mass transfer coefficient. *Energy Conversion and Management, 45, 765-783.*

Lola, A., Lawrence, O. O. and Adefunke, B. (2012). Effect of delayed processing on some physico-chemical properties of cassava starch. *American Journal of Food and Nutrition Print; ISSN 2157-0167, Online: ISSN 2157-1317, doi:10.5251/ajfn.2012.2.2.31.36 © 2012, ScienceHuß, http://www.scihub.org/AJFN*

Mujumdar, A. S. (1997). Drying fundamentals. In: Baker, C. G. J. (Editor) Industrial Drying of foods, Blackie Academy and Professional, ISBN 0-7514-0384-9, 7-30.

Olufayo, A. A. and Ogunkunle, O. J. (1996). Natural drying of cassava chips in the humid zone of Nigeria. *Bioresource Technology, 58, 89–91.*

Ong, K. S. (2003). A mathematical model of a solar chimney. *Renewable Energy 28, 1047-1060.*

Ong, K. S. and Chow, C.C. (2003). Performance of a solar chimney. *Solar Energy, 74, 1-17.*

Onyenwoke, C. A. and Simonyan, K. J. (2014). Cassava post-harvest processing and storage in Nigeria: A review. *African Journal of Agricultural Research, 9 (53) 3853-3863.*

Okos, M. R., Narsimhan G., Singh R. K. and Weitnauer, A. C. (1992). Food Dehydration. In: Heldman, D. R., Lund D. B., (Editors) Handbook of Food Engineering. Marcel Dekker, Inc, New York, Basel, Hong Kong, 437-562

Owusu-Baah K, Workshop on ECOWAS policy (2004). (Accessed from the Ghana Homepage: http://www.ghaweb.com on 30/11/2004)

Pongsawatmanit, R., Temsiripong, T., Ikeda, S. and Nishinari, K. (2006). Influence of tamarind seed xyloglucan on rheological properties and thermal stability of tapioca starch. *Journal of Food Engineering. 77 (1), 41-50.*

Rogers, G. F. C. and Mayhew, Y. R. (1992). Engineering Thermodynamics, Work and Heat Transfer, 4th Edition, ISBN 0-582-04566-5

Sharma, A., Chen, C. R. and Lan, N. V. (2009). Solar-energy drying systems: A review. *Renewable and Sustainable Energy Reviews 13, 1185–1210*

Singh, S., Singh, P. P., Dhaliwal, S. S. (2004). Multi-shelf portable dryer. *Renewable Energy, 29, 753-765.*

Stone, G.D., 2002. Both Sides Now. *Current Anthropology 43(4):611-630.*

International Journal of Science and Engineering Applications
Volume 5 Issue 3, 2016, ISSN-2319-7560 (Online)

A Review on Maintenance and Troubleshooting of DC Machines

K. Mahesh Kumar
Department of EEE
Sethu Institute of Technology,
Pulloor, Kariapatti, India

A.Krishnaveni
Department of ECE
P.S.R Engineering College,
Sivakasi, India

D. Edison Selvaraj
Department of EEE
Panimalar Engineering College
Chennai, India

T. Gunasekaran
P.Manikandan
Lieutenant. J.Ganesan
Department of EEE
Sree Sowdambika College of
Engineering, Aruppukottai,
India

Abstract: This paper simply covers the maintenance of DC machines. In addition DC Generator, DC Motor types and applications are discussed neatly. DC motor troubles and their remedies are listed in simple figure. This paper would be helpful for the technicians to improve the plant efficiency.

Keywords: Motor, Generator, Commutator, armature, brush

1. INTRODUCTION

An electrical machine is a device which converts mechanical energy into electrical energy or vice versa. Now a day's dc motor plays important role in electric traction and industry. In industry routine maintenance is essential to reducing plant downtime.

2.TYPES OF DC MACHINES

DC machines classified in to two types DC Generator and DC Motor.

2.1 DC Generator

An Electrical generator is a rotating machine which converts mechanical energy into electrical energy. This energy conversion is based on the principle of electromagnetic induction. According to Faraday's laws of electromagnetic induction, whenever a conductor is moved in a magnetic field, dynamically induced e.m.f is produced in the conductor.

2.1.1 Types of DC Generator

DC generators can be classified according to their methods of excitation. There are two types of DC generators [4].

1. Separately excited DC generator

2. Self excited DC generator

   i. Series generator
   ii. Shunt generator
   iii. Compound generator
      a. Long shunt Compound generator
      b. Short shunt Compound generator

2.1.2 Applications of DC Generator

The table 1 shows the applications of DC generator.

S. No.	Type of Generator	Applications
1	DC shunt Generator	For electro plating Battery charging For excitation of Alternators
2	Series Generators	Used as Boosters Used for supply to arc Lamps
3	Compound Generator	Differential Compound generators are used to supply dc welding machines.
		Level compound generators are used to supply power for offices , hostels and Lodges etc.
		Over compound generators are used to compensate the voltage drop in Feeders
4	Separately Exited Generator	As a supply source to DC Motors, whose speed is to be controlled for certain applications. Where a wide range of voltage is required for the testing purposes

2.2 DC Motor

2.2.1 Basic Principle of DC motor

The basic principle of operation of a dc motor is a whenever a current carrying conductor is placed in a magnetic field, the conductor experiences a force tending to move it [4].

2.2.2 Types of DC motor

The classification of DC motors is based on the connections of filed winding in relation to the armature

1. Separately excited DC motor
2. Self excited DC motor
   a. Series motor
   b. Shunt motor
   c. Compound motor
      - Long shunt compound motor
      - Short shunt compound motor

2.2.3 Applications of DC Motors

The table 2 shows the applications of DC motor.

The Table 2 Applications of DC motor

S. No.	Type of Motor	Applications
1	DC Shunt Motor	Blowers Fans Centrifugal and Reciprocating pump Lathe machines Machine tools Milling Machines Drilling Machines
2	DC Series Motor	Cranes Hoists Elevators Trolleys Conveyors Electric Locomotives
3	Cumulative Compound Motor	Rolling mills Punches Shears Heavy planers Elevators
4	Differential Compound Motor	Not suitable for practical applications

3. PROCEDURE FOR STARTING OF DC GENERATOR

The following figure 1 shows the procedure for starting of DC generator.

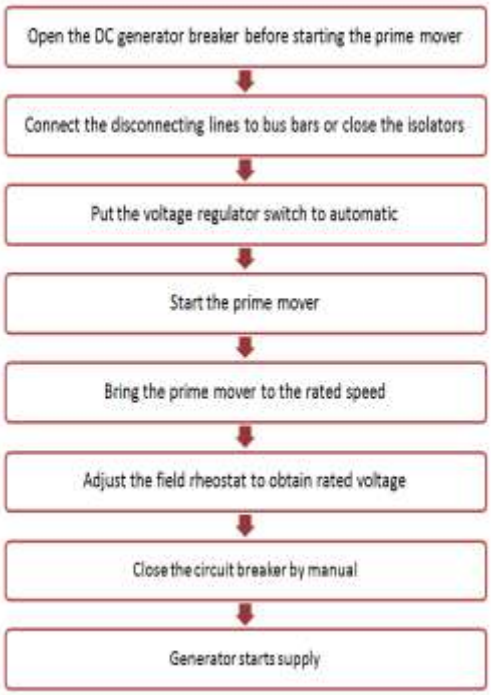

Figure 1 Procedure for Starting of DC Generator

4. CAUSES OF VOLTAGE FAILURE OF DC GENERATOR

Voltage failure is mainly caused by failure to build up the flux and low speed. The following figure 2 shows the various causes of voltage failure of DC Generator [1].

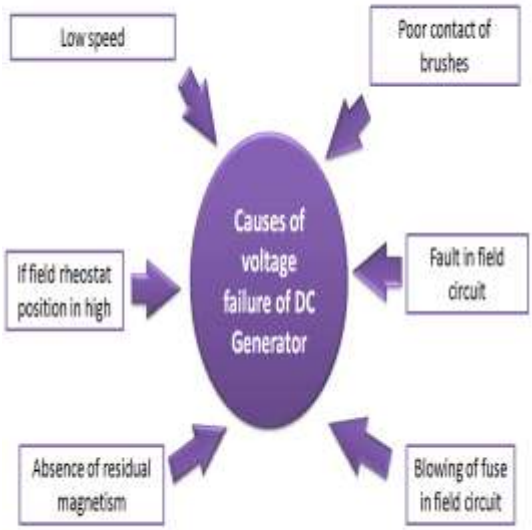

Figure 2 various causes of voltage failure of DC Generator

5. PROCEDURE OF INSTALLATION AND COMMISSIONING OF DC MOTOR

The following figure 3 shows the Procedure of installation and commissioning of DC Motor

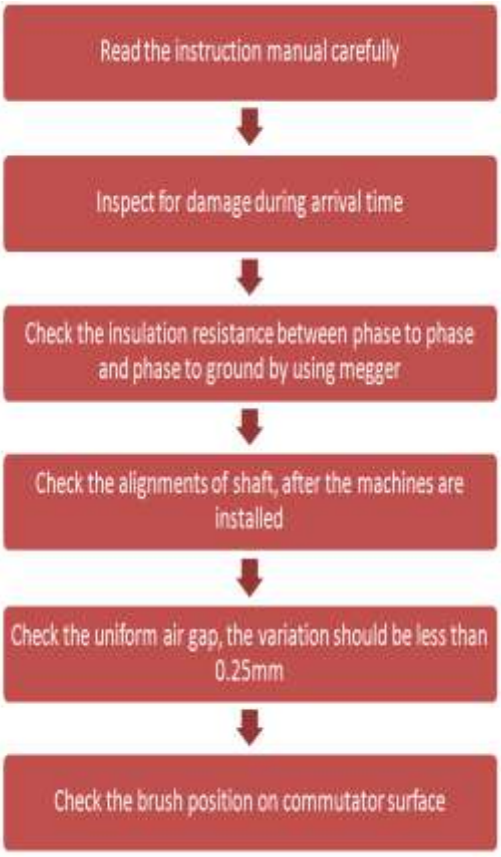

Figure 3 Procedure of installation and commissioning of DC Motor

The following figure 4 shows the Primary check during installation of DC Motor

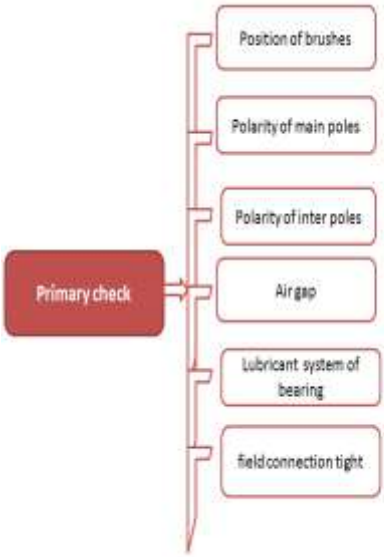

Figure 4 Primary checks during installation of DC Motor

The following figure 5 shows the Running checks after installation of DC Motor

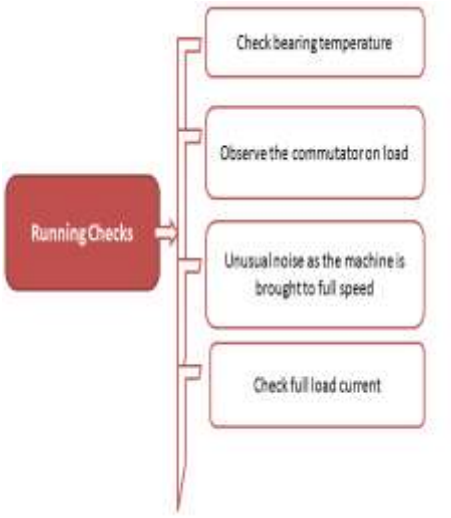

Figure 5 Running checks after installation of DC Motor

6. PREVENTIVE MAINTENANCE

6.1 Preventive maintenance

1. Includes electrical testing and visual inspection of the armature, commutator, brushes and filed coils [2].
2. Insulation to ground tests on DC equipment to evaluate the condition of insulation.
3. Checking brushes and commutator condition are very important parts of preventive maintenance

6.2 Armature

1. Visual inspection of the armature should include the search for cracked or brittle insulation, loose or broken banding and any dirt or oil contamination.
2. Leakage to ground testing of the armature indicates the insulation condition.
3. Bar to bar resistance check indicates shorted winding or defective solder joints at the risers.
4. Infrared inspection of the armature can reveal overheating of the brushes, commutator, loose or hot connections on the risers [3].

6.3 Fields

1. Visual inspection of the filed coils will expose cracked or brittle insulation.
2. Leakage testing provides the insulation level.
3. Drop test are used to find out shorted winding. In this test 110 v ac is applied to the field leads. The voltage drop across each filed pole is measured with a voltmeter. In healthy motor, all voltage drops should be equal.

6.4 Commutator

Check the commutator surface, brush and brush holder tension.

6.4.1 High Mica

1. Mica is the insulation material used between each segment in a commutator.
2. Mica should be approximately 1/16” lower than the adjacent commutator bars

3. If the commutator bars are worn the result will be brush chatter. Putting the dumb end of a lead pencil or other insulated device, on a brush while the motor is rotating and feeling for vibration can identify this.

6.4.2 High Commutator bars

Usually caused by the wedge or wedge ring [3].

7. DEFECTS IN ARMATURE WINDING, COMMUTATOR

The following types of faults occurred in armature winding. They are Open circuit fault, Short circuit fault and Earth fault or ground fault [5]

7.1 Open circuit fault:

Occurs when the armature conductors get broken or when a joint with commutator pulls out.

7.2 Short circuit fault

If the insulation between armature conductors in failure, a current floes between them. This is called short circuit.

7.3 Earth fault:

Due to failure of insulation of armature conductor and slot insulation a faulty current flows from armature conductor to core. This fault is called earth fault [6].

7.4 Causes of sparking in commutator

Sparking is the production of an arc due to jumping of current occurs due to the following reasons

1. Overloading
2. Brushes may be sticking in the holders.
3. Spring pressure may not be sufficient.
4. Brushes may be burned on the edges.
5. Commutator surface may be rough having high bars.
6. Grade of carbon brushes may be incorrect.
7. Mica may be high in the slots. Brushes will wear act rapidly with high mica.
8. Pressure on some brushes may be more, resulting in sparking.
9. Brushes may be too loose in the holders.
10. Pig tails may be loose in the same of the brushes.
11. Sparking can also be due to defects in the armature and field circuits.
12. If there is an open circuit in the commutator riser, a bright flying spark will occur.

8. TROUBLE SHOOTING

The following figure 6 to 10 shows the different type of DC Motor troubles and their remedies [5].

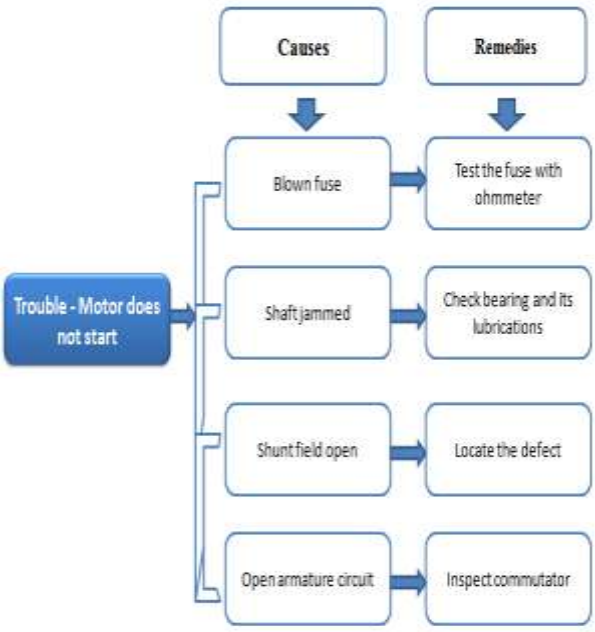

Figure 6 Motor does not start trouble and their remedies

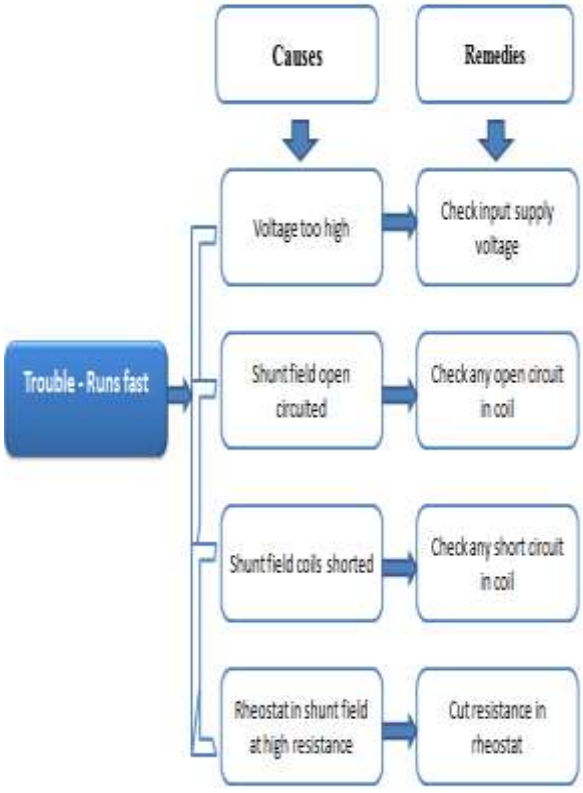

Figure 7 Motor runs fast trouble and their remedies

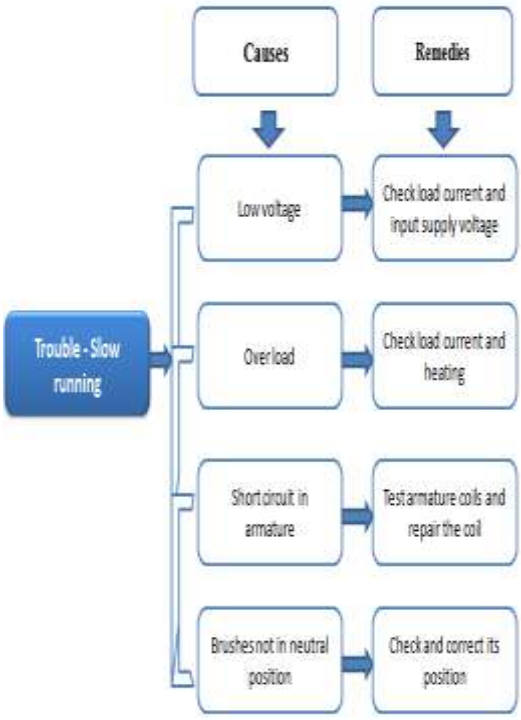

Figure 8 Motor slow running trouble and their remedies

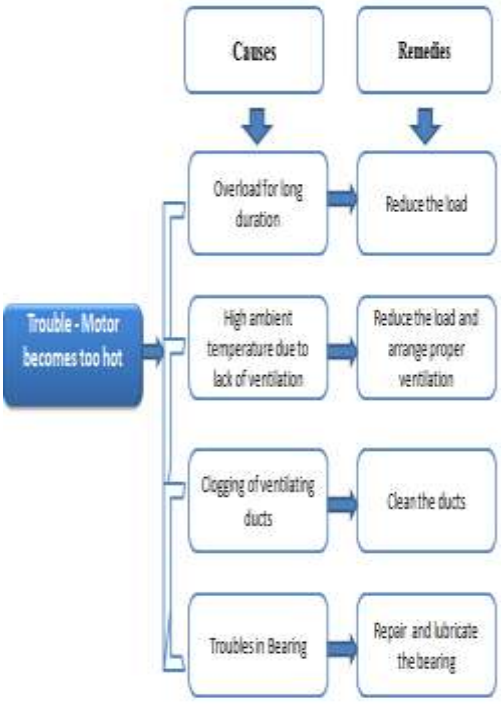

Figure 9 Motor becomes too hot trouble and their remedies

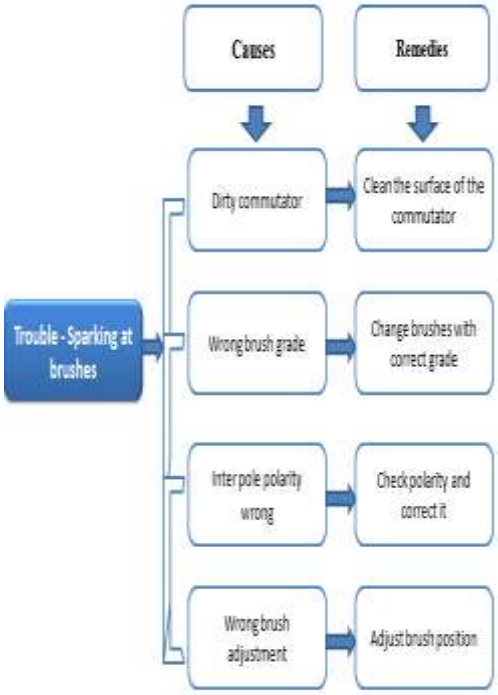

Figure 10 sparking at brushes trouble and their remedies

9. CONCLUSION

In this paper maintenance of DC machines were discussed in simple. Proper Maintenance of DC motor reduces unplanned downtime. Preventive maintenance can improve the motor efficiency and reduces energy consumption which will results in improved plant efficiency.

10. ACKNOWLEDGEMENT

We express our sincere thanks to the God, the Almighty, and Lord Jesus Christ. We express our gratitude towards our Tamil Scientist Dr. A.P.J. Abdul Kalam. We express our deep heart feelings towards His death and the people who have lost their lives in Tamil Nadu floods, 2015.

11. REFERENCES

[1] Basic Electrical Engineering, M.L.Anwani, Dhanpat Rai & Co.
[2] http://www.pdma.com/pdfs/Articles/DC_Motor_Analysis.pdf
[3] http://www.ohioelectricmotors.com/2015/07/a-general-guide-to-dc-motor-maintenance
[4] Electrical Machines -1 J. Gnanavadivel et. Al, Anuradha Publications.
[5] Testing commissioning Operation and maintenance of electrical equipment S.Rao, Khanna Publishers
[6] Brumbach, Michael.E and Clade, Jeffery. A, Indusdtrial Maintenace Thomson Delmar Learning, 2003

International Journal of Science and Engineering Applications
Volume 5 Issue 3, 2016, ISSN-2319-7560 (Online)

Copper and Copper Oxides Nanoparticles Synthesized by Electrochemical Technique in Chitosan Solution

F. A. Omar, M. M. El-Tonsy, A. H. Oraby, Fikry M. Reicha

Physics Department, Faculty of Science, Mansoura University, Mansoura, 35516, Egypt

Abstract

A synthesis of chitosan copper and copper oxides nanoparticles (Cs-Cu, CuO) NPs via electrochemical technique has been reported. Chitosan copper complexes were prepared by electrochemical oxidation technique at duration time followed by reduction using different reducing agents for producing chitosan copper nanoparticles, Cs used as stabilizer and capping agent. The nanocomposites were characterized by using ultraviolet-visible spectroscopy (UV-vis). Transmission electron microscope (TEM) images were investigated emphasized formation the formation of NPs with different shapes. The average size of formed NPs is 28 nm. X-ray diffraction (XRD) is used to investigate the formation of the crystalline structure of prepared samples exhibited presence of copper and copper oxides in the formed complexes and nanocomposites. Analysis of FTIR showed chelation of Cu^{+2} with chitosan in complex form and electrostatic interaction between chitosan and copper nanoparticles.

Keywords: Chitosan, Chitosan Copper complex, copper and copper oxide nanoparticles

1. INTRODUCTION

In recent years, many researches were carried out on preparation of nanomaterials. Nanoparticles (NPs) show different physical, chemical and biological properties rather than bulk materials due to a high specific surface area to volume ratio [1]. The nanophase is intermediate between microstate and macrostate showed different properties than them. In last decades metallic NPs are widely used in many fields of science, industry and in medical applications due to their properties. They are utilized in many biomedical applications such as in the cosmetics industry, drug delivery and hyperthermia [2].

Nowadays, chitosan metal complexes and chitosan metal nanocomposites were studied extensively due to their applications in biological fields. Copper is considering as one of the most important nanometal in such composites. Chitosan copper $[Cs\text{-}Cu]^{+2}$ complexes and nanocomposites of chitosan (copper and copper oxides) have excellent antimicrobial activity against various bacterial strains [3], also exhibited antitumor applications [4, 5].

Copper is essential for metabolic processes and organs function, also provides a role in development and maintenance of cardiovascular system, the skeletal system, human immune system and function of the nervous system. It has good antimicrobial and antibiotic properties [6].

For the last years, many efforts have been made on the synthesis of metallic copper nanoparticles in condensed phase with shape, size and growth control [7]. Copper NPs syntheses by many methods such as metal-vapor synthesis[8], radiation methods[9], vacuum vapor deposition[10], thermal reduction [11], chemical reduction[12], laser ablation[13] and microemulsion techniques[14]. The major limitation in these syntheses are their highly costing and toxically for environment. Electrochemical technique first developed by Reetz and Helbig in 1994 is a very promising technique for the production of metal nanoparticles because of their simplicity, environment-friendly process (eco-friendly) and their versatile application in the preparation of particles with different shapes and sizes. In their setup, a sacrificial anode is used as the metal source, which released ions and the resulting metal ions were reduced at cathode, forming metallic particles stabilized by tetraalkylammonium salts [15]. Usually, the electrolytic solution used for the production of metal nanoparticles contains (metal salt in acidic medium, surfactant stabilizer to form complexation or chelation with metal ions and reducing agent). Chitosan has been used as electrolytic solution for preparing green nanocomposites. Nowadays, most important copper nanocomposites are copper chitosan complexes and nanocomposites [16]. Chitosan is a partially deacetylated derivative of chitin. Chitosan is the second most used natural polysaccharides after cellulose [17]. Chitosan extracted from the shells of crustaceans like crabs, lobsters and prawns. Owing to its unique properties such as biodegradability, biocompatibility, and biological activity, chitosan has been widely applied in the food and cosmetics industry as well as the biomedical applications in relation to tissue engineering, antimicrobial, non-toxicity, anti-tumor properties, and the pharmaceutical industry relating to drug delivered [18]. It is recommended that chitosan of lower molecular weight exhibited strong bacterial and superior biological activities than high molecular weight [19]. It have been pointed out that the –OH and $–NH_2$ groups on the chitosan back bone are very active chelating groups to coordinate with transition metal ions to form two types of chitosan metal complexes named "bridge model" and "pendant model [20]. Also it is shown that coordinating bond may lead to weak point on the chitosan chain which in turn leads to degradation of chitosan [21]. Degradation of chitosan and chitosan metal complexes can be occurred by electrochemical oxidation technique [22, 23]. Degradation rate found to be dependent on the time of process, which lead to controlling the molecular weight [24].

The aim of our study in the present manuscript describes a strategy which depends on preparation of chitosan copper complex having different copper/chitosan ratio by electrochemical oxidation technique and followed by reduction (using ascorbic acid, $NaBH_4$ and N_2H_4 reducing agents) to produce chitosan copper nanocomposites.

2. EXPERIMENTAL TECHNIQUES

2.1. Chemical and methods

Chitosan Mw = 600,000 g/mol and Deacetylation degree (DD) is 75% (Aldrich chemical co.), De-ionized water (resistivity $>2x10^8\Omega cm$) was used for all samples preparation, Acetic acid of analytical grade, Platinum sheets Sigma-Aldrich, used as

counter electrode (cathode). Copper plates from Sigma-Aldrich of purity 99.999%, was used as source electrode (anode).

2.2. Synthesis of chitosan Copper Complex and copper nanoparticles

[Cs-Cu] $^{+2}$ complexes were produced by using the electrochemical technique of copper metal in an aqueous acidic medium. The electrochemical process was carried out at constant potential of 1.5V to avoid the hydrolysis of water. Electrolytic solution was prepared by dissolving 1 wt% chitosan into 100 ml deionized water containing 1% acetic acid, then solution placed on magnetic stirrer for 24 hrs. The pH of solution is adjusted at 4.6 before running the experiment. This pH value was fixed for the preparation of used complexes. The cell used to prepare chitosan copper complex $[Cs\text{-}Cu]^{+2}$ consists of Platinum sheet (cathode) and Copper sheet (anode) were dipped in the electrolytic solution separated by a fixed distance 5 cm from each other. The electrodes were connected to a suitable variable resistor and constant-voltage power supply (Model 1030A, U.S.A). The temperature was held constant at 25˚C by using a rotating water bath (VEB MLW, Type U4; GDR).Preliminary experiments were carried out for different running times ranged at (8hrs, 12 hrs, 16 hrs., and 20 hrs.). The solution was centrifuged by IEC Micromax microcentrifuge at speed (10,000 rpm for 30 min.), and filtered to remove any debris. Then the pH value is readjusted at 5 for the chitosan-copper complexes. These complexes were reduced by different types of reducing agent such as ascorbic acid, hydrazine hydrate and sodium borohydride. The samples were casted onto petri dishes (diameter 11cm) and left to dry at room temperature. After complete drying, samples are removed from the dishes and divided into pieces for measurement of some physical properties with different techniques.

2.3. Characterization

Chitosan, chitosan copper [Cs-Cu] $^{+2}$ complexes and Cs-Cu nanocomposites were characterized by following measurements. ATI Unicom UV–Vis spectrophotometer which working in the range of 200–900 nm. (NICOLET-IS10 FTIR located at chemistry department, faculty of science, Mansoura University) show spectra of [Cs- Cu] $^{+2}$ complexes and NPs. Transmission Electron Microscope (JEOL JEM - 2100 located in Mansoura University) with acceleration voltage of 160 kV was utilized to determine the size and distribution of nanoparticles in prepared samples. X-ray powder diffraction (XRD) patterns of Cs-Cu NPs were obtained by using Siemens D5000 diffractometer. The source of X-ray was Cu Kα radiation (40kV, 30mA). Differential thermal analyzer (DTA) (sltimad24 Japan located in Cairo University) under nitrogen gas.

3. RESULTS AND DISCUSSION

3.1. Chitosan copper complexes

The atomic absorption spectrometry is used to record the amount of copper molar ratios in prepared samples (chitosan copper complexes) at different duration time (8h, 12h, 16h, and 20h). It was found that the amount of copper content increase by increasing the complexation time. This behavior is shown in Figure (1) and represented by the polynomial empirical formula:

$$C = A + B_1 t + B_2 t^{2+} B_3 t^3$$

Where C is the concentration at any time (t) and, where A is constant= 47.26 and B_1 is constant = 58.58, B_2 = -3.38 and B_3 = 0.067

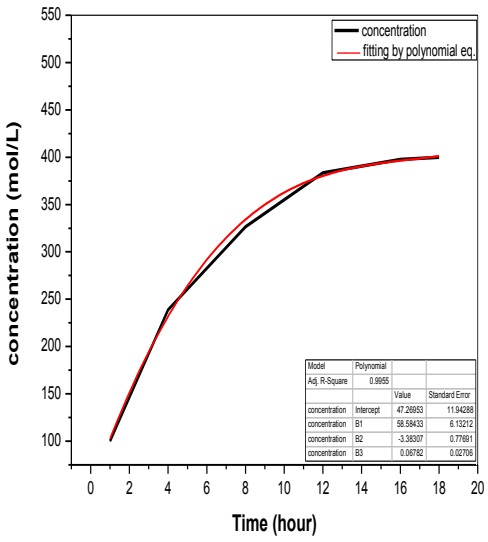

Figure (1) copper concentration in chitosan solution.

3.2. Optical characterization

A- UV/Vis absorption spectra of chitosan copper complexes

Figure (2) represents the UV/Vis absorption spectra of copper ions with chitosan at different experimental duration time of electrochemical oxidation. It shows the appearance of absorption peaks at 258 nm, 294 nm and broad one at 750 nm for all prepared samples. Band at 258 nm may be due to Cu(I) ions, and at 258 nm due to Cu (II) ions chelated with chitosan [25]. The peak around 750 nm is a common peak at all complexation of copper with any ligands, appeared due to complexation of copper with chitosan, this broad peak is existed in all formed complexes. This hump peak is attributed to the d–d transition of Cu^{+2} ions [26]. The intensity of this peak was increased by increasing the duration time. This peak vanished when using reducing agent due to conversion of [Cs-Cu] $^{+2}$ complex to chitosan copper and copper oxides nanocomposites as shown in figure (3).

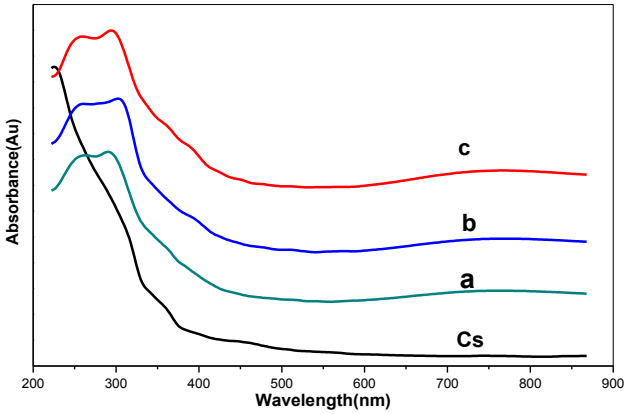

Figure (2): UV spectra of CS and its complexes at different complexation time (a) 8h, (b) 12h and(c) 16h.

B- UV/Vis absorption spectra of chitosan copper nanocomposites

UV-Vis spectra of chitosan copper nanocomposites with different reducing agents. From this spectrum the broad band of complex is completely disappeared while new characteristic bands appeared as represented in figure (3). Figure (4) exhibits peaks at about 360 nm and 314 nm that may be attributed to oxides nanocomposites phase (CuO, Cu_2O) [22, 27]. The sample which reduced by ascorbic acid (a), has peaks of Cu NPs appeared at 314 nm, 360 nm and 400 nm, which refer to Cu NPs in different shape and size [28]. The sample which reduced by $NaBH_4$ (c), showed the peaks of copper and copper oxides at 314 nm, 360 nm and 427 nm. The sample which reduced by N_2H_4 (d) contains a set of peaks for copper and copper oxides at 314 nm, 360 nm and 484 nm. The peak at 484 nm is a very broad peak is due to existence of different sizes of Cu NPs. The chemical reduction method using copper salt usually characteristic peak of copper around at (556-600 nm), but in our experimental it has not appeared at this wavelength. This is due to the lack of homogeneity in the shape and size of nanoparticles NPs, where the dipolar plasma resonance is found dependent on the shape of NPs ((spheres- pentagonal – triangular prisms)) [29].

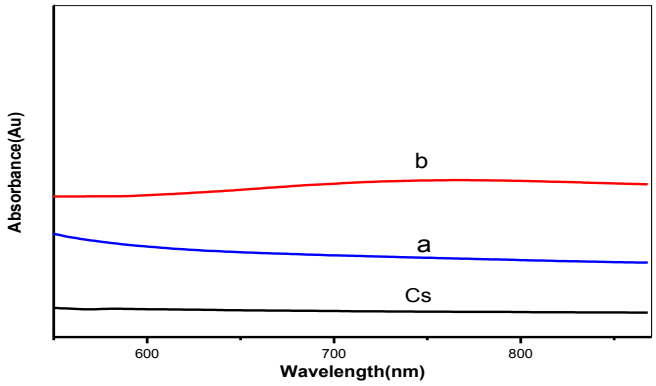

Figure (3): UV spectra of the disappeared of hump peak: CS and it's (a) after reduction and (b) complex at time16h.

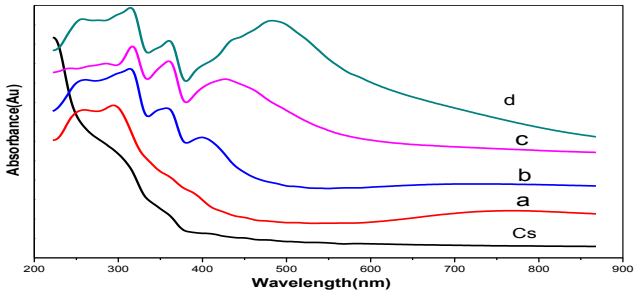

Figure (4): optical absorption spectra of: (a) complex at duration time (16h), (b) reduced chitosan copper complex at

complexation time (16h) with ascorbic acid, (c) reduced with $NaBH_4$, (d) reduced with hydrazine.

3.3. Fourier transformation Infra-Red (FTIR) analysis

FTIR characteristic bands of chitosan there are shown in figure (5). Chitosan exhibit abroad band at 3482 cm^{-1} attributed to $–NH_2$ symmetrical stretching and hydrogen bonded –OH [30]. The peaks at 2918 cm^{-1} and 2827 cm^{-1} corresponded to CH_2 asymmetrical and symmetrical stretching [31]. Furthermore, the peak at 1423 cm^{-1} assigned to CH_2 bending vibration[32]. The band at 1648 cm^{-1} assigned to C=O stretching vibration of amide bond resulted from traces of chitin [20]. The band at 1598 cm^{-1} corresponds to NH_2 bending vibration [33]. The peak at 1384 cm^{-1} attributed to C-H asymmetrical bending vibration. The band at 1253 cm^{-1} assigned to C-N stretching vibration, the peak at 1067 cm^{-1} related to O-H groups of chitosan.

FTIR spectra of chitosan copper complexes exhibited some vibrational modes that differ from chitosan as shown in figure (5). The broad band at 3482 cm^{-1} shifted to 3434 cm^{-1} assigned to stretching vibration of $–NH_2$ and –OH groups, with increasing the Cu^{+2} content in complexes through increasing the duration time of oxidation, the band become less broadening, which also indicated decrease the intermolecular force (hydrogen bond) within the molecules and become more ordered. The bands at 1598 cm^{-1} corresponds to NH_2 bending vibration shifted toward 1561 cm^{-1} this referred to the chelation of NH_2 and OH functional groups of chitosan with Cu^{+2}.

Figure (6) shows FTIR spectra for $[Cs\text{-}Cu]^{+2}$ complex at duration time (16h) that reduced by different types of reducing agents (N_2H_4 (a), $NaBH_4$ (b) and ascorbic acid (d)). With ascorbic acid (d) the peak at 2927 cm^{-1} attributed to C-H asymmetric stretching vibration has become more sharp after reduction by ascorbic acid, a two peaks at 1634 and 1770 cm^{-1} attributed to NH_2 bending and C=O stretching respectively. The peak at 774 cm^{-1} assigned to Cu-N stretching vibration, which an evidence for electrostatic attraction between Cu and chitosan. There is no peak for oxidation of Cu due to ascorbic acid act as antioxidant[34]. In samples which reduced by N_2H_4 (a) and $NaBH_4$(b) the peak at 525 cm^{-1} and 646 cm^{-1} were assigned to the stretching vibration N with cupric oxide (Cu_2O) and cuprous oxide (CuO) respectively [35, 36].

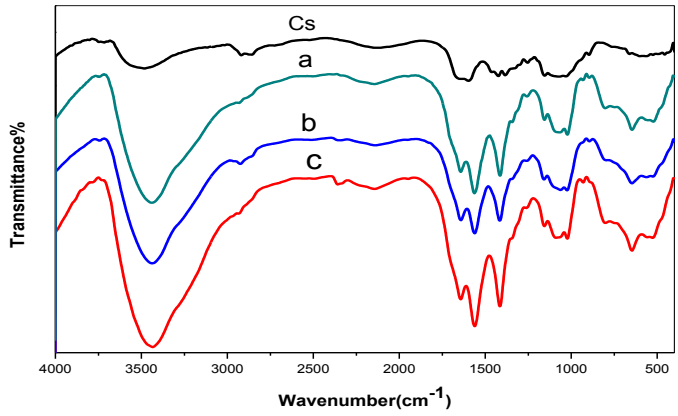

Figure (5) FTIR spectra of Cs, Chitosan copper complexes prepared at different duration time: (a) 8h, (b) 12h, and (c) 16h

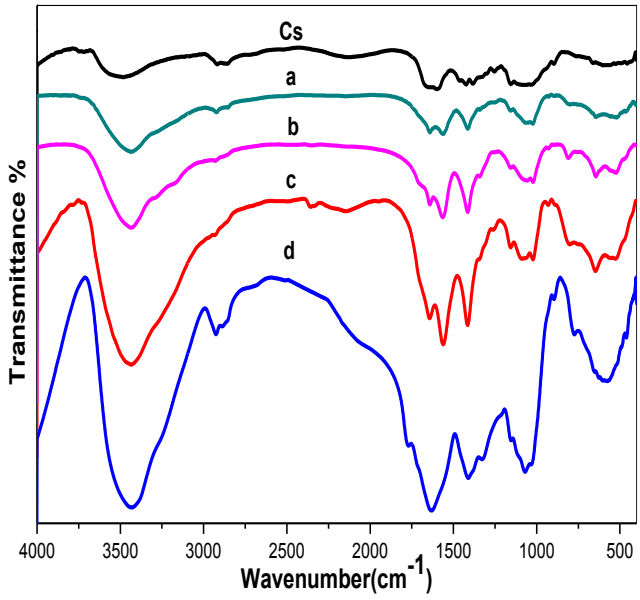

Figure (6): FTIR spectra of Cs, (c) chitosan – Cu complex 16h, (a) reduced the $[Cs\text{-}Cu]^{+2}$ complex with hydrazine, (b) reduced $[Cs\text{-}Cu]^{+2}$ complex with $NaBH_4$, (d) reduced $[Cs\text{-}Cu]^{+2}$ complex with ascorbic acid.

3.4. X-Ray diffraction (XRD)

X-Ray powder diffraction patterns of pure chitosan, chitosan copper complex and Cu NPs are shown in Figure (7).The diffraction pattern of chitosan is characteristic of amorphous structure, diffractogram of Cs has the characteristic peaks at diffraction angle 2θ equal to 10° and 20° were found in

literatures [37, 38] and it contains a crystalline seed at angle 2θ equal to 29.7 °. When the process was running to form the [Cs-Cu] $^{+2}$complex lead to formation of different crystalline forms of chitosan their characteristic peaks appeared at angle 2θ equal to (11°, 12.6°, 17°, 19°, 22°, 25°) and a small peaks at angle 2θ equal to 32.6°, 34°, 36.7° and 40.8° referred to formation small amount of copper and copper oxides nanoparticles [39]. The existence of copper and copper oxides nanoparticles confirmed that the chitosan act as reducing and capping agent [40]. The intensity of [Cs-Cu] $^{+2}$complex become sharper after adding different types of reducing agents. A number of peaks at angle 2θ equal to 32.6°, 34°, 36.7°, 40.8° and 44° in samples which reduced by N_2H_4 and $NaBH_4$ (c and d) characterized for formation CuO and Cu_2O. In sample which reduced by ascorbic acid (b) which contain peaks characteristic for copper NPs at diffraction angle 2θ equal to 43.19°, 50.36° and 74.12° corresponding to (111), (200) and (220) planes of FCC crystalline structures of Cu respectively [41] . Ascorbic acid act as antioxidant and strong reducing agent, lead to disassembles of CuO and Cu_2O NPs[42].

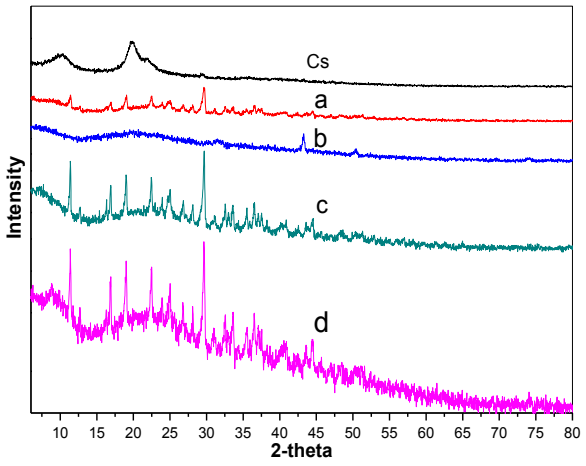

Figure (7): (XRD) for Cs, (a) [Cs-Cu] $^{+2}$ complex (16h), (b) reduction by ascorbic acid, (c) reduction by hydrazine, (d) reduction with $NaBH_4$.

3.5. Differential thermal analysis (DTA)

DTA Thermograms for pure chitosan (Cs) is shown in figure (8). For pure chitosan, we can notice that the endothermic peak at 15.7 C° is due to lose of free water or moisture evaporation. The broad peak indicates that Cs has amorphous structure. Chitosan is a non-thermoplastic material, the melting endothermic temperatures peak was completely absent in the curve because Cs does not have the melting or glass transition temperatures [43, 44]. In the samples (c and d) the [Cs-Cu] $^{+2}$complex show endothermic peaks at 42.19C°, 47.9 C° and 52.6 C° respectively due to moisture evaporation. Sample (b) doesn't contain any peaks due to the presence of copper NPs and have no copper oxide. The samples (a), (c) and (d) contain two crystalline phases at exothermic peaks at 306 C°, 309 C° and 324 C° which may be characteristics for crystalline behavior of both CuO and Cu_2O, existing due to building up of atoms, self-arrangements, in an ordered shape.

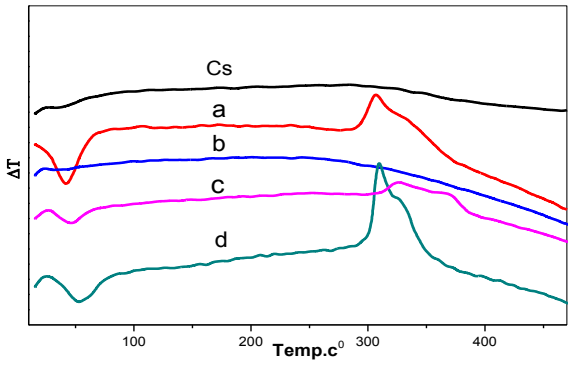

Figure (8) DTA for Cs, (a) [Cs-Cu] $^{+2}$ complex (16h), (b) reduction by ascorbic acid, (c) reduction with $NaBH_4$, (d) reduction by hydrazine.

3.6. Particle size and structure

The Cu NPs were synthesized and confirmed with particles size as shown in TEM micrograph (9). These particles, essentially, were very fine and roughly monodispersed, revealing that the presence of chitosan, indeed, restricted the growth of Cu nanoparticles efficiently. The average size of formed NPs is 28 nm. Figure (9) illustrate high resolution transmission electron microscopy images (HRTEM) of formed NPs. Most of formed crystals have FCC structure in samples that reduced by ascorbic acid which also confirmed by electron diffraction and lattice space images as shown in figure 9 (b and c). Figure 9 (e and f), shows the formation of fivefold crystals of reduced copper nanoparticles by $NaBH_4$ formed Cu this attribution was frequent in the literature [45].

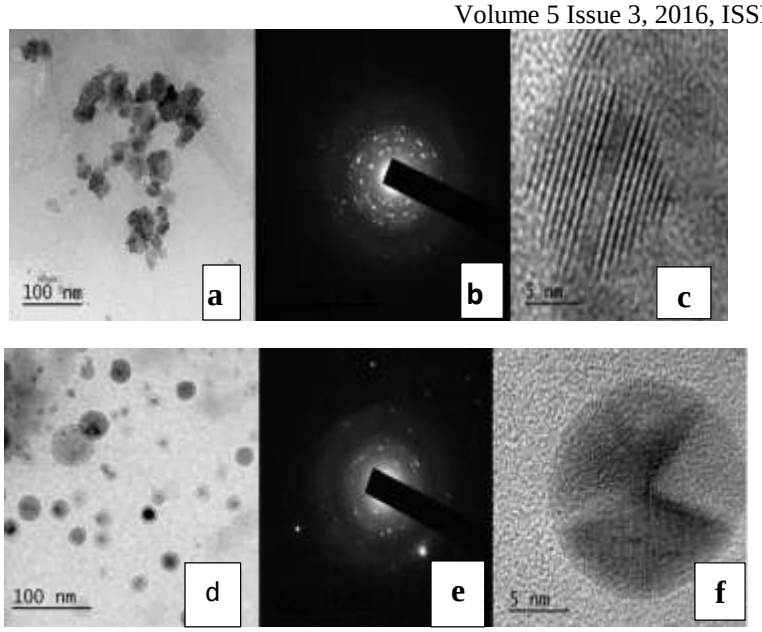

Figure (9): (a, d) TEM images of the CS-Cu NPs for samples reduced with ascorbic acid and $NaBH_4$. (b, e) electron diffraction for sample reduced with ascorbic acid and $NaBH_4$. (C and f) HRTEM image of lattice fringes were corresponding to CS-Cu and CuO or Cu_2O NPs planes for the samples (a) and (d).

4. CONCLUSION

In this paper, chitosan copper and copper oxides nanoparticles were successfully synthesized at room temperature by using electrochemical technique. Chitosan copper complex were reduced by different types of reducing agents such as (ascorbic acid, N_2H_4, $NaBH_4$). The presence of copper metal and copper oxides nanoparticles were confirmed by the appearance of the surface Plasmon resonance on these colloids, which their bands appeared in the FT-IR to investigate the interaction between copper nanoparticles and $–NH_2$, -OH function groups of chitosan. The TEM studies showed that the mean size of the NPs is 28 nm. The electrochemical technique is simple, cost-effective and the product which could use in many pharmaceutical and biomedical applications, all the materials used in the study were non-toxically for environment.

5. REFERENCES

1. Ferrando, R., J. Jellinek, and R.L. Johnston, *Nanoalloys: from theory to applications of alloy clusters and nanoparticles.* Chemical reviews, 2008. **108**(3): p. 845-910.
2. Egorova, E.M., A.A. Kubatiev, and V.I. Schvets, *Biological Effects of Metal Nanoparticles*. 2014, Springer.
3. Ahamed, M., et al., *Synthesis, Characterization, and Antimicrobial Activity of Copper Oxide Nanoparticles.* Journal of Nanomaterials, 2014. **2014**: p. 4.
4. Qiao, X., et al., *Study on potential antitumor mechanism of a novel Schiff Base copper (II) complex: synthesis, crystal structure, DNA binding, cytotoxicity and apoptosis induction activity.* Journal of inorganic biochemistry, 2011. **105**(5): p. 728-737.
5. Santini, C., et al., *Advances in copper complexes as anticancer agents.* Chemical reviews, 2013. **114**(1): p. 815-862.
6. Chen, Z., et al., *Acute toxicological effects of copper nanoparticles in vivo.* Toxicology letters, 2006. **163**(2): p. 109-120.
7. Suresh, Y., et al. *Characterization of green synthesized copper nanoparticles: A novel approach*. in *Advanced Nanomaterials and Emerging Engineering Technologies (ICANMEET), 2013 International Conference on*. 2013. IEEE.
8. Vitulli, G., et al., *Nanoscale copper particles derived from solvated Cu atoms in the activation of molecular oxygen.* Chemistry of materials, 2002. **14**(3): p. 1183-1186.
9. Joshi, S., et al., *Radiation induced synthesis and characterization of copper nanoparticles.* Nanostructured materials, 1998. **10**(7): p. 1135-1144.
10. Liu, Z. and Y. Bando, *A novel method for preparing copper nanorods and nanowires.* Advanced Materials, 2003. **15**(4): p. 303-305.
11. Dhas, N.A., C.P. Raj, and A. Gedanken, *Synthesis, characterization, and properties of metallic copper nanoparticles.* Chemistry of materials, 1998. **10**(5): p. 1446-1452.
12. Cheng, X., et al., *Modifier effects on chemical reduction synthesis of nanostructured copper.* Applied surface science, 2006. **253**(5): p. 2727-2732.
13. Aye, H.L., S. Choopun, and T. Chairuangsri. *Preparation of nanoparticles by laser ablation on copper target in distilled water*. in *Advanced Materials Research*. 2010. Trans Tech Publ.
14. Chen, D.-H. and S.-H. Wu, *Synthesis of nickel nanoparticles in water-in-oil microemulsions.* Chemistry of Materials, 2000. **12**(5): p. 1354-1360.
15. Reetz, M.T. and W. Helbig, *Size-selective synthesis of nanostructured transition metal clusters.* Journal of the American Chemical Society, 1994. **116**(16): p. 7401-7402.
16. Zheng, Y., et al., *Preparation of chitosan–copper complexes and their antitumor activity.* Bioorganic & medicinal chemistry letters, 2006. **16**(15): p. 4127-4129.
17. Kumar, M.N.R., *A review of chitin and chitosan applications.* Reactive and functional polymers, 2000. **46**(1): p. 1-27.
18. Annapurna, S., et al. *Characterization of Green Synthesized Copper Nanoparticles Stabilized by Ocimum Leaf Extract*. in *MRS Proceedings*. 2014. Cambridge Univ Press.
19. Lavertu, M., et al., *High efficiency gene transfer using chitosan/DNA nanoparticles with specific combinations of molecular weight and degree of deacetylation.* Biomaterials, 2006. **27**(27): p. 4815-4824.
20. Mekahlia, S. and B. Bouzid, *Chitosan-Copper (II) complex as antibacterial agent: synthesis, characterization and coordinating bond-activity*

correlation study. Physics Procedia, 2009. **2**(3): p. 1045-1053.
21. Yin, X., et al., *Metal-coordinating controlled oxidative degradation of chitosan and antioxidant activity of chitosan-metal complex.* Arkivoc, 2004. **9**: p. 66-78.
22. Reicha, F.M., et al., *Electrochemical synthesis, characterization and biological activity of chitosan metal complexes.* Int. J. of Basic and Applied Chemical Sciences, 2012. **2**: p. 7-22.
23. Cai, Q., et al., *Degradation of chitosan by an electrochemical process.* Carbohydrate Polymers, 2010. **79**(3): p. 783-785.
24. Kousalya, G., et al., *Preparation and metal uptake studies of modified forms of chitin.* International journal of biological macromolecules, 2010. **47**(5): p. 583-589.
25. Chiessi, E., et al., *Copper complexes immobilized to chitosan.* Journal of inorganic biochemistry, 1992. **46**(2): p. 109-118.
26. Rhazi, M., et al., *Contribution to the study of the complexation of copper by chitosan and oligomers.* Polymer, 2002. **43**(4): p. 1267-1276.
27. Brunel, F., N.E. El Gueddari, and B.M. Moerschbacher, *Complexation of copper (II) with chitosan nanogels: Toward control of microbial growth.* Carbohydrate polymers, 2013. **92**(2): p. 1348-1356.
28. Dang, T.M.D., et al., *Synthesis and optical properties of copper nanoparticles prepared by a chemical reduction method.* Advances in Natural Sciences: Nanoscience and Nanotechnology, 2011. **2**(1): p. 015009.
29. Tiwari, A.D., et al., *Stabilisation of silver and copper nanoparticles in a chemically modified chitosan matrix.* Carbohydrate polymers, 2013. **92**(2): p. 1402-1407.
30. Bian, Y., et al., *Preparation and study on anti-tumor effect of chitosan-coated oleanolic acid liposomes.* RSC Advances, 2015. **5**(24): p. 18725-18732.
31. sani Usman, M., *Synthesis, characterization, and antimicrobial properties of copper nanoparticles.* International journal of nanomedicine, 2013. **8**: p. 4467-4479.
32. Dhawade, P.P. and R.N. Jagtap, *Characterization of the glass transition temperature of chitosan and its oligomers by temperature modulated differential scanning calorimetry.* Adv Appl Sci Res, 2012. **3**(3): p. 1372-82.
33. Usman, M.S., et al., *Copper nanoparticles mediated by chitosan: synthesis and characterization via chemical methods.* Molecules, 2012. **17**(12): p. 14928-14936.
34. Zain, N.M., A. Stapley, and G. Shama, *Green synthesis of silver and copper nanoparticles using ascorbic acid and chitosan for antimicrobial applications.* Carbohydrate polymers, 2014. **112**: p. 195-202.
35. Manikandan, A. and M. Sathiyabama, *Green synthesis of copper-chitosan nanoparticles and study of its antibacterial activity.* Journal of Nanomedicine & Nanotechnology, 2015. **2015**.
36. Prakash, I., et al., *Preparation and characterization of nanocrystallite size cuprous oxide.* Materials Research Bulletin, 2007. **42**(9): p. 1619-1624.
37. Li, L.-H., et al., *Preparation, characterization and antimicrobial activities of chitosan/Ag/ZnO blend films.* Chemical Engineering Journal, 2010. **160**(1): p. 378-382.
38. Qi, Z.-m., et al., *Characterization of gold nanoparticles synthesized using sucrose by seeding formation in the solid phase and seeding growth in aqueous solution.* The Journal of Physical Chemistry B, 2004. **108**(22): p. 7006-7011.
39. Primo, A., et al., *High catalytic activity of oriented 2.0. 0 copper (I) oxide grown on graphene film.* Nature communications, 2015. **6**.
40. Guo, Y., et al., *One pot preparation of reduced graphene oxide (RGO) or Au (Ag) nanoparticle-RGO hybrids using chitosan as a reducing and stabilizing agent and their use in methanol electrooxidation.* Carbon, 2012. **50**(7): p. 2513-2523.
41. Chmielová, M., J. Seidlerová, and Z. Weiss, *X-ray diffraction phase analysis of crystalline copper corrosion products after treatment in different chloride solutions.* Corrosion science, 2003. **45**(5): p. 883-889.
42. Dang, T.M.D., et al., *The influence of solvents and surfactants on the preparation of copper nanoparticles by a chemical reduction method.* Advances in Natural Sciences: Nanoscience and Nanotechnology, 2011. **2**(2): p. 025004.
43. Shalumon, K., et al., *Fabrication of aligned poly (lactic acid)-chitosan nanofibers by novel parallel blade collector method for skin tissue engineering.* Journal of biomedical nanotechnology, 2012. **8**(3): p. 405-416.
44. Lu, J.Z., et al., *Chelating efficiency and thermal, mechanical and decay resistance performances of chitosan copper complex in wood–polymer composites.* Bioresource technology, 2008. **99**(13): p. 5906-5914.
45. Yang, H.-J., S.-Y. He, and H.-Y. Tuan, *Self-Seeded Growth of Five-Fold Twinned Copper Nanowires: Mechanistic Study, Characterization, and SERS Applications.* Langmuir, 2014. **30**(2): p. 602-610.

International Journal of Science and Engineering Applications
Volume 5 – No.3, May 2016

Predicting Medicine-Stocks by Using Multilayer Perceptron Backpropagation

The Prediction Medicine Stock based Multilayer Perceptron Backpropagation

Eka MalaSari Rohman
Faculty of Engineering,
University of Trunojoyo
Madura, Indonesia

Imamah
Faculty of Engineering,
University of Trunojoyo
Madura, Indonesia

Aeri Rachmad
Faculty of Engineering,
University of Trunojoyo
Madura, Indonesia

Abstract: Artificial neural network has a lot of ability in controlling the error rate to formulate some of its functions as a supervised method. Medicine is one of the major needs for each patient, so that every hospital should know how much inventory of drugs is used and needed by patients every day. This study uses artificial neural network with multilayer perceptron backpropagation as a solution for predicting drug stocks. Prediction of drug stocks using medicine prior period stock data for three years is used to get the predicted results with a small error rate. Backpropagation algorithm using the error output is used to change the weights in the backward direction. To get this error, forward stage should be done first. The results of experiments using backpropagation with the configuration of 0.04 mementum which has training rate of 0.001 gets the value of MSE of 0.00001.

Keywords: artificial neural network, backpropagation, medicine stocks, hospital, predictions

1. INTRODUCTION

Neural networks have been shown to be effective in modelling and forecasting nonlinear time series with or without noise [1]. There are several works which has been done for time series prediction based on neural network for prediction of stock price, financial and economic time series, stock exchange. Medicine is one of the essential needs of a hospital. Health patient at a hospital depends on the availability of drugs, especially for patients who are hospitalized and in a worrying condition. Therefore, the hospital must provide the drug in sufficient quantities for their patients [2]. However, having medicine in a very big-stock is not good enough because the medicine is composed of chemicals that if the expiration runs, it would be dangerous to consume. Data stock of drugs is one of the data which is included in the time series data. Various studies time series, especially statistical time series forecasting has become the most popular technique for a short time scale [3]. Smoothing of time series data is a task that occurs in many applications and is used for prediction or forecasting.

Data preparation is an important step in building a successful model of Neural Network. Without good data collection, adequate and representative, it is not possible to develop a predictive model of Neural Network useful. Thus, the reliability model of Neural Network depends on the extent of how much the quality of data [4].An artificial neural network (ANN), another powerful mathematical tool, is capable in making extremely complex – modeling and non-linear systems with many inter-related parameters, and does not require detailed information on the physical parameters of the system [5].

This paper will be focusing on objective forecasting method. We proposed to apply neural network of backpropagation to predict the medicine stock. There are 3 categories of prediction methods [6], they are:

• Objective forecasting method (quantitative prediction methods) – based on mathematical and statistical calculations
• Subjective forecasting method (qualitative prediction methods) – based on expert opinions
• Prophecy (educated guessing)

2. SYSTEM DESIGN

Prediction or forecasting is an activity which predicts the recurrence in the future through a testing-state in the past. In social life, everything is uncertain, it is difficult to accurately predict. In this case there should be a forecasting. Forecasting is always made in order to minimize the effect of this uncertainty of an issue. In other words, the prediction aims to get results that can minimize errors in the predicted future (forecast error) which is usually measured by the mean square error, mean absolute error, and so forth.

A good prediction has several important criterion, such as accuracy, cost, and convenience, they are described as follows::

- **Accuracy**.Accuracy of a forecasting results measured by habits and consistency forecasting. A forecasting may results bias, if is too high or too low compared with the fact that actually happened. Forecasting result is said to be consistent if the magnitude of forecasting error is relatively small.
- **Costs.** The cost required for the manufacture of a forecast depends on the number of items which are predicted, the length of the forecast period, and the forecasting method used**.**
- **Easy.** The use of forecasting methods which are simple, easy to make and easy to apply will benefit the company.

In this case the medicine by the time stock data will be processed with the formula to obtain the autocorrelation time lags which make the time could be significant for the predicted time. Then the significance of medicine stock data at a time will be the input data in the process of training the neural network backpropagation ANN.

To evaluate price forecasting parameters, we can use the size of the forecast error. The best price of forecasting parameters is the price that gives the smallest value of forecasting error. There are different sizes that errors can be classified into standard size in statistics and relative size.

Artificial neural network information is a paradigm of information processing that is inspired by biological nervous systems, such as information processing in the human brain [7]. Each neuron can have multiple inputs and has a single output. Input lines on a neuron may contain raw data or processed data from the previous neuron. While the output of a neuron can be the end result or input to the next neuron.

Input on the network will be processed by a function that will add up the values of all weights. The results of the sum will be compared to a threshold value through the activation function of each neuron. One function of activation on neural network is a binary sigmoid function. This function has a value in the range of 0 to 1, which is expressed as:

$$y = f(x) = \frac{1}{1+e^{-\sigma x}} \quad (1)$$

$$f(x) = \text{SIN}\, x = [-1, 1] \quad (2)$$

The value of y = f (x) uses the value of sin x because based on the research [8] , this value can be better than the sigmoid function [0,1] because the share value is 0, which do not have a significant value. The methodwhich is used to perform Predictive stock prices in this study is Backpropagation method. This method is selected because it is a method of ANN multi-layer that matches the nature of the data which is non-linear and time series.

Once the efficient parameter values are specified, prediction performances of ANN and SVM models can be compared to each other. This performance comparison was performed on the entire data set considering the parameter values specified using the parameter setting data set. That is, the prediction models must be re-trained using a new training data set which must be a new part of the entire data set and must be larger than the training subset of parameter setting data set [9]. After re-training, out-of-sample evaluation of models must be carried out using a new holdout data set, which is the remaining part of entire data set.

The training stage shown in Figure 1 is a step to process data patterns that have been through the process of autocorrelation and normalization for the system to determine the weights that can map between the input data with target data output is desired. After the feedforward and backward, it will get the best weights according to the target error and epoch maximal or maximal iterations desired.

Before the data is processed into the ANN which the aim is to normalize the data input of medicine stock. Stock data must be normalized first, because ANN can only recognize the value range of (0.1) which the equation can be seen in equation (1). It can reduce the prediction error by adjusting the weight of the node-node when the training phase.

One form of analysis in Statistics theory is the analysis of time series data, that is the analysis of data is a function of time or place. Analysis of time series data is a special analysis of the regression analysis, because the time series data involves a quantity which is called autocorrelation. The existence of autocorrelation can be a periodic autocorrelation, which the period of autocorrelation value is more than one. It is also widely available in time series data that has periodic seasonal component.

Backpropagation is a method in conducting the production solutions for the basic number of neurons (n) in the hidden layer, value of learning rate, momentum and number of iterations. Those are ANN model parameters which must be efficiently determined [9].

The architecture of the three-layered feedforward ANN is one neurons input, four ouput layers, one output layers with 0.001 learning rate, the momentum of 0.02 and the maximall iterations 10000.

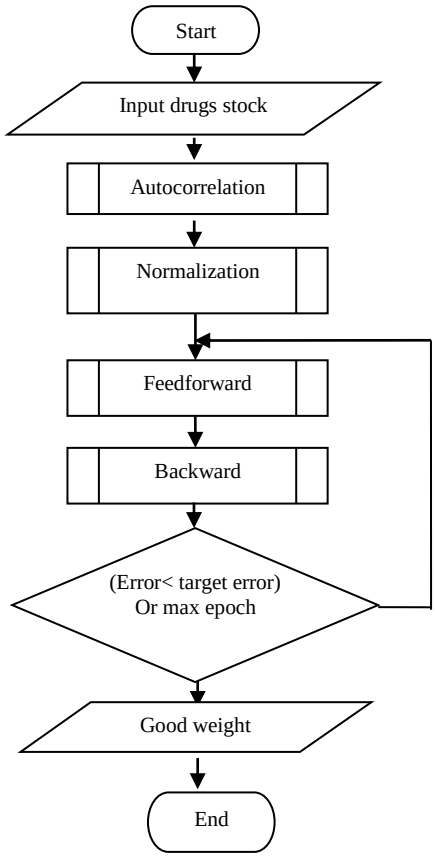

Figure 1. Flowchart Training

Autocorrelation formulates together with the formulation of the correlation between two variables. In the method of Statistics, the sample holds on bivariate data (X, Y).

Autocorrelation process is performed to find the closeness of the data and is used to find data patterns stationary or non-stationary. Once the weights are the best at this stage of training which could be obtained, then the weighted value is used to process the input data to generate the appropriate output. It is used to test whether the ANN can work well to predict patterns of data that has been drilled with a small error rate.

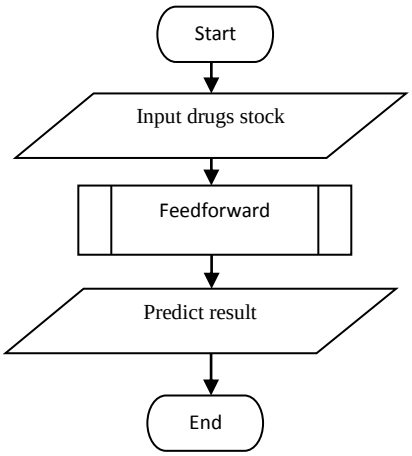

Figure 1. Flowchart Testing

Weighting is done on the training process, if the number of neurons and the number of lower layer lead to a low value

to weight the training process [10]. The architectural design for the number of neurons in each layer is instrumental in improving accuracy.

Feedforward process is performed to obtain the output error by summing the input weights and the weight bias shown in Figure 2. And the performance of the activation functions for hidden summing the weights and the bias. Once the best weights at this stage of training is obtained, then the value of the weights are used to process the input data to generate the appropriate output. It is used to test whether optimal ANN can work to predict patterns of data that have been trained with a small error rate. This process continues until the epoch value is reached. When the price-stock could be obtained, then it can calculate the fitness value. The value which is used is the RMSE.

2.1 Normalization and Denormalization

Normalization process used in this system uses normalized minimum-maximum. Denormalization existing data is done by dividing the value of that data with the value of the data range (maximum data value-minimum data value). The aim of data input normalization is to adjust the value range of data with the activation function in a propagation system. This means that the value of the square of the input should be in the range of 0 to 1. So the input range that qualifies is the input data which values from 0 to 1 or from -1 to 1. Therefore the resulting output will be in the range of 0 to 1. Then image to get the true value of output is necessary to normalize the process.

Normalization of data using the formula in equation (3):

$$f(x) = \frac{X_i - X_{\min}}{X_{\max} - X_{\min}} \quad (3)$$

X_i is the i-th of data, while theX_{min}, is the minimum value data and X_{max} is the maximum value of data.

In the testing process, the output is produced by the network which ranges from 0 to 1. So it is necessary to normalize it to be useful to convert the output result of the network back into normal medicine-stocks. After all it will do a comparison between the actual data with the data from predictive, so it can the error and its percentage could be calculated.

The image of normalizing the data by using the formula in the equation (4):

$$X_i = y(X_{\max} - X_{\min}) + X_{\min} \quad (4)$$

2.2 RMSE (Root Mean Squared Error)

Selection of the best forecasting method should be based on the level of prediction errors. Measurement error is made to see if the methods that have been used are adequate for predicting a data, because there is no forecasting method to predict future data appropriately. The smaller the margin of error is generated, the more precise a method in generating predictions.

Size accuracy of forecasting results are used to calculate the error value of the calculation process by the system to the initial value in accordance with the original data using the average of squared errors. RMSE is the square root of the Mean Squared Error (MSE). Error suggests how minimum predicted results with the actual value. This is the formula of the average error square root or Root Mean Squared Error (RMSE) with equation (5):

$$RMSE = \sqrt{\frac{\sum_{t=1}^{n}(X_t - F_t)^2}{n}} \quad (5)$$

RMSE is obtained from the roots number X_t is the value of forecasting the expected period t is reduced F_t as the value of the forecasting system in period t is squared and then averaged for n number of data.

3. RESULT AND DISCUSSION

The data which are used in this research is secondary data that is quantitative (show in Table1). The source of the data were obtained from hospitals Syarifah Ambami Bangkalan. In consideration of the relatively more stable condition, this study used the study period 2007-2009. Historical data were chosen because it reflects the actual condition of medicine-stocks, so that this research results will be used as valuable information for the hospital.

Training data that will be used in this study to training is as many as 500 on data from January 2007 - December 2008. And since January 2009 - December 2009, the total of 119 data is used as a test

Table 1. Medicine-stock data in December 2008.

NO	DRUGS NAME	DRUGS Stock Desember 2008	Drug Price
1	ACTAZOLAM 0.5 MG TAB/ BOX 30	-	1,300.00
2	ACTRAPID HM PENFILL 100 INJ/10	-	181,830.00
3	ACTRAPID INJ	-	290,000.00
4	ACTRAPID NOVOLET 5X3ML INJ	-	84,813.00
5	ACYCLOVIR 200 TAB (50/BOX)	90	320.00
6	ACYCLOVIR 400 MG (100/BOX)	125	535.46
7	ACYCLOVIR 400 MG (50`S/BOX)TAB NOVELL	-	650.00
8	ACYCLOVIR KRIM 5 % 5 G (TUBE) INDO	12	2,646.48
9	ADALAT OROS 20 MG TAB/DOS 30`S	-	2,700.00
10	ADALAT OROS 30 MGTAB/BTL 30`S	-	3,300.00
11	ADALAT TAB 10 MG/BOX 50`S	44	2,120.00
12	ADALAT TAB 5 MG/BOX 50`S	-	1,420.00
13	ADULT OXIGEN MASKER AMS	-	70,000.00
14	AERIUS/30	-	5,311.33
15	AGNUCASTON TAB 30`S	-	4,500.00
16	ALBAPURE 20% 100 ML	-	517,335.00
17	ALBOTHYL 100 CC	-	
18	ALBOTHYL CONC 10 ML (BTL)	-	17,325.00
19	ALBUMIN 25%	-	
20	ALBUMIN BEHRING 20% - 100 ML	-	1,310,000.00
21	ALDIAB TAB / BOX 40`S	-	750.00
22	ALGANAX TAB 0.5	-	1,430.00
23	ALINAMIN INJ - BOX 5 AMP	-	7,630.00
24	ALINAMIN TABLET	21	
25	ALKOHOL 70% /LT	15,000	25.00
26	ALKOHOL 95%	6,000	30.80
27	ALKOHOL 96%	-	19.80
28	ALKOHOL SWAB / BOX @ 200 SACHET	600	200.00
29	ALLOPURINOL 100 MG TAB/100`S	1,616	100.00

Bacpropagation has the training phase which is aimed to find the best weights on each layer.Network is trained with medicine sales data from the years 2008-

2009 as many lags which were obtained by autocorrelation and normalization before.

Artificial neural network architecture consists of an input layer, four hidden layer (hidden layer) and an output layer (1-4-1).The number of input and output node in accordance with the number of lags arise from the process of autocorrelation.While the number of hidden layer were obtained from the trial itself.The condition of the system will stop if the generated-error value is smaller than the tolerances error or the number of iterations which had been stated.

The process of propagation neural network with 4acyclovir medicine code 200 TAB (50 / BOX) produces some value, among others:

Table 2. The results of Bacpropagation Trial in the change of momentum

hidden	Iterasi	(δ)/mom	(a)/Lrate	Error	MSE
4	9000	0.04	0,001	0.0006	0,000001
4	9000	0.035	0.001	0.0006	0,000001
4	9000	0.03	0.001	0.0006	0,000001

Table 3. Results of Trial Backpropagation rate changes Training

hidden	Iterasi	(δ)/mom	(a)/Lrate	Error	MSE
4	9	0.02	0,1	0.008	0,083
4	969	0.02	0.001	0.008	0,083
4	31	0.02	0.025	0.008	0,083

4. CONCLUSION

Implementation of the results of experiments which was conducted five times to get the RMSE is getting smaller.Table 1 and table 2 are the result of an experiments on the change in momentum and also the experiments on the changes learning rate. The conclusions are as follows:

1. By adding the stock prices of medicine with Backpropagation neural network, it can be used as a solution for and determine the initial stock of drugs.
2. From the test results in determining the forecasting model parameters, it can be concluded that the best performance can be obtained by using the parameters of the artificial neural network with as many as 9000 the number of iterations, mementum parameter of 0.04 learning rate of 0.1, fault tolerance error of 0.0001 and a target at 0.0006. For all types of medicine- stocks daily data, it uses structures 1-4-1 BPNN architecture (one neuron in the input layer, four in the hidden layer, and a single neuron in the output layer).

5. ACKNOWLEDGMENTS

We thank the Indonesian government and Multimedia Computing Laboratory, University of Trunojoyo Madura, which has funded this research through research programs for lecturers.

6. REFERENCES

[1] Shamsul Faisal Mohd Hussein, MohdBadrilNor Shah, MohdRaziAbd Jalal, Shahrum Shah Abdullah. 2011. Gold Price Prediction Using Radial Basis Function Neural Network.Publish in Modeling, simulation and Applied(ICMSAO), 4th international Conferende. Pp 1 – 11.

[2] Anief, M. 1999. Disperse Systems, Suspension and Emulsion Formulation, Gadjah Mada University Press. Yogyakarta.

[3] Zhang, G. P. 2004. Neural Networks in Business Forecasting. (G. P. Zhang, Ed.)Review of Economic Sciences. IGI Global.Journal of Intelligent Systems Vol 6.

[4] Indah Suryani. 2015. Application of Exponential Smoothing for Transforming Data to Improve Neural Network on Prediction Accuracy Gold Prices. Jurnal of Intelligent System Vol. 1, No. 2.

[5] Ming Tan, Gaohong He, Xiangcun Li, Yuanfa Liu, Chunxu Dong, JinghaiFeng. 2012. Prediction of the Effects of Preparation Conditions on Pervaporation Performances of Polydimethylsiloxane (PDMS)/ Ceramic Composite Membranes by Backpropagation Neural Network And Genetic Algorithm. Separation and Purification Technology 89.pp 142–146.

[6] Sven F. Crone, 2005, Lancaster University Management School, Forecasting with Artificial Neural Networks, Lecture Notes.

[7] Kusumadewi, S. 2003. Artificial Intellegence. Jogjakarta: Graha Ilmu.

[8] Kara, Y., Boyacioglu, M. A., & Baykan, O. K. 2011. Predicting Direction Of Stock Price Index Movement Using Artificial Neural Networks And Support Vector Machines: The Sample Of The Istanbul Stock Exchange. Expert Systems with Applications 38 , 5311–5319.

[9] Yakup Kara, Melek Acar Boyacioglu, Ömer Kaan Baykan. 2011. Predicting direction of stock price index movement using artificial neural networks and support vector machines: The sample of the Istanbul Stock Exchange. Expert Systems with Applications 38, 5311–5319.

[10] Chang, P. C., Wang, D. d., & Zhou,ion C. l. 2012. A Novel Model By Evolving Partially Connected Neural Network For Stock Price. Expert Systems with Applications 39 , 611–620.